
Theses and Dissertations

Fall 2016

Development of metrics to describe cerebral aneurysm morphology

Benjamin Micah Berkowitz
University of Iowa

Copyright © 2016 Benjamin Micah Berkowitz

This dissertation is available at Iowa Research Online: <http://ir.uiowa.edu/etd/2181>

Recommended Citation

Berkowitz, Benjamin Micah. "Development of metrics to describe cerebral aneurysm morphology." PhD (Doctor of Philosophy) thesis, University of Iowa, 2016.
<http://ir.uiowa.edu/etd/2181>.

Follow this and additional works at: <http://ir.uiowa.edu/etd>



Part of the [Biomedical Engineering and Bioengineering Commons](#)

DEVELOPMENT OF METRICS TO DESCRIBE CEREBRAL ANEURYSM
MORPHOLOGY

by

Benjamin Micah Berkowitz

A thesis submitted in partial fulfillment
of the requirements for the Doctor of Philosophy
degree in Biomedical Engineering in the
Graduate College of
The University of Iowa

December 2016

Thesis Supervisor: Professor Suresh M.L. Raghavan

Copyright by
Benjamin Berkowitz
2016
All Rights Reserved

Graduate College
The University of Iowa
Iowa City, Iowa

CERTIFICATE OF APPROVAL

PH.D. THESIS

This is to certify that the Ph.D. thesis of

Benjamin Berkowitz

has been approved by the Examining Committee for
the thesis requirement for the Doctor of Philosophy degree
in Biomedical Engineering at the December 2016 graduation.

Thesis Committee:

Suresh M.L. Raghavan, Thesis Supervisor

Joseph Reinhardt

Sarah Vigmostad

Gary Christensen

David Hasan

ACKNOWLEDGEMENTS

I would like to thank my advisor, Professor Suresh M.L. Raghavan, for his mentorship. While Dr. Raghavan is clearly an accomplished researcher, he also holds the education and success of his students above all else. I am very happy to have spent my undergraduate and graduate education under his guidance.

Thank you to my committee members for serving on my committee. A special thanks goes to Dr. David Hasan for his additional work with several of my side projects.

Thank you to Dr. Hasan and Dr. Bob Harbaugh for their assistance with the collection of the selection bias patient data. Thank you to Dr. Manasi Ramachandran, Dr. Rohini Retarekar, Steve Lin, Ben Dickerhoff and Tatiana Correa whose efforts and results from previous studies were built upon in this work.

Tatiana Correa, Kevin Johnson and Elizabeth Niedert made significant contributions to my dissertation research. Tatiana assisted with data collection for the selection bias study, Kevin assisted with data processing of the BioMOST study data, and Elizabeth assisted with performing the protocol, as well as with the inter-user variability and sensitivity studies. I would like to thank them for their hard work and assistance.

Thank you to Luca Antiga, Marina Piccinelli and the VMTK community, whose work this dissertation builds upon, in addition to the work of Ma et al. 2004, Raghavan et al. 2005, Dhar et al. 2008, Lauric et al. 2011, Piccinelli 2012 and Ramachandran et al. 2016.

I would like to thank my fellow BioMOST Lab students for their support and friendship over the years. Each has given me a new perspective on scientific research and shown me the possibilities of where my career could take me.

I would also like to thank my family. My wife, Becky, for her strength, support and flexibility throughout my time as a graduate student. She has been a great partner throughout school, pushing me to enjoy life when I worked too hard, and to work harder when I needed the motivation. My sister, Shelly, for her friendship. And most of all, my parents, Dan and Holly, for providing me with the guidance and opportunity to attain what I have.

ABSTRACT

Cerebral aneurysm is a pathology of the circulatory system in the brain in which an arterial wall balloons into a blood-filled sac. If the aneurysm ruptures, stroke can occur and has a high probability of causing permanent disability or death. Aneurysm surgery carries a high rate of morbidity and mortality compared to the natural rate of aneurysm rupture, so physicians must take care in recommending surgery for an aneurysm patient. However, very little is known about the etiology of brain aneurysm rupture and what prognostics exist. The International Study for Intracranial Aneurysms suggested that large aneurysm size and posterior location are important factors in identifying high rupture risk. However, many small aneurysms and aneurysms in other portions of the circulation still rupture. Many studies have assessed morphological traits, identified from aneurysm appearance on diagnostic medical images, and found such traits to be different in aneurysms that ruptured and aneurysms that did not rupture. In fact, more than 50 such morphological indices have been introduced in the literature, and many of them redundantly quantify particular morphological characteristics. In order to demonstrate the prognostic ability of morphology as an indicator of rupture risk, however, a large longitudinal cohort study must be carried out. A study such as this is time-consuming and expensive, and each additional hypothesis that a particular morphological index is predictive of rupture risk would require increasing the study population size in order to fulfill the necessary statistical power requirements for a rigorous test. Thus, a minimal set of physically meaningful, independent metrics that fully describe the aneurysm morphology is needed.

In this dissertation an automated protocol was developed to process segmented medical images and extract an exhaustive set of morphological indices that quantify all relevant morphological features. Each morphological index was then analyzed for robustness to inter-user variability and for sensitivity to the particular morphological characteristic that it was designed to quantify. A factor analysis was then performed using the most robust, sensitive metrics on a population of unruptured aneurysms from five data centers and 276 patient-specific aneurysms. The results from the factor analysis were utilized to ascertain what morphological features those metrics truly described, if there were any redundancies in definition, and the variance each morphological trait described in the population. Four underlying morphological constructs were uncovered through the factor analysis. The first factor, sac size, was highly aligned with morphological indices that measured volume and one-dimensional size measurements. Sac size described 50% of the variance in the data set. The second factor, sac irregularity, was highly aligned with morphological indices that described various aspects of irregular shape. A set of variables that all were implicated in causing irregular shape, but in reality measured sac-neck size relation, also merited inclusion of a second metric to describe the variance seen in the second factor. Sac irregularity described 20% of the variance in the data set. The third factor, sac ellipticity, aligned highly with morphological indices that described the overarching ellipticity of the aneurysm sac independent of other non-spherical characteristics. Sac ellipticity described 13% of the variance in the data set. The fourth factor, sac-vessel size relation, aligned highly with morphological indices that described the size of the aneurysm sac in relation to its parent vessel. Sac-vessel size relation described 7% of the variance in the data set. All four of these factors in combination

described 91% of the variance in the data set. Five morphological indices – non-planar isolation sac volume (Vnp), Voronoi diagram core evolution irregularity index (IRRvdc), tissue stretch ratio (TSR), Voronoi diagram core evolution ellipticity index (EIvdc) and size ratio (SRang) were determined to be the key indices for describing aneurysm morphology. Finally, the proposed metrics were used to test the hypothesis that aneurysms that are chosen for untreated observation are morphologically different than those that are treated – commonly referred to as selection bias. Study population was 27 patient-specific aneurysms that were placed on untreated observation (observation group) and 27 patient specific aneurysms that were size- and location-matched but were chosen for treatment (treated group). A significant difference was found in the morphological index that measured ellipticity between the two groups, indicating that physicians already commonly select highly elliptical aneurysms for treatment. This result may give insight into physicians' choices, and merits further investigation with a larger data set for confirmation. Additionally, because the same result was replicated in both of the metrics chosen to quantify ellipticity (for both manual and automated methods), this highlighted the use of the morphological factors in determining an minimal set of independent, robust morphological indices.

PUBLIC ABSTRACT

Brain aneurysm is a disease in which a blood vessel in the brain weakens and balloons into a blood-filled sac. In the US alone, sixteen million people are estimated to have aneurysms, and if one of these aneurysms ruptures a part of the brain can lose its blood supply and die. An aneurysm is like a ticking time bomb, but it is impossible for a physician to know whether or not an aneurysm will rupture. Aneurysms are treatable with brain surgery, but because brain surgery is so risky and aneurysm rupture rate is so low, physicians need a way to tell how likely an aneurysm is to rupture. Currently, little is known about how to tell whether an aneurysm will be one of the 98% that never rupture, or one of the 2% that will cause severe brain injury. This dissertation introduced software that was developed to automatically assess aneurysms on medical images to quantify their appearance. The software was then tested to see if it was robust, and then the software in combination with statistics was used to tell future researchers what characteristics of an aneurysm's appearance to look for on medical images. Lastly, the software was utilized to test whether physicians are already choosing to treat aneurysms with these appearance characteristics, or if they can be used to improve doctors' abilities to make the right treatment decision.

TABLE OF CONTENTS

List of Tables	xii
List of Figures	xiii
Introduction.....	1
Cerebral aneurysm	1
Treatment options	2
Current prognostic assessment techniques.....	4
Current research on the determination of rupture risk from medical images	5
Objectives	15
Specific Aim 1: Development of All Morphological Indices.....	17
Methods for obtaining geometric data	17
Geometric data preparation protocol	18
Morphological indices from literature	21
Novel Indices	33
Summary of indices calculated by automated protocol	49
Specific Aim 2: Identification of Optimal Set of Morphological Indices	53
Background.....	53
Study data.....	54
Procedure to determine an optimal set of morphological indices.....	56
Study on robustness of morphological indices to inter-user variability	57
Study on sensitivity of morphological indices.....	62
Discussion of robustness in definition and application.....	77
Factor analysis	78

Conclusions toward an optimal set of morphological indices	95
Limitations	100
Specific Aim 3: Demonstration of use of optimal metrics to test hypothesis.....	102
Background.....	102
Study groups	102
Procedure	103
Results.....	103
Discussion	106
Conclusions.....	108
Appendix A Distributions of the morphological indices	110
Appendix B User variability plots	118
Appendix C User variability isolations.....	126
References.....	129

LIST OF TABLES

Table 1. Listing and description of each index and its source.....	50
Table 2. Summary of the data utilized for Specific Aim 2.....	55
Table 3. Inter-user variability statistics, regression line slope and Pearson coefficient, for each morphological index.....	59
Table 4. Description of the idealized aneurysm models used for the sensitivity analysis.....	64
Table 5. Summary of the sensitivity analysis.....	76
Table 6. Normality and transformations of variables.....	80
Table 7. Pattern matrix for the factor analysis.....	88
Table 8. Proportion of variance explained by each factor.....	88
Table 9. Factor correlation matrix.....	89
Table 10. Overall assessment results.....	95
Table 11. Recommended choices for morphological indices using either automated or manual measurements. The most highly recommended morphological index for each morphological factor is highlighted in bold.....	100
Table 12. Results from Wilcoxon test between observational and treatment groups using the marquee morphological indices derived using automated measurement. EIVdc was significantly different between the treated aneurysms and the follow-up aneurysms.....	105
Table 13. Results from Wilcoxon test between observational and treatment groups using the marquee morphological indices derived using automated measurement. MaxDRatioMagnitude was significantly different between the treated aneurysms and the follow-up aneurysms.....	106

LIST OF FIGURES

Figure 1. Types of cerebral aneurysms	1
Figure 2. Definitions of Raghavan et al. shape indices (Raghavan et al. 2005)	8
Figure 3. Example of a reconstruction of an aneurysm surface model using increasing orders of Zernike moments (Millán et al. 2007)	9
Figure 4. Illustration of vessel angle and aneurysm angle (Dhar et al. 2008)	10
Figure 5. Definition of vessel centerline curvature using the osculating plane and osculating circle tangent to the curve (Piccinelli et al. 2011)	11
Figure 6. Normalized centroid radii model parameter plotted on surface of an unruptured aneurysm and corresponding histogram (Lauric et al. 2011)	12
Figure 7. Comparison of convex hull (light grey), Voronoi diagram core (red), and aneurysm (dark grey) surfaces. (Piccinelli et al. 2012)	13
Figure 8. Visual demonstration of the data preparation protocol. The aneurysm geometry was first obtained as a segmented surface model (top left). The parent vessel was reconstructed, blue, from the segmented surface model, grey (top right). The surface meshes were optimized using triangular elements with the VMTK surface re-meshing algorithm (middle left). The aneurysm was next isolated using a planar isolation (middle right). The aneurysm was then isolated using a non-planar isolation, red, utilizing the parent vessel reconstruction, blue (bottom left). The dome, blue, was then isolated from the ostium, red, on both models (bottom right)	20
Figure 9. Planar isolation volume (red) overlaid on aneurysm geometry (gray) on left, non-planar isolation (red) overlaid with parent vessel reconstruction (blue) on parent vasculature (gray) in middle, and Voronoi diagram core volume (red) overlaid on parent vasculature (gray) on right	22
Figure 10. Different definitions for the measurement of cerebral aneurysm height	23
Figure 11. Different definitions for the measurement of diameter (black) overlaid on the corresponding measurements of height (gray)	24
Figure 12. ND_{avg} is calculated using the average distance from the ostium centroid (black circle) to the ostium boundary (grey line). $ND_{hydraulic}$ is calculated from the area of the ostium (blue)	25
Figure 13. Demonstration of vessel diameter, VD , with the maximum inscribed spheres, red, and centerline, blue, of a terminal (left) and lateral aneurysm (right)	25

Figure 14. Illustration of the derivation of bottleneck factor metrics. BF_{area} (left) uses a planar ostium, red plane, medial axis, red line, and its perpendicular max contour, blue line. BF (right) uses the maximum height, red dot, from the planar ostium, red plane, and its parallel max contour, blue line. 27

Figure 15. Largest maximally inscribed sphere (blue) and non-planar ostium (red)..... 29

Figure 16. Parent vessel (light blue), non-planar convex hull (grey), non-planar ostium (red), and largest maximally-inscribed sphere of the non-planar convex hull (dark blue) 30

Figure 17. Planar isolation of an aneurysm (red) with convex hull overlaid (grey). 31

Figure 18. Planar ostium (red), sac unit vector (green), vessel centerline (blue), and vessel unit vector (yellow). 33

Figure 19. ESDI uses measurements for the volume of the aneurysm geometry (grey) isolated by the planar ostium (blue) and the non-planar ostium (red). This figure displays front and side views of this hypothetical idealized aneurysm geometry. For this moderately fusiform hypothetical idealized model the ESDI value was 0.22..... 34

Figure 20. The two points of maximum distance and the line between them (green) are found for the aneurysm (grey) isolated by the nonplanar ostium (red plane). A contour perpendicular to the line between the two points of maximum distance is progressed from the first to second point. The contour of largest area (blue) is found. The centroid of that contour is found (red dot). A line passing through that point along the contour is rotated until the two points of maximum distance are found (purple). Finally, a line perpendicular to that line is used to find the two nearest points on the contour (orange). 36

Figure 21. Examples of covariance ellipse (blue) fit to an aneurysm (grey) isolated using a non-planar ostium (red). 38

Figure 22. Demonstration of surface area measurements obtained before (left) and after (right) the introduction of small surface undulations. No volume change was observed despite a 4% change in surface area 40

Figure 23. Demonstration of how two slight differences in cutting plane angle (red and blue) could give a misleading representation of aneurysm size based on surface area alone..... 41

Figure 24. The aneurysm and vasculature is shown in gray, non-planar ostium in blue, and the VDC in red. By increasing the cutoff value of the inclusion radius of the Voronoi spheres from 0% of the largest Voronoi sphere (left), 75% of the largest Voronoi sphere (center), and 99% of the largest Voronoi sphere (right), progressively larger shape features can be smoothed out from the VDC..... 42

Figure 25. Plot of the VDC evolution. The same VDC cutoff values from Figure 24 are demonstrated along the curve.	44
Figure 26. VDC evolution curve for aneurysm (grey in photo, blue on plot) and covariance-fit ellipsoid (red in photo, orange on plot).	45
Figure 27. VDC evolution curves of a spherical shape and a prolate shape with major-to minor-axis ratio of 1.66 to 1.	46
Figure 28. VDC evolution curve of a spherical shape and an otherwise spherical shape with concave irregularities.	47
Figure 29. VDC evolution curve comparison of an ellipsoidal shape (grey), and the same shape with hemispherical concave irregularities (red). In the 3D surface model above the ellipsoidal shape is transparently overlaid onto the ellipsoidal-irregular shape.	48
Figure 30. VDC evolution curve from which ideal sphere AUC of 1.0 (red + orange + blue), covariance-fit ellipsoid AUC (orange + blue), and aneurysm AUC (blue) are calculated.	49
Figure 31. Computational time to isolate aneurysm and calculate morphological indices generally increased with volume.	56
Figure 32. Demonstration of sensitivity of MaxD2 (and MaxD3) to different orientations of the MaxD1 measurement axis caused by a slight change in the ostium.	61
Figure 33. Examples of prescribed morphological changes in hypothetical idealized models. From left to right, the top row contains the models for low, medium and high prescribed height, and the bottom row contains the low, medium and high prescribed concave surface undulation.	63
Figure 34. Plots of the morphological index measurements from hypothetical idealized aneurysm models that modulate the morphological characteristic the index is designed to measure. Plots for Size Ratio, Neck-Sac Size Relation, Irregularity, Non-sphericity, Ellipticity, Prolateness, Oblateness and Fusiformity are normalized to the initial value of each index.	74
Figure 35. Scree plots with parallel analysis of simulated data. Four factors were extracted as a result.	82
Figure 36. Factor diagram. The arrows indicating association between a variable and its underlying factor associate the variable with its factor of highest loading.	84
Figure 37. Biplots showing the alignment of the variables with each factor.	87

Figure 38. Aneurysm with ARang of 4.72 and IRRvdc of 0.36, left; and ARang of 0.6 and IRRvdc of 0.64, right. The increased IRRvdc in the aneurysm with a lower aspect ratio was likely caused by the indentation and sharp-edged regions of the aneurysm geometry near the ostium. 90

Figure 39. Specificity study of EIIms using a spherical hypothetical idealized aneurysm with increasing irregularity (or undulation). Ellipticity should not theoretically increase, while non-sphericity should increase..... 91

Figure 40. Factor diagram using 5 factors. 94

Figure 41. Comparison of observational and treatment groups using marquee morphological indices for automated measurement. EIVdc showed a significant difference between the observational and treatment groups. 104

Figure 42. Comparison of observational and treatment groups using marquee morphological indices for manual measurement. MaxDRatioMagnitude was significantly different between the observational and treatment groups. 105

Figure A.1. Distribution plots of the morphological indices prior to transformation. 118

Figure B.1. Comparison of the results of the analysis by User 1 and User 2. 126

Figure C.1. Renderings of the non-planar ostium (left) and planar ostium (right) from user 1 (red) and user 2 (blue). 129

INTRODUCTION

Cerebral aneurysm

Cerebral aneurysm is a pathology of the arterial wall that is characterized by an outward bulging of the lumen. Approximately 90 percent of all cerebral aneurysms occur in a saccular form (Vega et al. 2002), and more rarely in a fusiform or dissecting manner, as shown in Figure 1. Saccular aneurysms form as a consequence of a weakening of the internal elastic lamina. The exact etiology of any particular cerebral aneurysm's formation varies from case to case. However, hereditary traits (including Marfan syndrome, previous familial occurrence, and female gender) and acquired risk factors (such as age over 50 years, tobacco use, and hypertension) may indicate a higher risk for aneurysm manifestation (Vega et al. 2002).

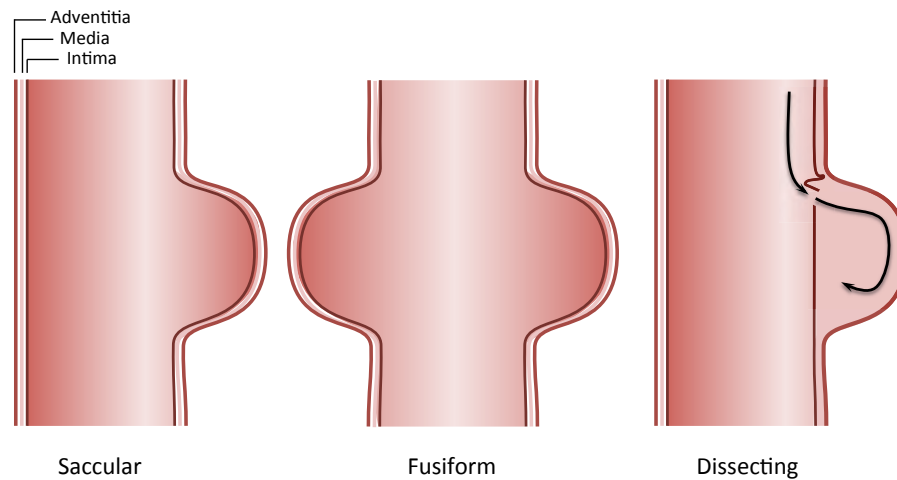


Figure 1. Types of cerebral aneurysms.

Cerebral aneurysm is a relatively common condition with an estimated prevalence of 3.6 to 6 percent in the general population. Aneurysm rupture is a major cause of death and disability. It occurs in approximately 1.9% for those patients presenting with an aneurysm (Rinkel et al. 1998). The risk of short term death from the hemorrhage associated with rupture is high (10 to 20%), and an additional number (12 to 30%) of patients never recover from the initial bleed (Hop et al. 1997).

Treatment options

Traditionally, the most common cerebral aneurysm treatment procedure has been surgical clipping of the aneurysm neck, which involves a craniotomy to access the affected vessel. Complication risk is a concern because of the invasiveness of the surgery. However, given an eligible patient the surgery is generally very effective, with complete occlusion rates reported around 93% (Raftopoulos et al. 2003).

The growing treatment of choice in recent years is endovascular coil embolization. This is an outpatient procedure that has relatively low associated complication risk and a short recovery period. The first endovascular coiling device approved by the FDA for general use was the Guglielmi detachable coil in 1991 (Guglielmi et al. 1991). The International Subarachnoid Aneurysm Trial (ISAT), a European study involving 2,143 patients across 42 neurosurgical centers, found that endovascular coiling provided absolute risk reduction of 6.9% and relative reduction in risk death or dependence of 22.6% over surgical clipping (van den Berg et al. 2003). However, endovascular coiling outcomes are highly dependent on aneurysm sac geometry. Studies have shown that initial treatment and aneurysm sac recanalization and

continued growth occurs in 22-42% of endovascular coil-treated cases (Grunwald et al. 2007; Sluzewski et al. 2003).

Flow diverters are a more recent development for cerebral aneurysm treatment. Arterial stents, such as those used in conjunction with cerebral aneurysm coils or to maintain patency of an atherosclerotic artery had previously been observed to occlude aneurysms by diverting flow away from the aneurysm sac (Wakhloo et al. 1994). Flow diverters take this idea beyond the observation of this phenomenon and bring it to clinical use. A flow diverter's mesh porosity is optimized for use specifically to occlude cerebral aneurysms over time, while maintaining long-term patency of perforating and branching arteries that may be covered by the device. Flow diverters are very new to the market having been approved in mid-2011, and are only indicated for the treatment of large or giant aneurysms located on specific portions of the internal carotid artery (ICA). This, unfortunately, precludes treatment of a large number of patients.

All surgical treatment of the brain carries a large inherent risk. One site-specific study found that as much as many as 25% of surgical clipping patients and 10% of endovascular coiling patients experienced an adverse event (Johnston et al. 2001). For many cerebral aneurysm patients this risk is amplified by their age and co-morbidities. Because 98% of patients will never experience a rupture, only patients with a high risk of rupture will be recommended for surgery. In other patients, for those whom risk of rupture is lower than risk from treatment (Wiebers et al. 2003), the treating physician will recommend that a patient not undergo treatment, and instead return periodically for follow-up observation. These patients will return on a semi-annual or annual basis for

clinical follow-up and image-based evaluation to assess the aneurysm for signs of growth, which might indicate aneurysm instability.

Current prognostic assessment techniques

In order to determine an effective treatment plan for a patient, a physician must first assess a patient's relative likelihood of aneurysm rupture. While it is hypothesized that aneurysm rupture occurs due to a gradual thinning and weakening of the vessel wall this phenomenon is impossible to discern non-invasively because the tissue thickness of an aneurysm dome ranges from 16 to 400 μm (Kadasi et al. 2012), well below the resolution of modern medical imaging modalities. Furthermore, because even the thickest tissue in this range is on the order of only one voxel with standard computed tomography (CT) and magnetic resonance imaging (MRI), which are conventional medical imaging techniques; therefore, it is unlikely that any information about the thickness of an aneurysm sac can be measured in-vivo. This is a limitation in evaluating aneurysm rupture risk in large clinical studies (Ramachandran et al. 2016).

The only large-scale, prospective longitudinal study to evaluate cerebral aneurysm rupture risk is the International Study of Unruptured Intracranial Aneurysms (ISUIA), which indicated that rupture risk increases with size, and therefore suggests aneurysms larger than 10mm should be treated (Wiebers et al. 2003). The ISUIA study also found that aneurysms in the posterior vasculature of the brain are more likely to rupture than those in other locations. For aneurysms smaller than the 10mm threshold and outside the posterior communication, there is a smaller chance of rupture than larger aneurysms, but ruptures do occur, and there is very little known about what factors contribute to rupture

in these aneurysms. As a result, there is a lack of consensus in the field, and there is a great range of strategies neurosurgeons employ to assess rupture risk with small aneurysms.

One study sought to characterize the factors that physicians take into account when determining treatment decisions, and found that physicians view size, irregular and elongated geometry, vessel location, growth over time, de novo formation and contralateral steno-occlusive vessel disease as factors that are thought to be important in determining the risk of aneurysm rupture risk (Etminan et al. 2014). However, this study merely reveals neurosurgeons' opinions formed from their own experiences, which form the current basis for treatment. Further scientific research into markers that identify high-risk aneurysms could improve outcomes for patients who would otherwise not be treated, and allow doctors to avoid performing invasive cranial surgery for those patients who do not need it.

Current research on the determination of rupture risk from medical images

While the ISUIA study is currently the only large study that has sought to determine the indicators of rupture risk, it is clear that there is more to learn about the risk factors for aneurysms outside the highest-risk categories determined by ISUIA. Although ISUIA concluded that large aneurysms and aneurysms on the posterior circulation present the highest risk of rupture, many small aneurysms on other areas of circulation do rupture as well (Raghavan et al. 2005; Dhar et al. 2008). Therefore, researchers have focused on determining aneurysm rupture indicators from medical image analysis. Some research groups have performed computational fluid simulations on the arterial models obtained

from patient scans (Sforza et al. 2009; Cebal et al. 2009; Cebal et al. 2011; Retarekar et al. 2014). However, because of the lack of patient-specific information for fluid inlet parameters and material properties, some have argued that these simulations are purely reflective of the shape of the arterial models (Ramachandran et al. 2016; Retarekar et al. 2014). In order to analyze large datasets, it would therefore be ideal to reduce the complexity of the analysis by simply reducing it to a direct analysis of the morphology of the aneurysm and its surrounding vasculature. Analyzing the morphology of aneurysm sacs in isolation from the vasculature could also give insight into bulging of weakened tissue, continued growth, or other factors that could contribute to increased rupture propensity.

Many research groups have found differences in various morphological factors between ruptured and unruptured aneurysms. Many of these studies have followed a similar format in which a novel morphological index or set of indices is introduced, which are then compared between a small subset of ruptured and unruptured aneurysms. This type of study is quick to perform and gives some insight into whether there may be morphological differences between ruptured and unruptured aneurysms.

In 2005 Raghavan et al. introduced novel morphological indices and found that several of them stratified a small population of ruptured and unruptured aneurysms. Undulation Index (UI) was introduced as a descriptor of the undulation present in the dome of the aneurysm. It is computed by comparing the volume of the aneurysm to the volume of its convex hull (a similar geometry from which the concavities are removed). The thinking is that these undulations could represent stress concentrations and weakened inhomogeneous regions within the aneurysm dome; therefore, their presence could be an

indicator of increased rupture risk. Raghavan et al. also introduced Aspect Ratio (AR) as an index to describe the ratio of the aneurysm neck to its height as measured perpendicularly from the neck plane (Ujiie et al. 2001). This was intended as one measure of an aneurysm's similarity of a shape to an elliptical geometry, which would indicate an inhomogeneous stress distribution leading to generally higher peak stresses than a spherical geometry. Therefore, more elliptical aneurysms are thought to be prone to rupture. Ellipticity Index (EI) was introduced as another index seeking to measure the ellipticity of an aneurysm. It was measured from a ratio of the surface area to the volume, for which a hemisphere would produce a value of 0, and an elliptically shaped aneurysm would produce an indicial value near 1. Non-sphericity Index (NSI) was introduced to describe the overall deviation from a hemispherical geometry. Similar to EI it was measured from a ratio of surface area to volume, but differed in that these values were calculated from the aneurysm geometry directly. In this way, it combined non-spherical characteristics from elliptical shape as well as surface undulation. Conicity parameter (CP) was introduced to describe a potential measure of the location of growth of an aneurysm. The location of the cross-section of largest diameter was compared to the midpoint from the neck to the maximal height. In this way if an aneurysm's largest cross section was located near to the neck, the growth would be assumed to be near to the neck; if the cross section were located near the top of the dome, the growth would be assumed to be near the top of the dome. Bottleneck factor (BF) was introduced as a potential indicator for increased hemodynamic abnormalities. It was calculated as the ratio of the maximum diameter of the aneurysm to the diameter of the neck. The surface curvature-based indices Mean Curvature Norm (MLN) and Gaussian Curvature Norm (GLN) were

also introduced. A study of 9 ruptured and 18 unruptured aneurysms found NSI, UI, EI, AR, and MLN values to be significantly different between the ruptured and unruptured groups.








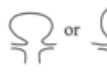


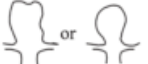



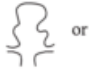



Shape Index	Low	Medium	High
Undulation index (UI)			
Aspect ratio (AR)			
Ellipticity index (EI)			
Non-sphericity index (NSI)			
Conicity parameter (CP)			
Bottleneck factor (BF)			

Figure 2. Definitions of Raghavan et al. shape indices (Raghavan et al. 2005).

In 2007 Millán et al. demonstrated the use of geometric and Zernike moment invariants to characterize the geometry of aneurysms. A database of 31 ruptured and 24 unruptured aneurysms was examined. It was shown that the Zernike moment invariants were able to classify ruptured and unruptured aneurysms (given the particular training set) with an accuracy of approximately 80%.

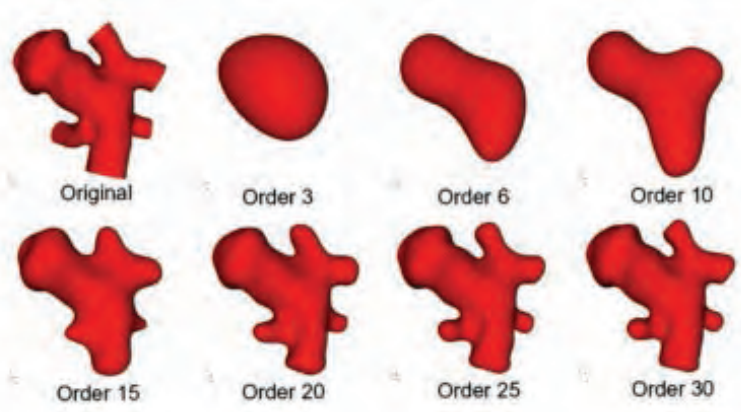


Figure 3. Example of a reconstruction of an aneurysm surface model using increasing orders of Zernike moments (Millán et al. 2007).

In 2008 Dhar et al. introduced vessel angle (the angle between the afferent vessel and the aneurysm clipping plane), aneurysm angle (the angle between the neck plane and the vector point from the center of the neck to the point of maximum height), and aneurysm-to-vessel size ratio. Differences in the morphology values between ruptured and unruptured aneurysms were statistically significant not only for aneurysm angle and size ratio, but also undulation index, non-sphericity index, ellipticity index, and aspect ratio. In 2010 the same research group published the results of prospective studies that again found size ratio to correlate with rupture status (Rahman 2010).

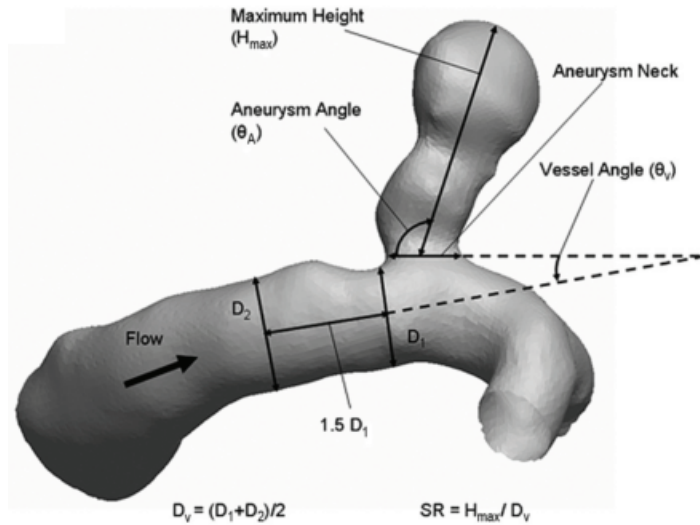


Figure 4. Illustration of vessel angle and aneurysm angle (Dhar et al. 2008).

In 2009 Piccinelli et al. introduced and demonstrated methods for characterizing the geometric analysis of vasculature with application to cerebral aneurysms (Piccinelli et al. 2009). An entire computational framework was built around the Vascular Modeling Toolkit (VMTK) (Antiga et al. 2008) to compute characteristics of a vessel centerline such as tube function, curvature, torsion, tortuosity, and bifurcation angle. A study was published in 2011 that analyzed the geometry of the internal carotid artery (ICA) of 17 ruptured and 37 unruptured aneurysms. The vessel geometry metrics curvature, torsion, length, and radius for each ICA bend and aneurysm position and orientation with respect to the parent vessel, angles between portions of the parent artery afferent and efferent to the aneurysm and to the aneurysm ostium were measured. Many of these metrics demonstrated statistically significant differences between the ruptured and un-ruptured aneurysm groups (Piccinelli et al. 2011).

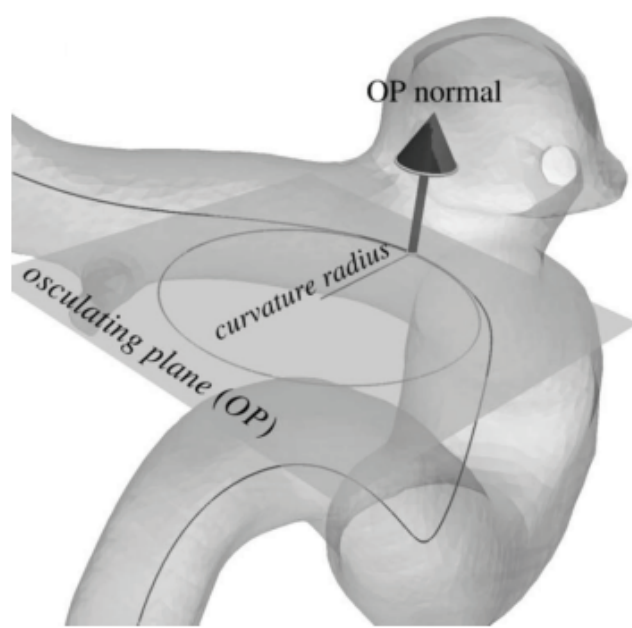


Figure 5. Definition of vessel centerline curvature using the osculating plane and osculating circle tangent to the curve (Piccinelli et al. 2011).

In 2011 Yasuda et al. introduced a metric of the aneurysm volume-to-ostium area ratio. The values of this metric were compared between groups of 62 ruptured and 93 unruptured aneurysms (Yasuda et al. 2011). Later that year Ryu et al. also published a study that evaluated the metric in 105 ruptured and 109 unruptured aneurysms. Both groups found that the trait was significantly higher in ruptured aneurysms than unruptured aneurysms (Ryu et al. 2011).

In 2011 Lauric et al. described a method for shape characterization called the centroid-radii model. The centroid-radii model computes the distance from an aneurysm model's centroid to the points on its surface mesh, and subsequently computes the entropy of the histogram of the normalized radii. A subsequent study of 73 ruptured and 81 unruptured aneurysms also found a significantly higher entropy value for ruptured aneurysms.

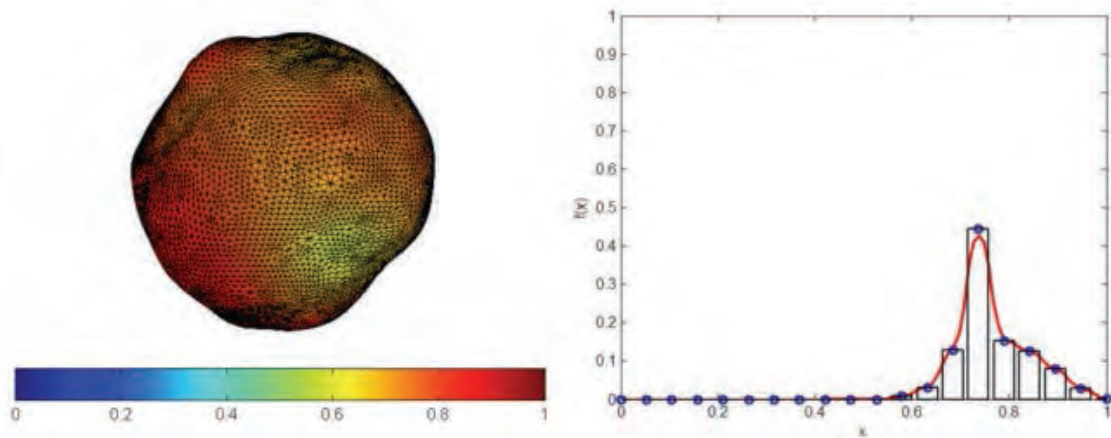


Figure 6. Normalized centroid radii model parameter plotted on surface of an unruptured aneurysm and corresponding histogram (Lauric et al. 2011).

In 2012 Piccinelli et al. explored several novel methods for computationally obtaining measurements from aneurysm sacs, including the introduction of the Voronoi diagram core – a hypothetical representation of the largest and most stable portions of the aneurysm sac, a centerline-based sac diameter measurement, and best-fit ellipsoid. This study utilized a subset of the Aneurisk database. The Aneurisk database was a project carried out from 2005-2008 in order to develop tools for the biomechanical and morphological analysis of cerebral aneurysms. It contains data from 153 consecutive patients who underwent 3D rotational angiogram (3DRA) at Niguardia Hospital in Milan, Italy between 2002 and 2006 (Piccinelli et al. 2012).

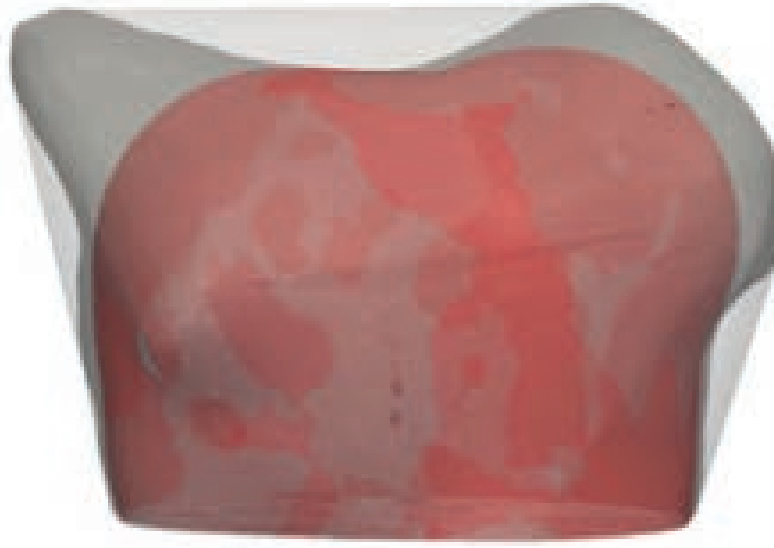


Figure 7. Comparison of convex hull (light grey), Voronoi diagram core (red), and aneurysm (dark grey) surfaces. (Piccinelli et al. 2012)

These studies have each examined a different morphological metric and demonstrated a difference in shape between ruptured and unruptured aneurysms. But while they do indicate that there is a discernible difference in shape between the two groups, they do not demonstrate the predictive ability of morphology as an indicator of rupture. The primary reason why these case-control type studies do not elucidate this predictive ability is because the time point of shape change in the aneurysm's development is unknown. They give no indication of whether this difference in morphology would be present early in the aneurysm's development and be visible at the time of diagnosis, whether it would appear very late in the aneurysm's development just prior to rupture, or whether morphological features appear only after rupture occurs. There is some evidence that there is not a morphological difference pre- and post-rupture, although there is not a strong consensus in the field (Kataoka et al. 2000). Because it is

very unlikely that an aneurysm would be imaged immediately prior to rupture this is likely to remain unknown outside of a few anecdotal cases.

The ultimate goal of aneurysm researchers is ultimately not simply to determine if aneurysm morphology is different in patients that ruptured, but rather to determine if, at an earlier time point, physicians could discern whether an aneurysm is benign or likely to go on to rupture. Longitudinal cohort studies, like the ISUIA study, directly measure the prognostic ability of biomarkers such as aneurysm morphology. However, because of the amount of time and the large cohorts needed to see disease presence, no large studies have been performed to study aneurysm morphology.

In a study much smaller than the ISUIA, Ramachandran et al. published a study that followed 198 aneurysms in a longitudinal cohort and examined morphology as an indicator of rupture risk (Ramachandran et al. 2016). It found that the morphological indices were not different between the group of aneurysms that grew and the group of aneurysms that did not grow. None ruptured. While this study is on too small of a scale to draw any sweeping conclusions about the predictive ability of morphology, it does give an indication that if there is any morphological difference between rupture resistant and rupture-prone aneurysms it may be subtle, or it is in morphological traits that were not measured. Researchers therefore must be careful to observe the morphological features that are present in aneurysms, and that the morphological indices that we use to observe these morphological features must be sensitive enough to discern a difference. This is especially important when studying the mainly small aneurysms that are placed under observational follow-up. It is also possible that physicians are already selecting aneurysms with these particular morphologies for treatment, which was an exclusionary

criteria for the Ramachandran et al. study. A study published by Etminan et al. suggests that physicians do already look at morphology as an indicator of rupture risk, and that this selection preference likely varies by clinical site (Etminan et al. 2014). If physicians do, in fact, select aneurysms with certain morphological traits for treatment, then the morphological features of the study populations of untreated aneurysms could differ from the full population of aneurysms that doctors would see at diagnosis. A measurement of this selection bias would be helpful in constructing future studies.

Objectives

The current state of research on aneurysm rupture risk assessment from medical images lacks a minimal set of physically meaningful, independent metrics that exhaustively describe the aneurysm morphology. Development of such a set of metrics requires that the myriad collection of morphological indices reported in the literature and any newly developed metrics are consolidated into a single collection, and assessed for robustness and common variance in a single study population database. Future studies that aim to evaluate hypotheses relating to the role of aneurysm morphology in clinical outcome (be that rupture or treatment complication) may then use these metrics. This precisely, is the overall goal of this project accomplished through three specific aims.

Specific aim 1 is the development of the ability to exhaustively quantify the aneurysm morphology. To that end, the aim is to a) consolidate and categorize all the reported metrics in the literature and develop new metrics where needed, in order to quantify all relevant morphological features; and b) develop algorithms for computing all these morphological metrics.

Specific aim 2 is to identify an optimal collection of meaningful metrics to describe aneurysm morphology. To that end, the aim is to use idealized aneurysm models for a sensitivity analysis, user variability studies and patient-specific aneurysm models from two large study populations totaling N=286 subjects to a) identify the metrics that best capture specific morphological features; and b) to employ statistical techniques to ascertain the features and their respective metrics that most uniquely describe the largest amount of variance among the relevant patient populations of unruptured cerebral aneurysms.

Specific aim 3 is to demonstrate the use of the optimal collection of metrics in testing clinically relevant hypotheses on the role of aneurysm morphology. Specifically, to test the hypotheses that the morphological characteristics of aneurysms that are chosen for treatment differ from those that are chosen for untreated observation – the so-called selection bias – in a human subjects population.

SPECIFIC AIM 1:

DEVELOPMENT OF ALL MORPHOLOGICAL INDICES

Morphological indices are metrics that quantify the measure of a morphological feature. A morphological index may be dimensional or non-dimensional, and it is intended to be utilized for comparative means among a set of geometric data. In applying this concept to aneurysm morphology the morphological indices are developed to describe morphological characteristics that potentially have implications on the fluid dynamics, wall tension, or shape features that indicate propensity for aneurysm growth or rupture.

Methods for obtaining geometric data

Diagnostic imaging for cerebral aneurysms is generally obtained at the time of original diagnosis. Because diagnosis is mainly incidental, the modality of the images can be diverse. Depending on the size, location and quality of the diagnostic scan, a follow-up scan may be performed. The modalities of these images include Computed Tomography Angiography (CTA), Contrast-Enhanced Magnetic Resonance Angiography (CE-MRA), Time-of-Flight Magnetic Resonance Angiography (ToF-MRA), and 3D rotational angiography (3DRA). The resolution in these images typically ranges from 0.4 to 0.6mm in CT and MRA to 0.2mm in 3DRA (Ramachandran et al. 2016; Larrabide et al. 2011). In order to obtain a 3D aneurysm geometry from these images they are generally segmented using semi-automated methods. Once the aneurysm and its contiguous vasculature is segmented from the image, a surface mesh is created from the

segmentation boundary (Antiga et al. 2008). The aneurysm geometry is then isolated from the contiguous vasculature using a planar or non-planar isolation scheme.

Geometric data preparation protocol

The following studies utilized pre-segmented data and focused on aneurysm isolation techniques and morphological analyses. The algorithms described were programmed in Python 2.7, and they utilized the VMTK 1.2 and VTK 5.10 libraries (Schroeder et al. 2006; Antiga 2002). The following protocol, demonstrated in Figure 8, was used in order to prepare a given aneurysm geometry in a consistent manner:

1. First, a pre-segmented model of a patient's aneurysm and contiguous vasculature should be obtained. The model should be a surface model composed of triangular elements. It should contain enough upstream and downstream contiguous vasculature to successfully perform the following steps. If it does not contain enough contiguous vasculature, it should be excluded from the study.
2. Second, the aneurysm should be digitally removed from the surface model to obtain a parent vessel reconstruction (Ford et al. 2009). This process should utilize the code included as part of the VMTK Apps.
3. The aneurysm parent vessel reconstruction and the original surface model should both be re-meshed and optimized using triangular elements.
4. The aneurysm should be isolated from the parent vessel using the automatic clipping plane technique (Piccinelli et al. 2012). If the automated clipping plane isolation fails due to algorithmic error the clipping plane should be manually placed by an expert user.

5. The aneurysm should also be isolated from the parent vessel using a non-planar technique. This technique should be similar to the approach outlined by Berkowitz 2012. However, instead of performing a direct Boolean operation of the mesh, a Boolean operation should instead be performed by converting the Voronoi diagram polyballs to image space, performing a Boolean subtraction in image space, and converting the resulting isolated aneurysm back to a surface mesh from image space.
6. The ostium and dome of both planar and non-planar isolated aneurysm geometries should be delineated.

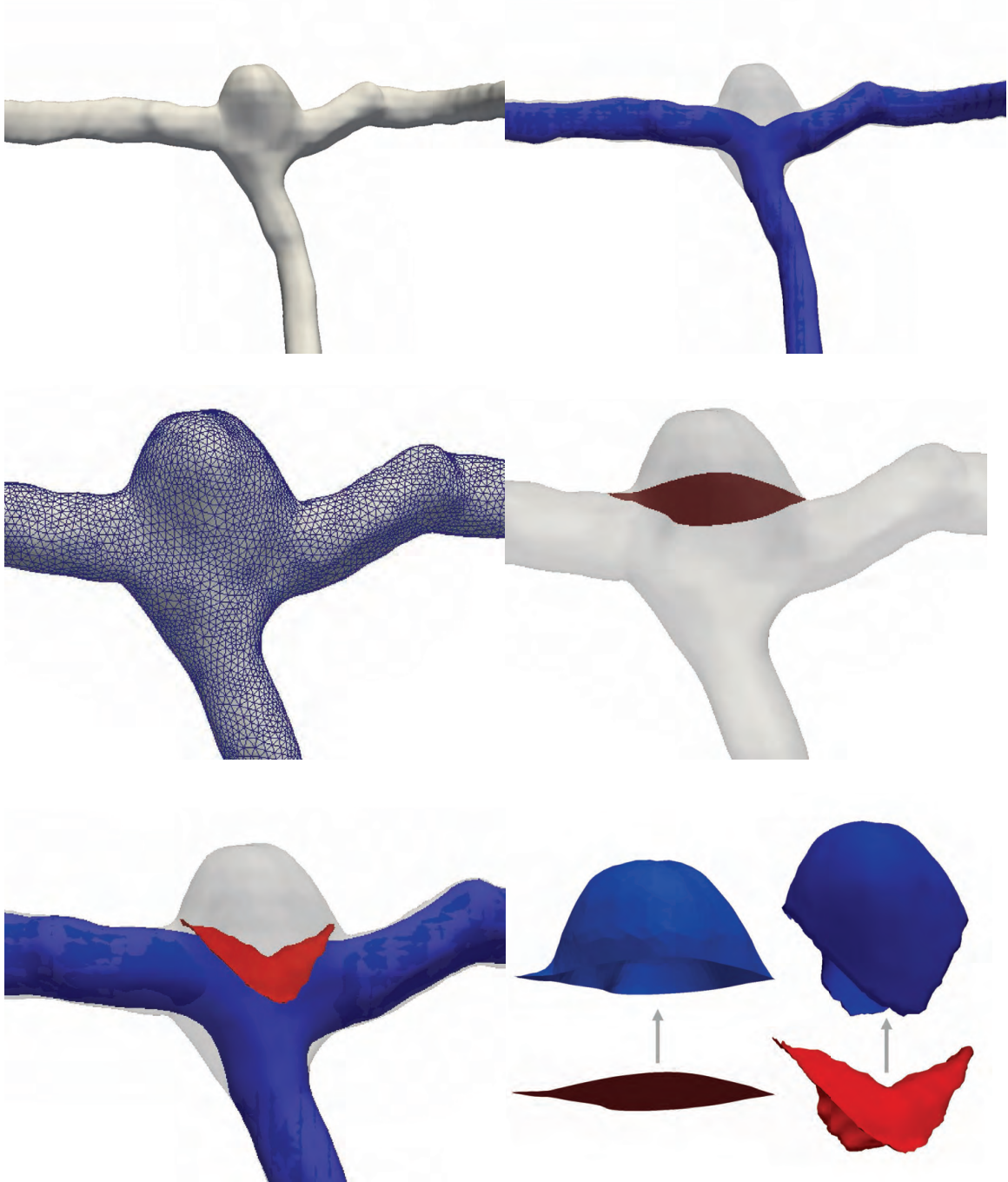


Figure 8. Visual demonstration of the data preparation protocol. The aneurysm geometry was first obtained as a segmented surface model (top left). The parent vessel was reconstructed, blue, from the segmented surface model, grey (top right). The surface meshes were optimized using triangular elements with the VMTK surface re-meshing algorithm (middle left). The aneurysm was next isolated using a planar isolation (middle right). The aneurysm was then isolated using a non-planar isolation, red, utilizing the

parent vessel reconstruction, blue (bottom left). The dome, blue, was then isolated from the ostium, red, on both models (bottom right).

After the aneurysm geometry was obtained via the protocol, a set of morphological indices was automatically measured by novel software that was developed for the purpose of this dissertation. This set of morphological indices contained a large portion of the morphological indices described in the literature. After a gestalt assessment of the remaining shape characteristics of cerebral aneurysms that had not yet been described in the literature several novel morphological indices were also developed. The non-planar isolation method more fully captures aneurysm geometry, especially in partially fusiform and terminal aneurysms; therefore, whenever possible the non-planar isolation method was utilized for the definition of the morphological indices.

Morphological indices from literature

Volume

Aneurysm volume is commonly assessed in the literature (Raghavan et al. 2005; Ryu et al. 2011; Ramachandran et al. 2016). In this study, three volume measurements were taken from each aneurysm geometry. First, denoted as V , was the volume of the planar isolation of the aneurysm geometry in mm^3 . Second, denoted as V_{np} , was the volume of the non-planar isolation of the aneurysm geometry in mm^3 . Third, denoted as V_{vdc} , was the volume of the Voronoi Diagram Core (VDC) in mm^3 (Piccinelli et al. 2012). It should be noted that in this instance the VDC was taken of the non-planar isolation of the aneurysm geometry in order to more fully capture the aneurysm's full volume in cases of fusiform or terminal aneurysms.

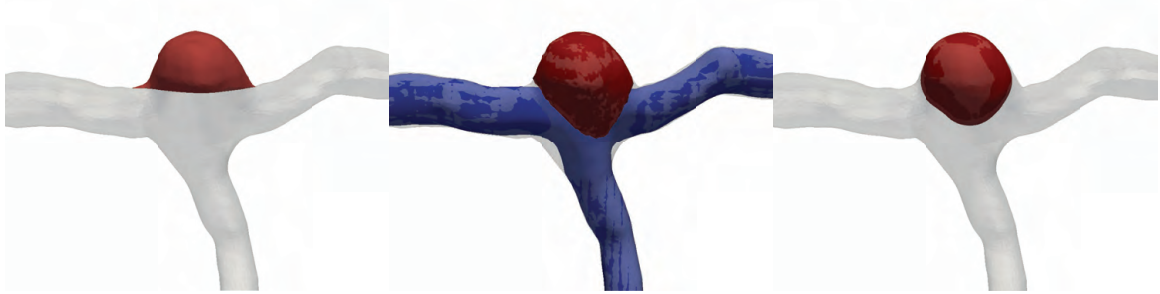


Figure 9. Planar isolation volume (red) overlaid on aneurysm geometry (gray) on left, non-planar isolation (red) overlaid with parent vessel reconstruction (blue) on parent vasculature (gray) in middle, and Voronoi diagram core volume (red) overlaid on parent vasculature (gray) on right.

Height

The height of an aneurysm has been used in the literature to describe the dimension of an aneurysm that is generally measured from the ostium to the top of the aneurysm dome. Raghavan et al., for example, defined height measurement as the maximum perpendicular distance from the ostium plane to the point of intersection with the dome (Raghavan et al. 2005). Piccinelli et al. defined height as the distance from the center of the ostium, along the medial axis of the aneurysm sac, plus the last maximal inscribed sphere radius of the centerline (Piccinelli et al. 2012). This method would hypothetically capture height from shape features that could be missed by the Raghavan et al. definition, but it is not as easily derived from an angiographic measurement in the clinic. Dhar et al. proposed an alternative definition as the straight-line distance from the ostium center to the furthest point on the surface of the aneurysm dome (Dhar et al. 2008). For this work, Raghavan et al. definition will be referred to as H_{perp} , the Piccinelli et al. definition will be referred to as H_{med} , and the Dhar et al. definition will be referred to as H_{ang} . The differences between the definitions is illustrated in Figure 10.

The quantity H_{perp} was computed using the planar isolation of the aneurysm, and the quantities H_{med} and H_{ang} were computed using the non-planar isolation of the aneurysm.

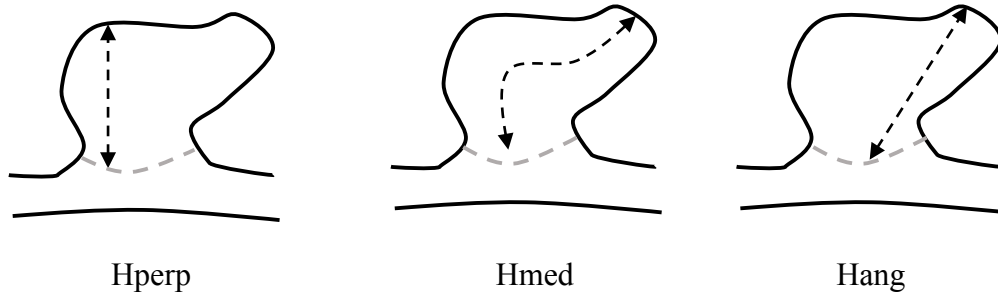


Figure 10. Different definitions for the measurement of cerebral aneurysm height.

Diameter

Diameter in the literature is often described as the dimension of the aneurysm perpendicular to the height. The same three definitions of height as defined above also define corresponding definitions of height. Raghavan et al. define diameter by extracting the cross-section of largest area parallel to the planar ostium, and using the hydraulic diameter $D = 4A/P$, where A is the area of the largest cross-section, and P is the perimeter of the largest cross-section, to estimate the aneurysm diameter (Raghavan et al. 2005). Dhar et al. do not define diameter with relation to their H_{ang} metric, however for consistency in this work D_{ang} will be defined as the hydraulic diameter of the cross-section of largest area that is perpendicular to the axis of measurement H_{ang} . Similarly, Piccinelli et al. do not define diameter with relation to their H_{med} metric, however for consistency in this work D_{med} will be defined as the hydraulic diameter of the cross-

section of largest area that is perpendicular to the medial axis of measurement H_{med} , as shown in Figure 11.

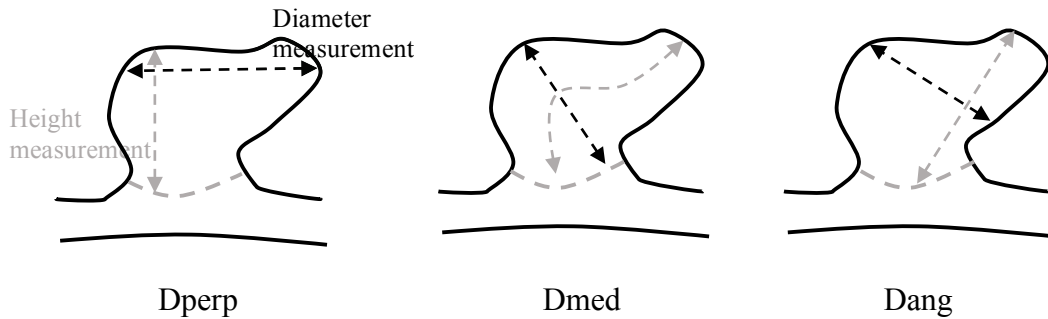


Figure 11. Different definitions for the measurement of diameter (black) overlaid on the corresponding measurements of height (gray).

Neck Diameter

The neck diameter of an aneurysm is a one-dimensional measurement of the ostium. Raghavan et al. proposed neck diameter, here referred to as $ND_{hydraulic}$, that is defined as the hydraulic diameter of the planar ostium. In order to accommodate for a non-planar ostium, a measurement method similar to that proposed by Dhar et al. was used in which the value ND_{avg} was calculated as twice the average distance from the ostium centroid to each point on the ostium edge (Dhar et al. 2008).

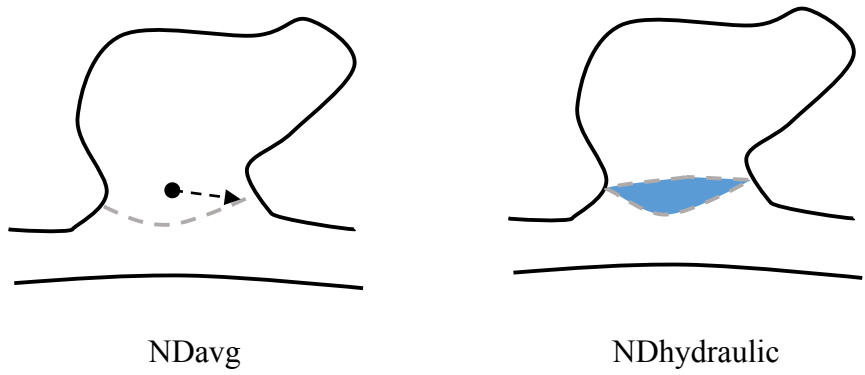


Figure 12. ND_{avg} is calculated using the average distance from the ostium centroid (black circle) to the ostium boundary (grey line). $ND_{hydraulic}$ is calculated from the area of the ostium (blue).

Vessel Diameter

Piccinelli et al. proposed a method for the measurement of vessel diameter, here defined as VD , as shown in Figure 13, in which the average maximum-inscribed sphere diameter along the centerline at each clipping point was measured (Ford et al. 2009).

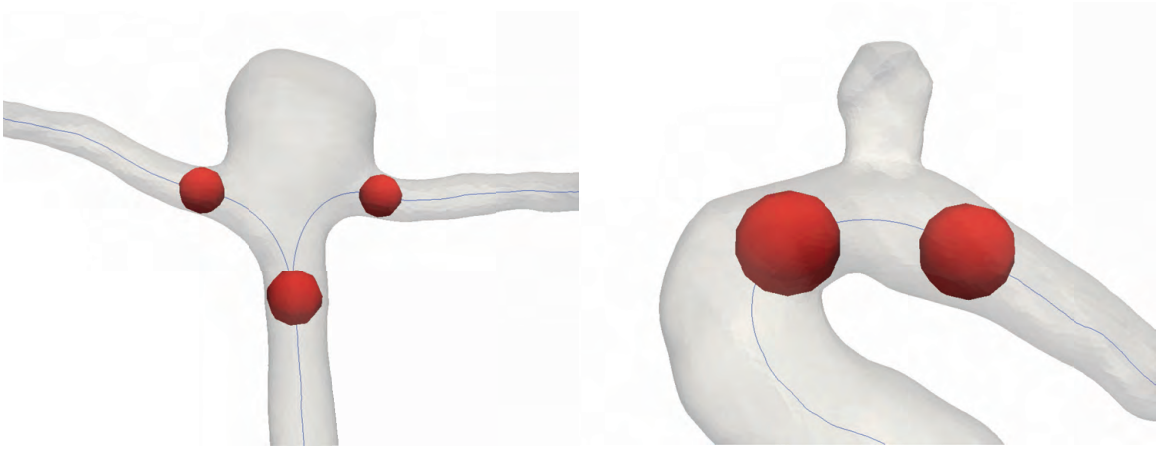


Figure 13. Demonstration of vessel diameter, VD , with the maximum inscribed spheres, red, and centerline, blue, of a terminal (left) and lateral aneurysm (right)

Size Ratio

Size ratio was proposed by Dhar et al. as the ratio of aneurysm height to vessel diameter, VD (Dhar et al. 2008). Piccinelli et al. proposed an alternate definition for size ratio using Hmed (Piccinelli et al. 2012). In regards to this work, size ratio was defined using Hperp, Hmed and Hang. These correspond, respectively, to the quantities Srperp, SRmed and SRang.

Aspect Ratio

Aspect ratio was first proposed by Ujiie et al. as the ratio between the aneurysm height to aneurysm neck width (Ujiie et al. 2001). Raghavan et al. further refined the definition using perpendicular height, Hperp, and the planar neck diameter. (Raghavan et al. 2005). Piccinelli et al. proposed an alternative definition in which aspect ratio was defined using the measurement of Hmed as a height measurement (Piccinelli et al. 2012). Additionally, this work proposes a third definition for aspect ratio in which the measurement of Hang is used as the height measurement. Therefore, ARperp is defined as the ratio of Hperp to NDhydraulic, ARmed is defined as the ratio of Hmed to NDavg, and ARang is defined as the ratio of Hang to NDavg.

Bottleneck Factor

Bottleneck factor was first proposed by Raghavan et al., and referred to here as BF, as the ratio between the diameter of an aneurysm sac and its planar ostium (Raghavan et al. 2005). Piccinelli et al. proposed an alternative definition, here referred to as BFarea, in which bottleneck factor was defined using the ratio of the area of the largest cross section perpendicular to the medial axis, to the area of the planar ostium (Piccinelli et al. 2012). BF and BFarea are illustrated in Figure 14.

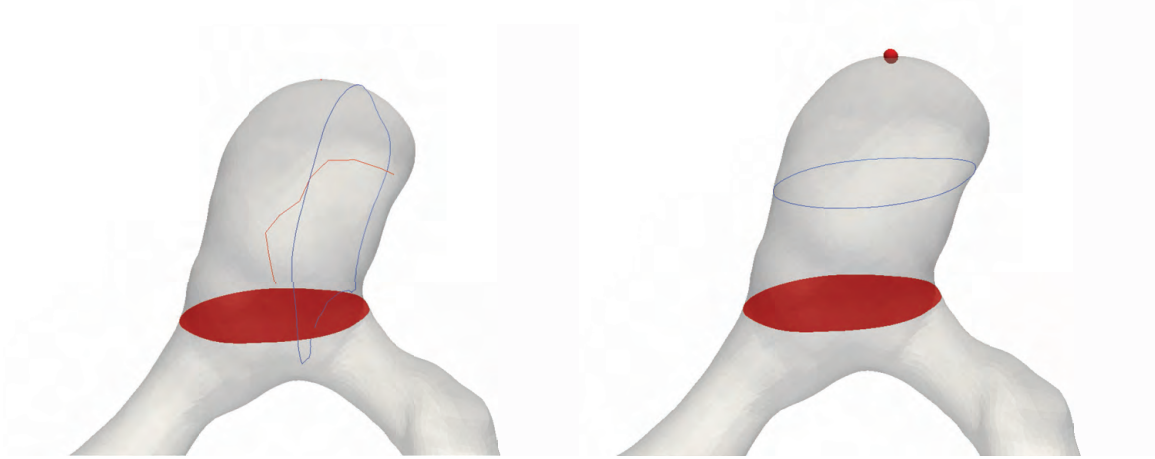


Figure 14. Illustration of the derivation of bottleneck factor metrics. BFarea (left) uses a planar ostium, red plane, medial axis, red line, and its perpendicular max contour, blue line. BF (right) uses the maximum height, red dot, from the planar ostium, red plane, and its parallel max contour, blue line.

Bulge Location

Bulge location, sometimes referred to as conicity parameter, was first defined by Raghavan et al. as the quantity $0.5 - \frac{H_b}{H_{perp}}$, where H_b is the distance perpendicular from the planar ostium to the largest cross-section. In order to avoid negative values, the bulge location, Blperp, is defined as simply the ratio of H_b to H_{perp} . Similarly, metrics Blang and Blmed were defined using the angled height, H_{ang} , and the medial-axis height, H_{med} , respectively.

Centroid-Radii Model Normalized Entropy

The centroid-radii model was proposed by Lauric et al. in order to describe the shape of an aneurysm (Lauric et al. 2011). It quantifies the entropy of the probability density function of the distances from the aneurysm's centroid to each point on its surface. The distances are either normalized or non-normalized. This work will utilize the entropy of the normalized centroid-radii model, Crhnorm.

Non-Sphericity Index

Non-sphericity index (NSI) was proposed by Raghavan et al. in order to describe the deviations of an aneurysm from a spherical shape (Raghavan et al. 2005). These deviations were based on the principle that aneurysms were most often similar to hemispherical shapes, and related the surface area-to-volume ratio of the aneurysm to that of a perfect hemisphere. However, a truly saccular aneurysm would be more similar to a perfect sphere, and would therefore have a higher NSI value under this definition than a hemisphere. To address this, definitions for both non-sphericity, $NSI_{36} = 1 - (36\pi)^{1/3} \frac{V^{2/3}}{S_{np}}$ where V is the volume of the aneurysm and S_{np} is the surface area of the non-planar isolation, and non-hemisphericity, $NSI_{18} = 1 - (18\pi)^{1/3} \frac{V^{2/3}}{S_{dome}}$ where S_{dome} is the surface area of the aneurysm dome, were utilized in this work.

An alternate definition for NSI was proposed by Berkowitz, in which the volume of the largest maximally-inscribed sphere, V_{lmis} , is compared to the volume of the non-planar isolated aneurysm, V_{np} (Berkowitz 2012). It is defined as $NSI_{lmis} = 1 - \frac{V_{lmis}}{V_{np}}$ and is illustrated in Figure 15.

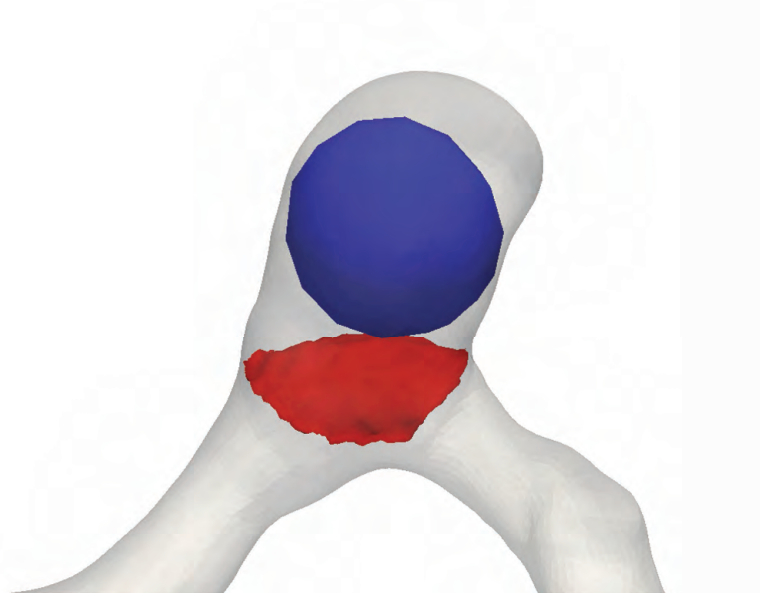


Figure 15. Largest maximally inscribed sphere (blue) and non-planar ostium (red).

Ellipticity Index

Ellipticity index (EI) was proposed by Raghavan et al. and is similar to NSI in that it describes the deviations of an aneurysm from a spherical shape, but by utilizing a convex hull it removes all concavities and only measures convex deviations from a spherical shape (Raghavan et al. 2005). Again in this work it was defined for both non-spherical ellipticity, $EI36 = 1 - (36\pi)^{1/3} \frac{V_{ch}^{2/3}}{S_{ch}}$ where V_{ch} is the volume of the convex hull of the planar isolated aneurysm, and S_{ch} is the surface area of the convex hull of the planar aneurysm; and non-hemispherical ellipticity, $EI18 = 1 - (18\pi)^{1/3} \frac{V_{ch}^{2/3}}{S_{chdome}}$ where S_{chdome} is the surface area of the dome of the convex hull of the planar aneurysm.

An alternate definition for EI was proposed by Berkowitz, in which the volume of the convex hull of the non-planar aneurysm, V_{ch} , is compared to its largest maximally-inscribed sphere, V_{chlmis} , and the non-planar isolated aneurysm, V_{np} (Berkowitz 2012).

It is defined as $Ellmis = 1 - \frac{V_{chlmis}}{V_{ch}}$. This alternative definition by Berkowitz is illustrated in Figure 16.

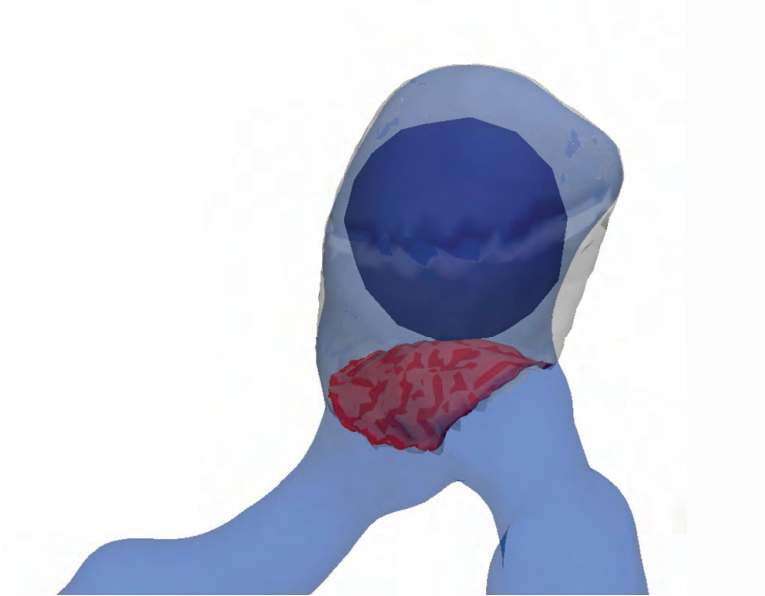


Figure 16. Parent vessel (light blue), non-planar convex hull (grey), non-planar ostium (red), and largest maximally-inscribed sphere of the non-planar convex hull (dark blue)

Undulation Index

Undulation index (UI) was proposed by Raghavan et al. to characterize irregularities in an aneurysm (Raghavan et al. 2005). It is defined as $UI = 1 - \frac{V}{V_{ch}}$, where V is the volume of the planar-isolated aneurysm and V_{ch} is the volume of the convex hull of the planar-isolated aneurysm.

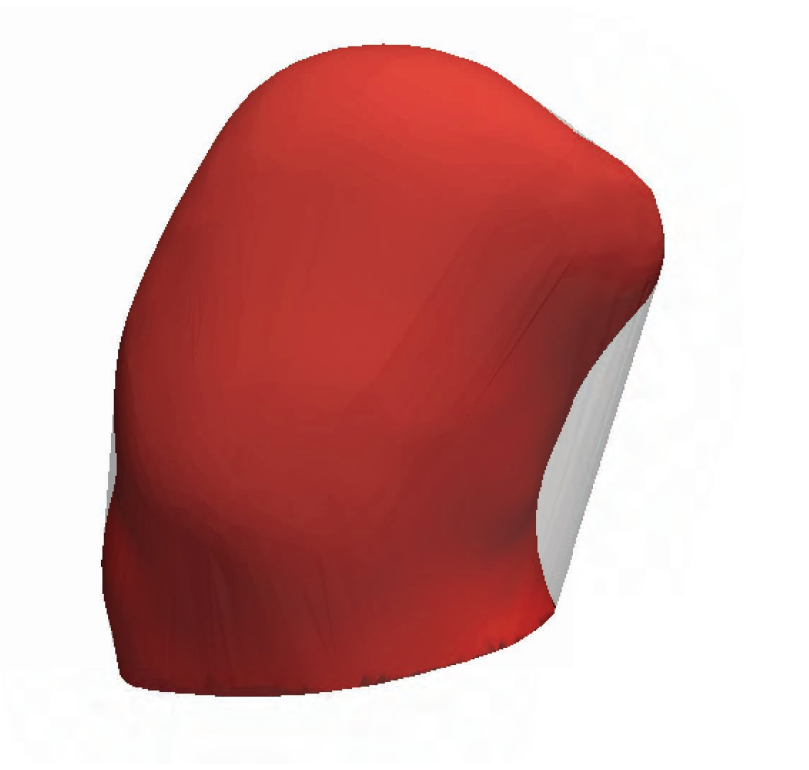


Figure 17. Planar isolation of an aneurysm (red) with convex hull overlaid (grey).

Tissue Stretch Ratio

Tissue stretch ratio (TSR) was introduced by Berkowitz to quantify the extent of tissue deformation undergone by the aneurysm (Berkowitz 2012). It was defined as

$$TSR = \frac{S_{dome}}{S_{ostium}},$$
 where S_{dome} is the surface area of the dome of the non-planar isolated aneurysm, and S_{ostium} is the surface area of the ostium of the non-planar isolated aneurysm.

aneurysm, and S_{ostium} is the surface area of the ostium of the non-planar isolated aneurysm.

Volume to Ostium Ratio

Volume-to-ostium ratio was first introduced by Yasuda et al., and was intended to assess the morphological features of an aneurysm that could lead to slow or stagnant hemodynamics (Yasuda et al. 2011). It is defined in this work using the planar isolated

aneurysm volume as $VOR = \frac{V}{S_o}$, where V is the planar isolation aneurysm volume and S_o is the surface area of the planar ostium. Piccinelli et al. introduced an alternative definition utilizing V_{vdc} , and this is defined as $VOR = \frac{V_{vdc}}{S_o}$ (Piccinelli et al. 2012).

Aneurysm, Neck and Vessel Angulation

Dhar et al. proposed the measurement of the angle at which blood-flow enters an aneurysm sac and at which blood-flow impinges upon the dome (Dhar et al. 2008), as shown in Figure 18. Piccinelli et al. utilized these concepts to define $\theta_{\text{sac-vessel}}$, the angle between the inflow artery centerline tangent at its clipping point and the unit vector of the measurement of Hang; and $\theta_{\text{neck-vessel}}$, the angle between the inflow artery centerline tangent at its clipping point and the aneurysm planar ostium normal vector. The calculation of these angles was incorporated into the dissertation's software. However, they were not included in the following analyses because the true inflow vessel was not identified as part of the geometric data protocol. Because of this the angles were not truly associated with the flow of blood and render the values meaningless for this application. This step was inadvertently omitted and should be included in a future protocol.

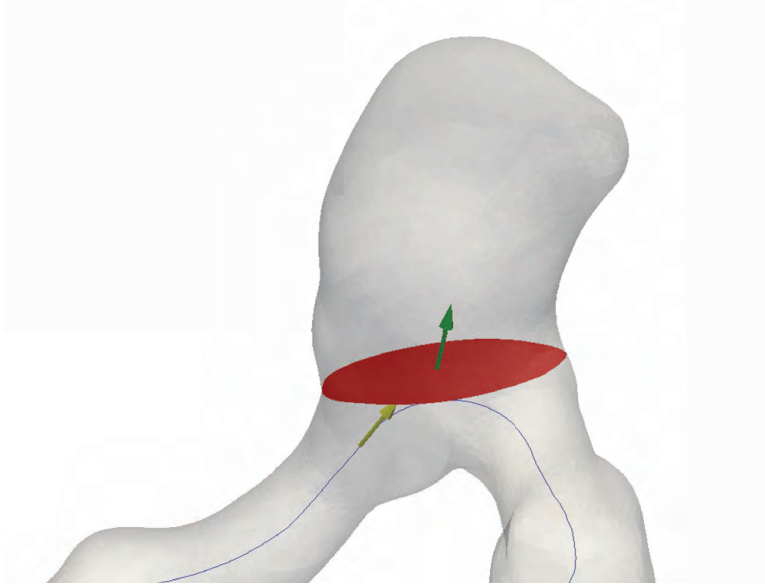


Figure 18. Planar ostium (red), sac unit vector (green), vessel centerline (blue), and vessel unit vector (yellow).

Novel Indices

After identifying all relevant morphological indices from literature and assessing the morphological characteristics they described, the morphological characteristics not yet described were identified. Once identified, morphological indices were developed to describe the morphological characteristics.

Extra-Sac Dilation Index

Extra-Sac Dilation Index (ESDI) was introduced in this study to quantify the fusiform nature of an aneurysm. A fusiform aneurysm is defined as an aneurysm whose dilation is symmetrically centered along the centerline of its parent vessel. Most brain aneurysms are considered to be saccular, and few are considered to be fusiform. However, most have geometries that are not fully saccular, meaning they do not have a pronounced narrowing that delineates the boundary between the sac and the parent vessel

and yet are not fully fusiform, or their dilation is not symmetrically centered along the centerline of their parent vessels. ESDI was developed in order to describe the degree to which an aneurysm may exhibit properties that would be considered partially fusiform. This index was defined as $ESDI = \frac{V_{np}-V}{V_{np}}$, where V_{np} is the volume of the non-planar isolation and V is the volume of the planar isolation. A planar isolation of a saccular aneurysm is able to fully isolate the same amount of volume as a non-planar isolation of the same aneurysm. However, for a fusiform aneurysm a non-planar isolation would be able to fully isolate the aneurysm volume from the parent vessel, while a single planar isolation would leave at least a portion of the residual volume of the aneurysm unisolated from its parent vessel.

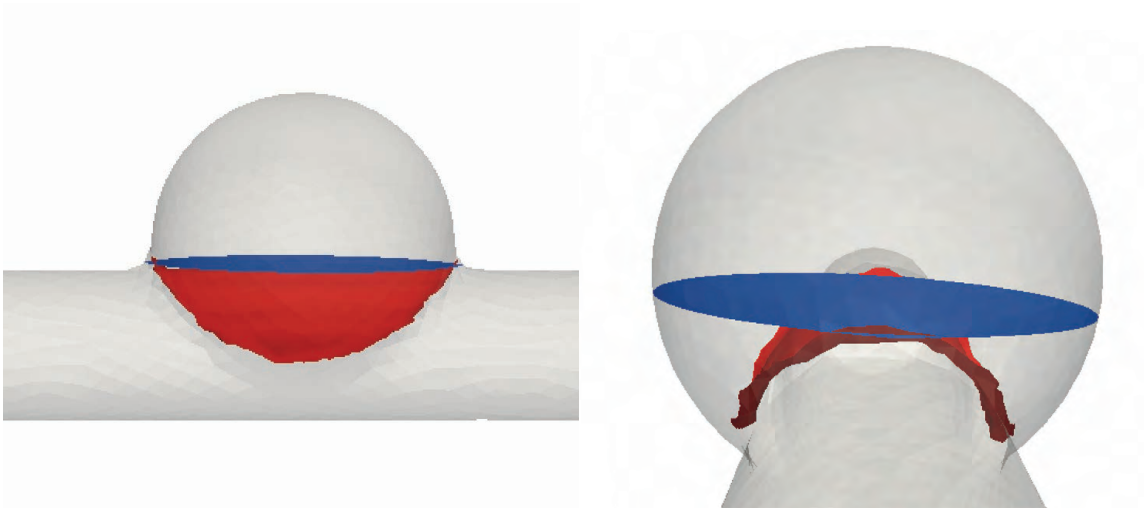


Figure 19. ESDI uses measurements for the volume of the aneurysm geometry (grey) isolated by the planar ostium (blue) and the non-planar ostium (red). This figure displays front and side views of this hypothetical idealized aneurysm geometry. For this moderately fusiform hypothetical idealized model the ESDI value was 0.22.

Maximum Dimensions

Diameter and height of an aneurysm have frequently been used as one-dimensional metrics of aneurysm size. As previously discussed, there are several different definitions in literature of both diameter and height so as to best capture the size characteristics of an aneurysm. However, these dimensions are constrained by the location of the ostium, and could therefore lead to inaccurate measurements of the true dimensions of an aneurysm. Therefore a set of three maximum dimension measurements that is unconstrained by the ostium, was developed. The first maximum dimension measurement, MaxD1, is defined by surveying all points on the surface mesh of an aneurysm for the largest distance between any two points. The second maximum dimension measurement is subsequently measured by first defining cross-sectional contours perpendicular to the line between the points used to define MaxD1. The contours of largest area is next determined, and this contour's centroid is computed. The distance between all points on this contour with a connecting line that passes through its centroid is measured. The largest distance that is measured in such a manner is defined as MaxD2. On the same cross-sectional contour, MaxD3 is defined as the distance between the points on the contour at the intersection of a line passing through its centroid and perpendicular to the line between the points that define MaxD2. This is demonstrated in Figure 20.

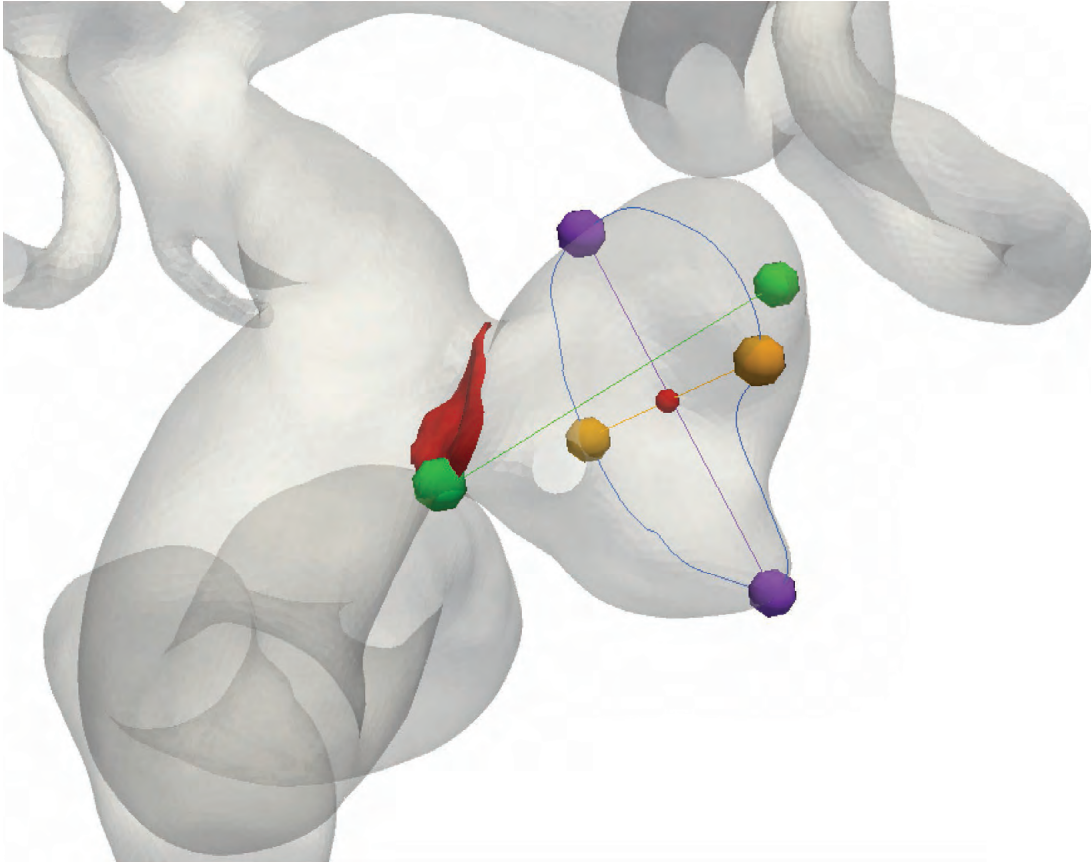


Figure 20. The two points of maximum distance and the line between them (green) are found for the aneurysm (grey) isolated by the nonplanar ostium (red plane). A contour perpendicular to the line between the two points of maximum distance is progressed from the first to second point. The contour of largest area (blue) is found. The centroid of that contour is found (red dot). A line passing through that point along the contour is rotated until the two points of maximum distance are found (purple). Finally, a line perpendicular to that line is used to find the two nearest points on the contour (orange).

Covariance-Fit Ellipsoid Dimensions

In reviewing the morphological indices in literature, it was recognized that all one-dimensional size measurements – height, diameter, and even the novel maximum dimension metrics defined above – were subjective to measurement error due to potentially irrelevant focal irregularities, imaging artifacts or meshing artifacts. Because of this a more gestalt size metric was necessary. Piccinelli et al. introduced a maximally-

inscribed ellipsoid, but this too is subject to similar insignificant irregularities – particularly small concavities. One solution to this problem is to prescribe an ellipsoid fit by using a covariance-fit ellipsoid.

The ellipsoid is first defined by extracting the covariance matrix of the X, Y and Z dimensions using the formula $COV = \frac{\sum_{i=1}^n (X_i - \bar{x})(Y_i - \bar{y})}{n-1}$, to fill in the covariance matrix

$$C = \begin{bmatrix} COV(X, X) & COV(X, Y) & COV(X, Z) \\ COV(Y, X) & COV(Y, Y) & COV(Y, Z) \\ COV(Z, X) & COV(Z, Y) & COV(Z, Z) \end{bmatrix}, \text{ where } (X, Y, Z) \text{ is the position of a}$$

respective surface point i (NIST/SEMATECH 2003). The square-root eigenvalues of this matrix were then calculated, and scaled such that the volume of an ellipsoid with diameters equivalent to the square-root of the resulting eigenvalues was equivalent to the volume of the non-planar aneurysm volume. The values of the scaled eigenvalues were then used to form an ellipsoid. The resulting ellipsoid could then be centered at the aneurysm's centroid, and oriented such that its axes aligned with the eigenvectors of the covariance matrix for a best-fit ellipsoid, as illustrated in Figure 22.

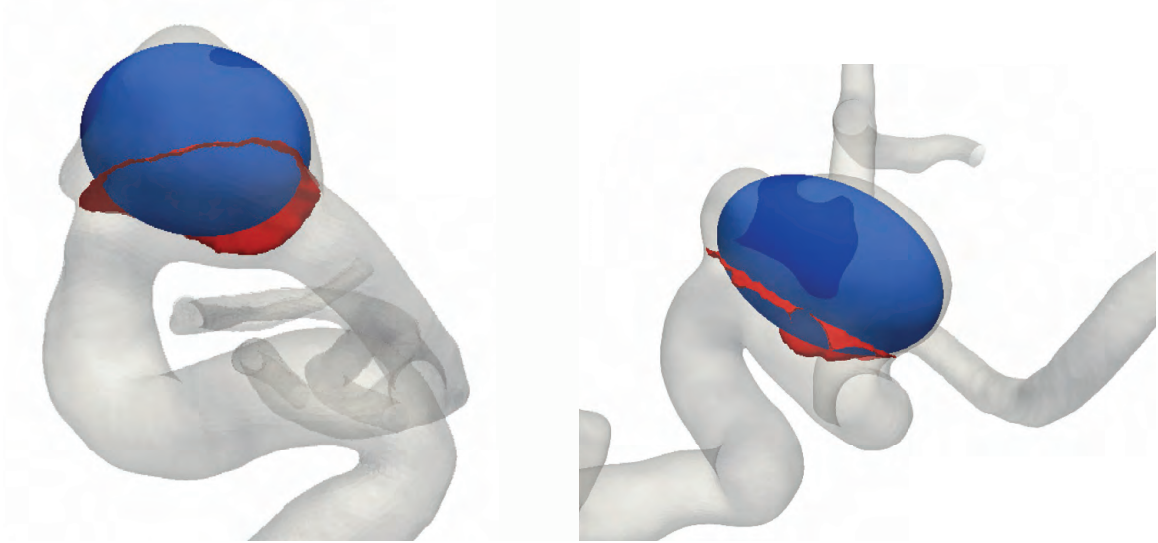


Figure 21. Examples of covariance ellipse (blue) fit to an aneurysm (grey) isolated using a non-planar ostium (red).

Prolaticity and Oblate Ellipticity

Prolate and oblate ellipticity describe the nature of an ellipsoid's appearance, and could have implications on the path of blood-flow within an aneurysm sac. Aspect ratio, the ratio of height to neck size, was also intended to be an indicator of prolate and oblate ellipticity. In hemispherical aneurysms a low aspect ratio value would indicate an oblate geometry, while a high aspect ratio value would indicate a prolate geometry. However, this is not necessarily the case for spherical aneurysms. In order to measure the extent to which an aneurysm was prolate or oblate two new indices were introduced. Utilizing the covariance matrix best-fit ellipsoid axis ratios allows for a more universal estimate of the extent of oblate or prolate ellipticity. By analyzing the ratio of covariance best-fit ellipsoid axes 1 to 2 (Cov12), a value of greater than 1 would indicate increased prolate ellipsoidal shape. By analyzing the ratio of covariance best-fit ellipsoid axes 2 to 3 (Cov23), a value of greater than 1 would indicate increased oblate ellipsoidal shape. In

order to capture the extent to which an aneurysm is prolate and/or oblate, rather than spherical, a magnitude function could be applied between Cov12 and Cov23, such that $CovRatioMagnitude = \sqrt{Cov12^2 + Cov23^2}$.

A similar approach was defined using MaxD1, MaxD2, and MaxD3 in the same manner as the covariance best-fit ellipsoid axes to define MaxDRatio12, MaxDRatio23 and MaxDRatioMagnitude.

Voronoi Diagram Core Evolution-Based Non-Sphericity, Ellipticity and Undulation

The surface area of a surface mesh is inherently a somewhat unreliable quantity. Meshing or imaging artifacts, as well as small differences in isolation plane placement, may cause large differences in surface area with very little difference in volume. To demonstrate this, a sphere of radius 1 cm was created in Rhinoceros 3D, as shown in Figure 22. Small undulations of a radius 5% of the sphere radius were then added to simulate surface noise. No change in volume was observed despite a 4% change in surface area as a result of the undulations. While this example illustrates a minor difference in surface area, it would be common to see surface area values much different due to meshing imaging artifacts. Similarly, Figure 23 demonstrates how two slightly different cutting planes could produce differing measurements that could cause significant errors in a surface area-to-volume comparison as a means of determining non-sphericity. Using the red cutting plane to isolate the aneurysm produces a surface area of 90.3 mm² and a volume of 62.9 mm³. Using the blue cutting plane to isolate the aneurysm produces a surface area of 94.8 mm² (5% increase) yet a volume of 62.3 mm³ (1% decrease). Again, this discrepancy could manifest itself to higher degrees in certain situations. In order to avoid problems such as this and provide a more robust

measurement of non-sphericity a more volume-focused approach is necessary.

Berkowitz's NSIImis and EIIImis are a step in the right direction, but because, similar to Piccinelli et al.'s maximally inscribed ellipsoid, it could experience large discrepancies from small concave irregularities, another more robust metric would be ideal.

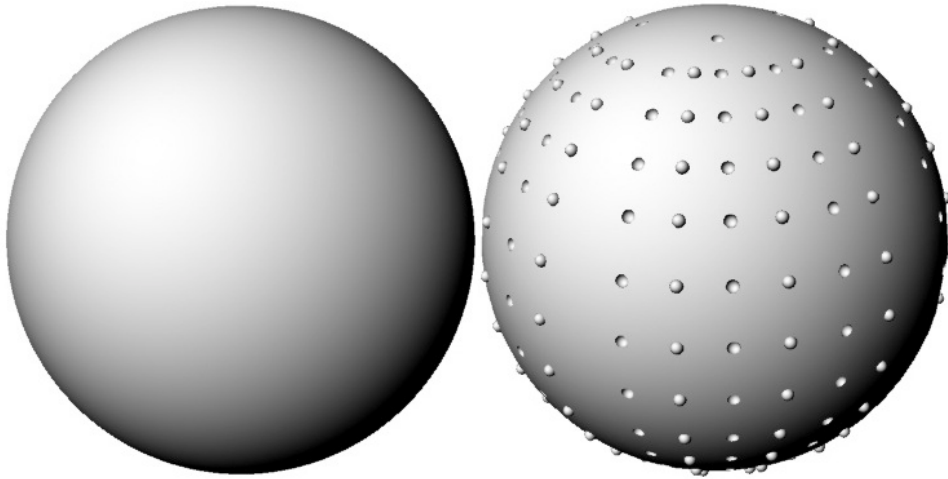


Figure 22. Demonstration of surface area measurements obtained before (left) and after (right) the introduction of small surface undulations. No volume change was observed despite a 4% change in surface area.

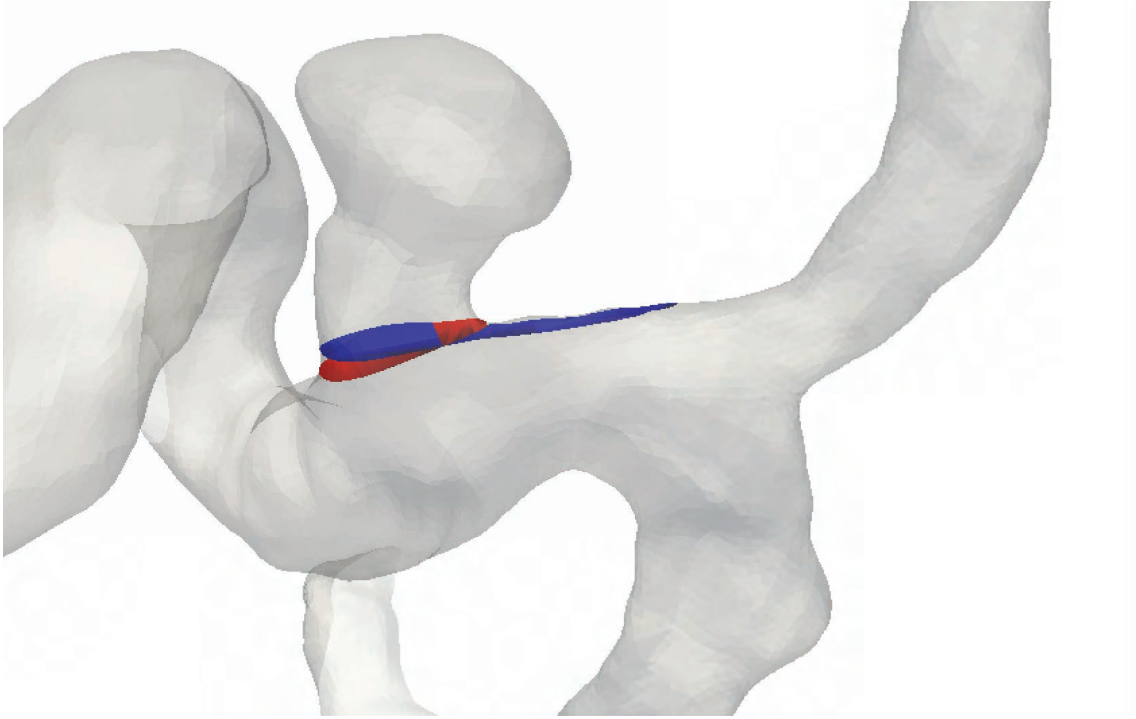


Figure 23. Demonstration of how two slight differences in cutting plane angle (red and blue) could give a misleading representation of aneurysm size based on surface area alone.

Piccinelli et al. proposed a volume metric called the Voronoi Diagram Core (VDC), which utilizes the Voronoi diagram inscribed spheres of radius 75% or greater of the largest inscribed sphere. This essentially produces a smoothed surface that eliminates small shape features, as seen in Figure 9. The cutoff of 75% was “chosen empirically as a reasonable level of smoothness” (Piccinelli et al. 2012).

However, one could envision the effects of perturbing this cutoff. On one end of the spectrum, a cutoff of inclusion for Voronoi spheres close to 0% or greater of the radius of the largest Voronoi sphere would produce a shape that would not smooth out any small shape features, and would be essentially the same shape as the input. On the other end of the spectrum, a cutoff of inclusion for Voronoi spheres slightly less than

100% (e.g. 99%) or greater of the radius of the largest Voronoi sphere would smooth out nearly all shape features and leave only a sphere that is the size of the largest Voronoi sphere. So by slowly incrementing this cutoff value, shape features of increasing sizes would sequentially be smoothed out, as demonstrated in Figure 24.

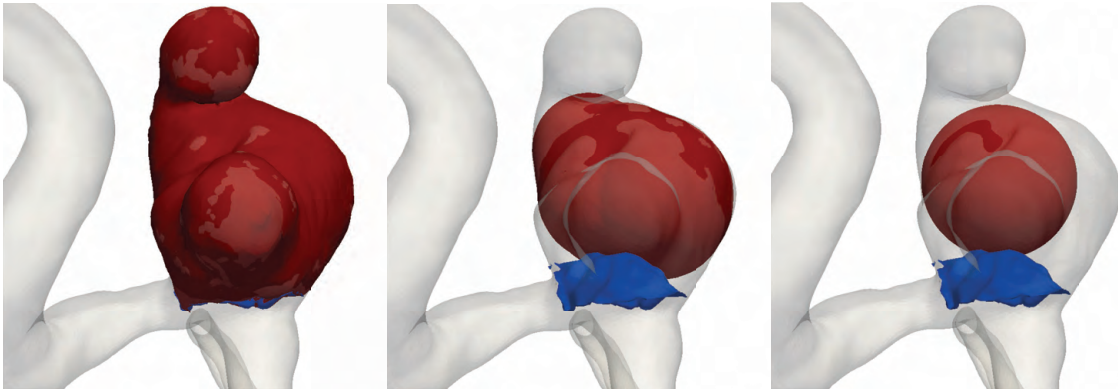


Figure 24. The aneurysm and vasculature is shown in gray, non-planar ostium in blue, and the VDC in red. By increasing the cutoff value of the inclusion radius of the Voronoi spheres from 0% of the largest Voronoi sphere (left), 75% of the largest Voronoi sphere (center), and 99% of the largest Voronoi sphere (right), progressively larger shape features can be smoothed out from the VDC.

By concurrently measuring the volume of the Voronoi diagram core at each sphere inclusion cutoff, a measure of the portion of the aneurysm's volume encompassed by a particular size of shape feature can be determined. If an aneurysm's volume is largely composed of small irregularities, its predominant volume would be high at low cutoff values and low at high cutoff values. For instance, the VDC volumes for those cutoff values shown in Figure 24 are 100% of the aneurysm's V_{np} for a Voronoi sphere cutoff of 0% of the largest Voronoi sphere, 66% of the aneurysm's V_{np} for a Voronoi sphere cutoff of 75% of the largest Voronoi sphere, and 38% of the aneurysm's V_{np} for a Voronoi sphere cutoff of 99% of the largest Voronoi sphere.

In the previous example the Voronoi sphere inclusion cutoff is framed as a percentage of the largest Voronoi sphere. However, to gain insight into how much of the aneurysm's volume is part of a particular size of morphological characteristic, the Voronoi sphere cutoff should rather be framed as a percentage of the aneurysm volume, V_{np} , instead of the largest Voronoi sphere. Plotting the fraction of V_{np} filled by the VDC against the fraction of V_{np} of the current Voronoi sphere cutoff results in Figure 25. This aneurysm, for instance, has a daughter sac that begins to be smoothed out once Voronoi spheres below approximately 9% of the V_{np} are cut out.

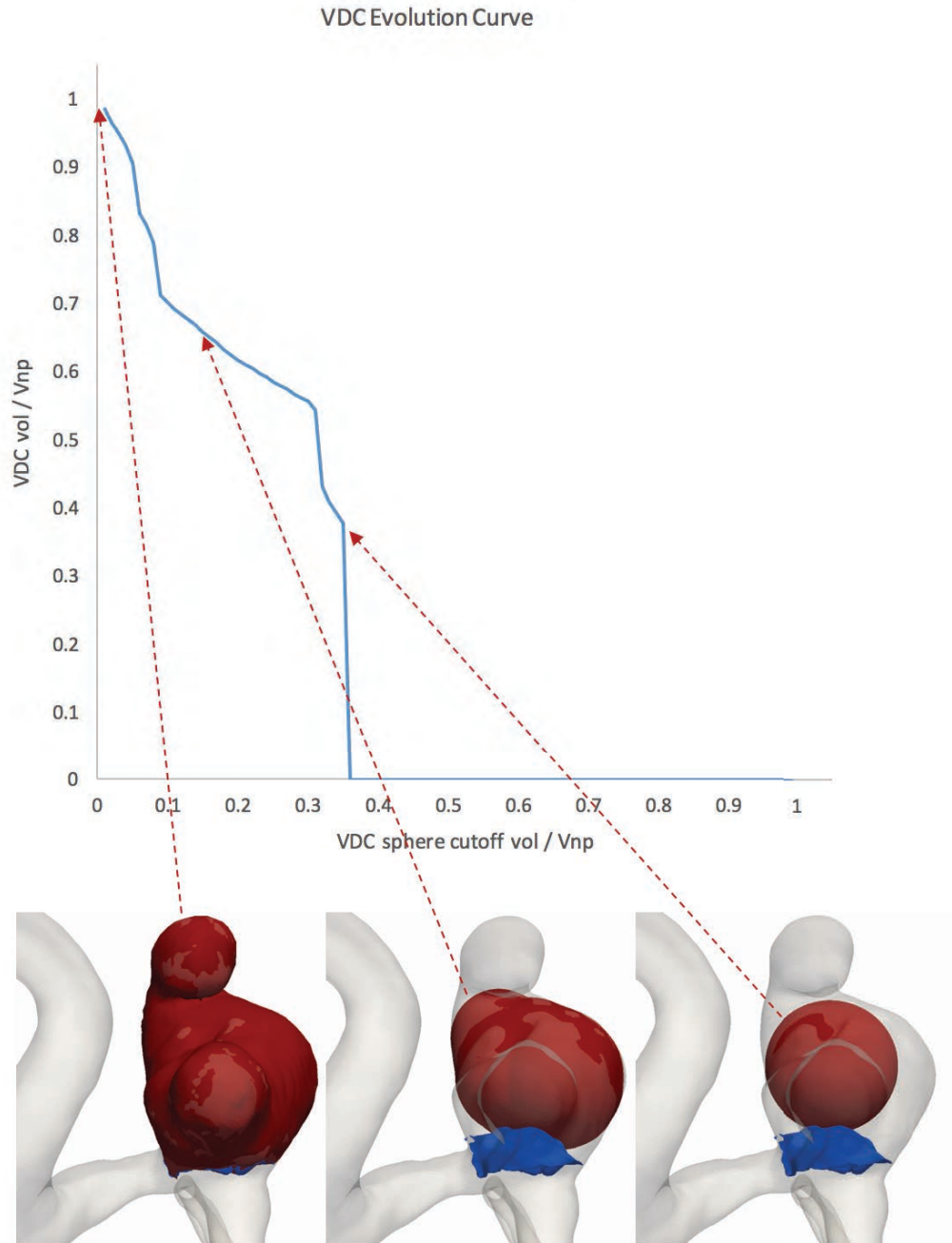


Figure 25. Plot of the VDC evolution. The same VDC cutoff values from Figure 24 are demonstrated along the curve.

This same type of plot could also be generated for the aneurysm's covariance-fit ellipse, as shown in Figure 26, where V_{np} is replaced with the volume of the ellipsoid.

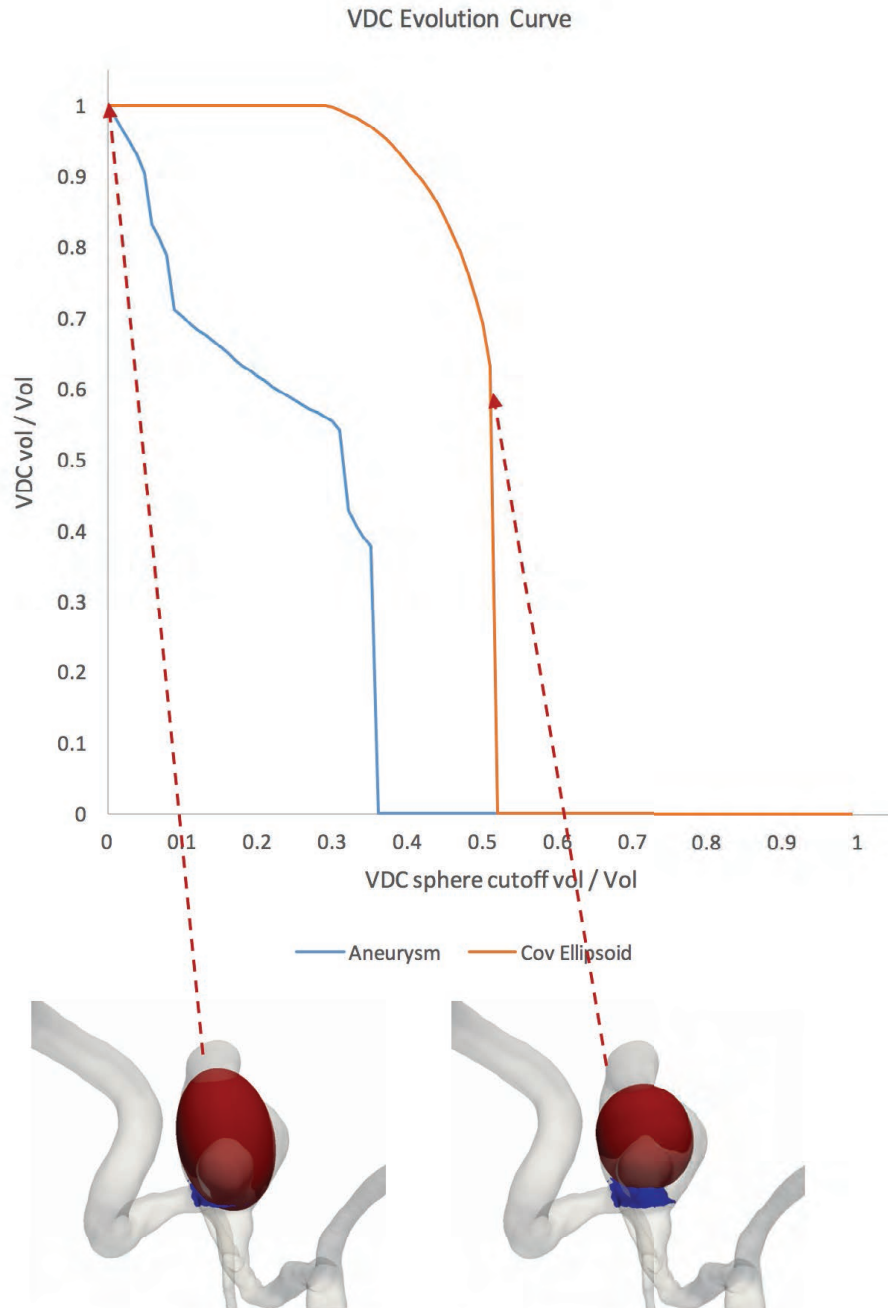


Figure 26. VDC evolution curve for aneurysm (grey in photo, blue on plot) and covariance-fit ellipsoid (red in photo, orange on plot).

An ellipsoid that was completely spherical would produce a VDC evolution curve with an area under the curve (AUC) of 1.0, and an ellipsoid that were very prolate or oblate (one or two very large axes compared to the third) would produce a VDC evolution curve with an area under the curve (AUC) that asymptotes towards 0 as the axis ratio becomes larger, as shown in Figure 27.

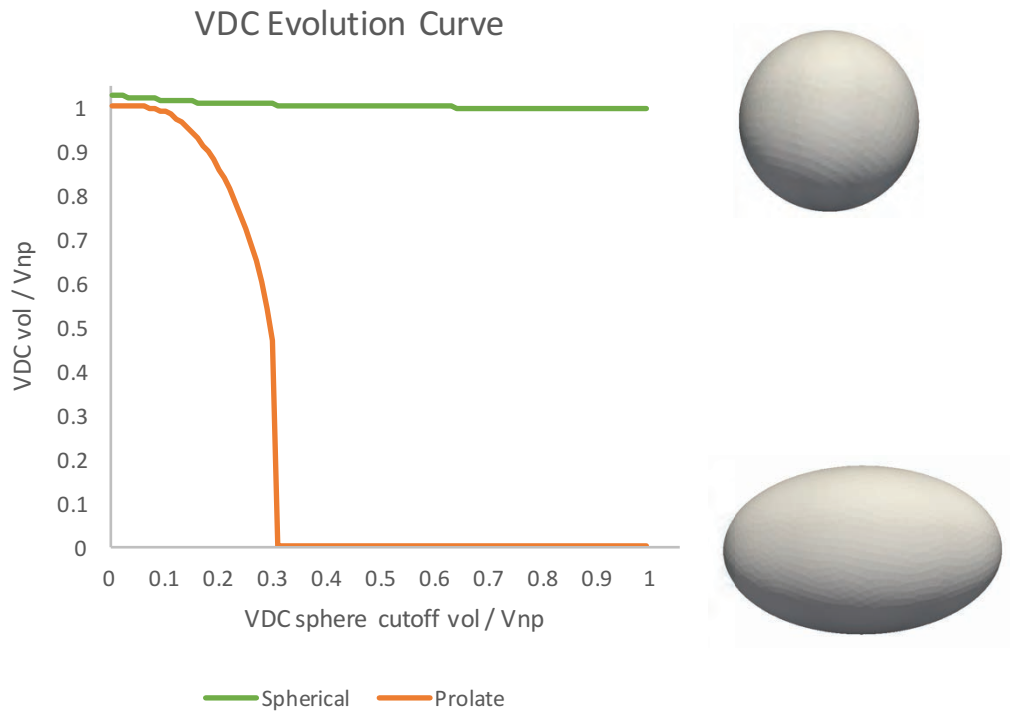


Figure 27. VDC evolution curves of a spherical shape and a prolate shape with major- to minor-axis ratio of 1.66 to 1.

Similarly, a spherical shape with added surface irregularities would also produce a VDC evolution curve that trends toward 0, as shown in Figure 28.

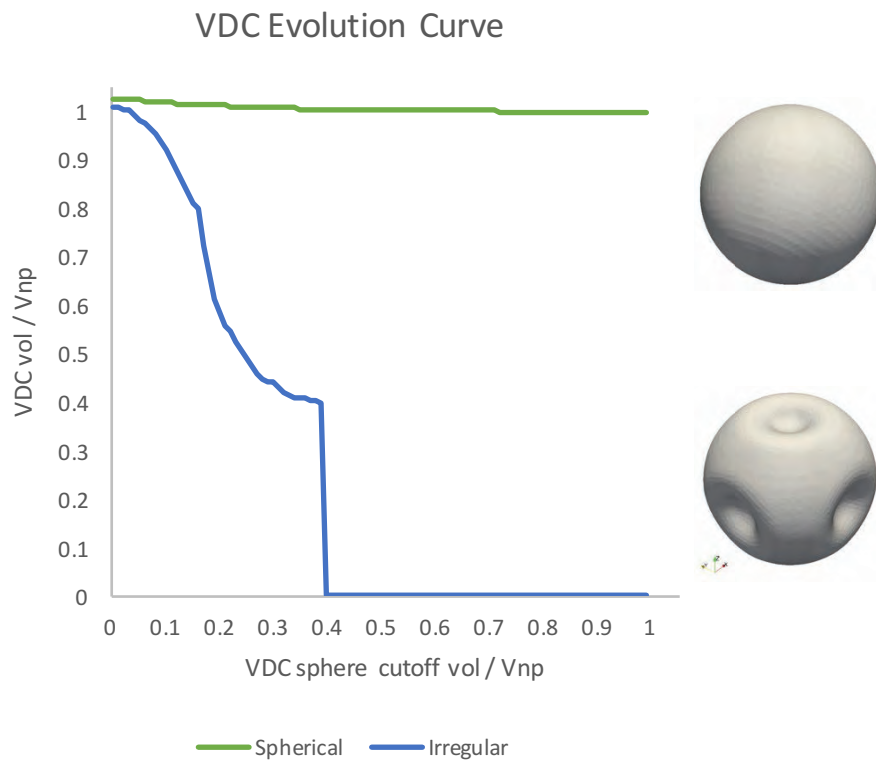


Figure 28. VDC evolution curve of a spherical shape and an otherwise spherical shape with concave irregularities.

Therefore, an aneurysm's VDC evolution curve will have a lower AUC the more irregular and the more ellipsoidal its surface is, as shown in Figure 29. By comparing the aneurysm to the VDC evolution curve of its best fit ellipsoid the aneurysm's irregular shape properties can be isolated from its ellipsoidal shape properties.

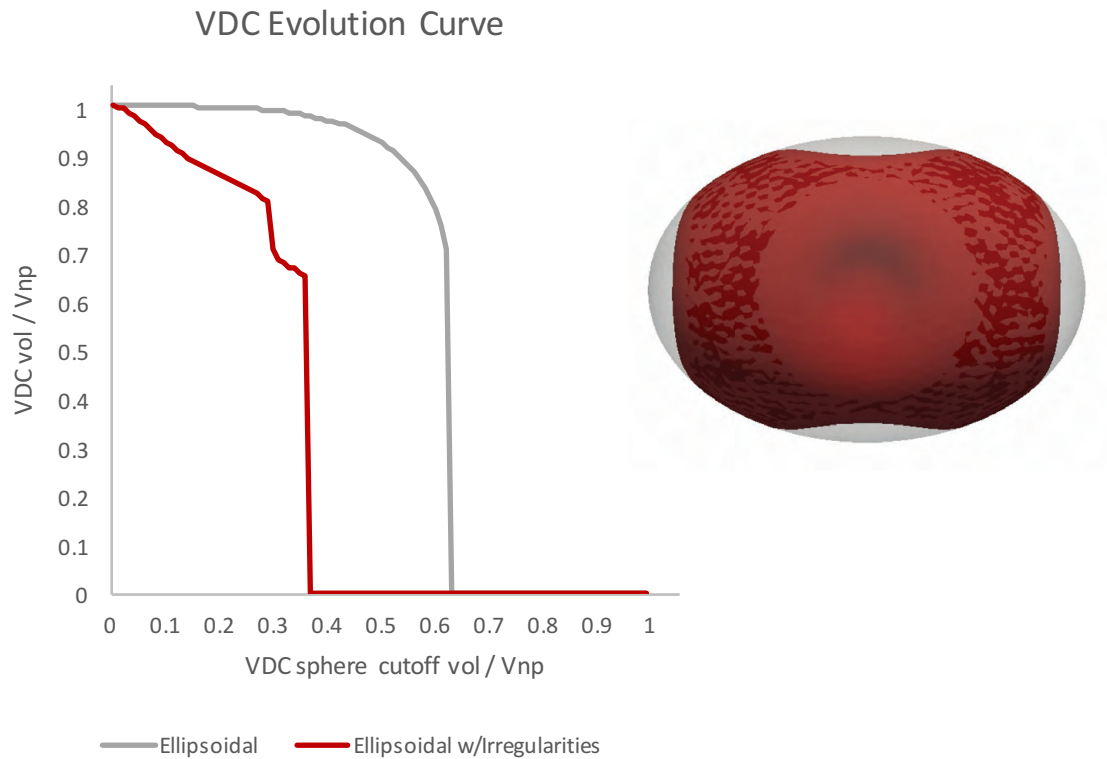


Figure 29. VDC evolution curve comparison of an ellipsoidal shape (grey), and the same shape with hemispherical concave irregularities (red). In the 3D surface model above the ellipsoidal shape is transparently overlaid onto the ellipsoidal-irregular shape.

By isolating the ellipticity from the irregularity as demonstrated in Figure 30, the VDC evolution curve's AUC values can serve as an indicator for undulation, ellipticity, and non-sphericity as a whole. Ellipticity can be quantified by observing the AUC of the covariance-fit ellipsoid VDC evolution curve. Undulation can be quantified by observing the AUC difference between the covariance fit VDC evolution curve and the aneurysm VDC evolution curve, as discussed above. Non-sphericity can be quantified by observing the AUC of the aneurysm VDC evolution curve. These quantities are demonstrated in Figure 30. The formulae for the quantities $Elvdc$ (Ellipticity Index calculated from the

VDC evolution curve), IRRvdc (Undulation Index calculated from the VDC evolution) and NSIvdc (Non-Sphericity Index calculated from the VDC evolution) are, then:

$$EIvdc = 1 - AUC_{ellipsoid}$$

$$IRRvdc = \frac{AUC_{ellipsoid} - AUC_{aneurysm}}{AUC_{ellipsoid}}$$

$$NSIvdc = 1 - AUC_{aneurysm}$$

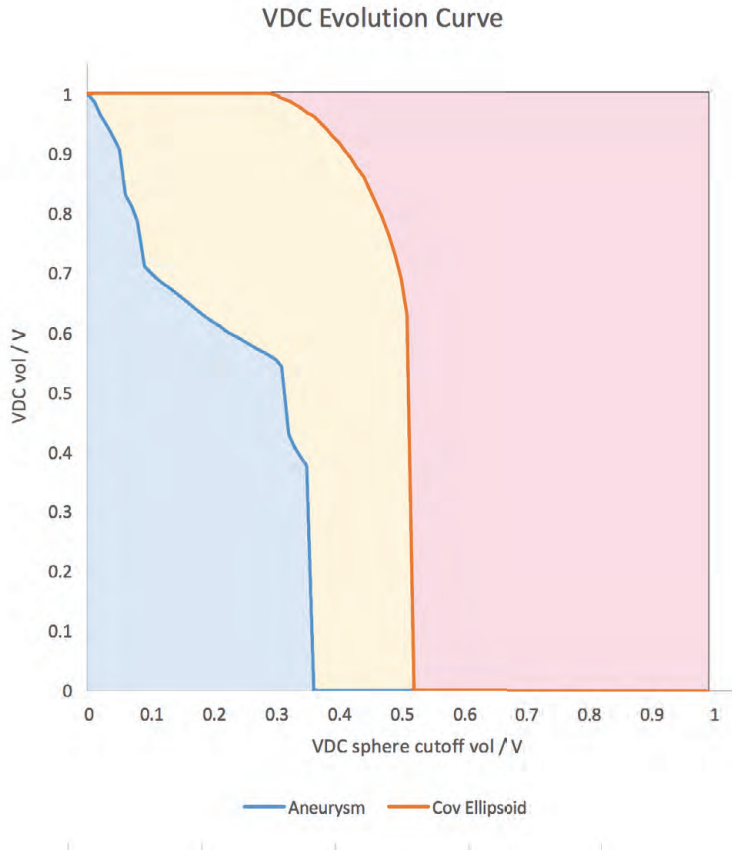


Figure 30. VDC evolution curve from which ideal sphere AUC of 1.0 (red + orange + blue), covariance-fit ellipsoid AUC (orange + blue), and aneurysm AUC (blue) are calculated.

Summary of indices calculated by automated protocol

All of the morphological indices described above were developed into software that isolates the aneurysm from its parent vessel and calculates each index. The software was written in Python 2.7 and utilizes VMTK and VTK Python libraries. Table 1 summarizes the output of this script.

Table 1. Listing and description of each index and its source.

Index	Name	Source
Vnp	Non-planar isolated aneurysm volume	(Berkowitz 2012)
V	Planar isolated aneurysm volume	(Raghavan et al. 2005)
Vvdc	Voronoi diagram core volume	(Piccinelli et al. 2012)
Hperp	Height perpendicular to planar ostium	(Raghavan et al. 2005)
Hmed	Height along medial axis	(Piccinelli et al. 2012)
Hang	Height to most distal point from ostium centroid	(Dhar et al. 2008)
Dperp	Diameter perpendicular to Hperp	(Raghavan et al. 2005)
Dmed	Diameter perpendicular to Hmed	(Piccinelli et al. 2012)
Dang	Diameter perpendicular to Hang	Novel
NDhydraulic	Neck diameter using hydraulic diameter of planar ostium	(Raghavan et al. 2005)
NDavg	Neck diameter using average distance to ostium centroid	(Dhar et al. 2008)
VD	Vessel diameter	(Piccinelli et al. 2012)
SRperp	Size ratio using Hperp	(Dhar et al. 2008)
SRmed	Size ratio using Hmed	(Piccinelli et al. 2012)
SRang	Size ratio using Hang	Novel
ARperp	Aspect ratio using Hperp	(Raghavan et al. 2005)

Table 1 – continued

ARmed	Aspect ratio using Hmed	(Piccinelli et al. 2012)
ARang	Aspect ratio using Hang	Novel
BF	Bottleneck factor	(Raghavan et al. 2005)
BFarea	Bottleneck factor using areas	(Piccinelli et al. 2012)
BLperp	Bulge location using Hperp	(Raghavan et al. 2005)
BLmed	Bulge location using Hmed	(Piccinelli et al. 2012)
BLang	Bulge location using Hang	Novel
Cov12	Covariance ellipsoid prolateness	Novel
Cov23	Covariance ellipsoid oblateness	Novel
CovRatioMagnitude	Magnitude of prolate and oblate ellipticity using covariance ellipsoid	Novel
CRhnorm	Centroid-radii model normalized entropy	(Lauric et al. 2011)
MaxD1	Maximum dimension 1	Novel
MaxD2	Maximum dimension 2	Novel
MaxD3	Maximum Dimension 3	Novel
MaxDRatio12	Prolateness using MaxD1 and MaxD2	Novel
MaxDRatio23	Oblateness using MaxD2 and MaxD3	Novel
MaxDRatioMagnitude	Magnitude of prolate and oblate ellipticity using max dimensions	Novel
NSI18	Hemispherical non-sphericity index	(Raghavan et al. 2005)
NSI36	Spherical non-sphericity index	Novel
NSIImis	Non-sphericity index using the largest maximally inscribed sphere	(Berkowitz 2012)
NSIvdc	Non-sphericity index using Voronoi diagram core evolution	Novel
EI18	Hemispherical ellipticity index	(Raghavan et al. 2005)
EI36	Spherical ellipticity index	Novel

Table 1 – continued

EIImis	Ellipticity index using the largest maximally inscribed sphere	(Berkowitz 2012)
EIvdc	Ellipticity index using Voronoi diagram core evolution	Novel
UI	Undulation index	(Raghavan et al. 2005)
IRRvdc	Undulation index using Voronoi diagram core evolution	Novel
TSR	Tissue stretch ratio	(Berkowitz 2012)
VOR	Volume-to-ostium ratio	(Yasuda et al. 2011)
VORvdc	Volume-to-ostium ratio using Vvdc	(Piccinelli et al. 2012)
ESDI	Extra-sac dilation index	Novel

SPECIFIC AIM 2:
IDENTIFICATION OF OPTIMAL SET OF MORPHOLOGICAL
INDICES

Background

There have been many studies that introduce novel morphological indices and successfully demonstrate the indices' ability to discern between ruptured and unruptured aneurysms. However, a comprehensive, large-scale longitudinal study is still needed. Examining every single metric in combination with all others would provide a thorough description of morphological traits for such a study, but it would not lend itself well to assessing the hypothesis that aneurysm morphology is an indicator of rupture risk. Since testing each metric itself constitutes a hypothesis, each additional metric requires increased study population size to keep up statistical power, presumably achieved from recruiting a larger number of patients in an already expensive and time-consuming endeavor. In order to effectively test this hypothesis, the fewest number of metrics that exhaustively describe aneurysm morphology should be used. Many morphological indices are redundant with others and equivalently measure the same morphological characteristic, some describe morphological characteristics that are similar enough to others that measuring both morphological indices is not necessary, some are not sensitive to the kinds of morphological differences that are present in the cerebral aneurysm population, and some are so sensitive to inter-user variability they do not produce meaningful results. By assessing which metrics uniquely and robustly describe the largest amount of morphological variance among several populations of unruptured, untreated

cerebral aneurysms the groundwork can be laid for a future large-scale, longitudinal study.

Study data

Three data sets were used for the following studies. The first data set used for this study was described in Ramachandran et al. 2016. It consisted of 178 patients with 198 unruptured aneurysms that were recommended for observational follow-up rather than treatment, and corresponding image sets were collected in a consecutive, longitudinal manner from 4 data centers. Institutional review board approvals were obtained at all participating clinical centers and the data analysis center. The image modalities consisted of 132 CTA, 7 CE-MRA and 30 TOF-MRA datasets. The data was pre-segmented as part of the Ramachandran et al. study. The second data set consisted of an additional 27 unruptured aneurysms that were chosen for treatment and were collected under the same IRB protocol as the Ramachandran et al. 2016 study. These images were not pre-segmented, and were segmented for this study under the same protocol as the Ramachandran et al. study, which used the level-set segmentation technique within VMTK. Further detail on this data set is elaborated upon in Specific Aim 3. In order to expand the breadth of the study population a third data set consisting of an additional 59 unruptured aneurysms were utilized from the Aneurisk study. The Aneurisk study collected aneurysm diagnostic medical images between 2005 and 2008 in order to perform analyses on geometry and hemodynamic conditions that might correlate with aneurysm rupture (Emory University Department of Math and Computer Science 2012). The Aneurisk data sets include aneurysms that were chosen both for treatment and for follow-up. The Aneurisk data sets were collected from 3DRA images and were pre-

segmented and meshed using VMTK by the Aneurisk research group. The data are summarized in Table 2.

Table 2. Summary of the data utilized for Specific Aim 2.

Research Group	Data center(s)	<i>N</i>	Treatment status	Imaging modalities	Used in
BioMOST	University of Iowa; Thomas Jefferson University; Mass. General Hospital; Penn. St. University-Hershey	198	Untreated	CTA, CE-MRA, TOF-MRA	Aim 2, Aim 3
Aneurisk	Niguardia Hospital Milan	59	Untreated and treated	3DRA	Aim 2
BioMOST	University of Iowa; Thomas Jefferson University; Mass. General Hospital; Penn. St. University-Hershey	27	Treated	CTA, CE-MRA	Aim2, Aim 3

The Specific Aim 1 protocol was performed for all cases. There were 5 cases of the 198 original BioMOST data sets (2.5%), 1 case of the 29 newly collected BioMOST cases (3.4%) and 2 cases of the 59 Aneurisk data sets (3.4%) that experienced errors during the protocol that prevented a successful completion of the protocol. One case failed during calculation of Hang metric in the protocol algorithm, and seven cases failed during the non-planar isolation section of the protocol algorithm. These cases were discarded, and the remaining 276 cases successfully completed the protocol. Of those 276 cases, 30 failed to automatically define a suitable clipping plane and had to use a manually-positioned planar isolation, but otherwise successfully completed the protocol.

The average time to run one data set through the protocol (not including parent vessel reconstruction) was 9 minutes 43 seconds, and the large majority of this time was spent in the computation of the VDC evolution. Run time generally increased with volume, as shown in Figure 31. Because the focus of this work was not on computational efficiency there is likely a good amount of room for improvement in computational time.

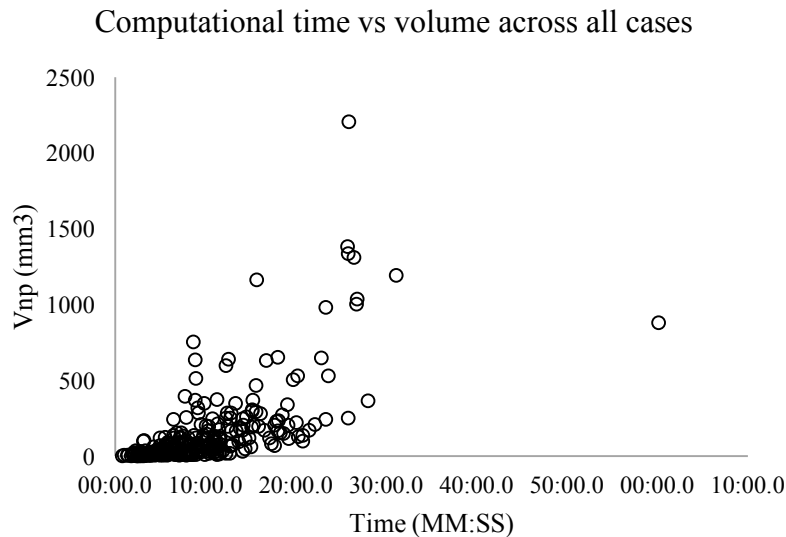


Figure 31. Computational time to isolate aneurysm and calculate morphological indices generally increased with volume.

Procedure to determine an optimal set of morphological indices

The Specific Aim 1 study protocol was performed on all data and compiled into a database. Using this data, the first step in determining which metrics were most robust was an analysis of its sensitivity to differences in the prescribed morphological characteristic that it was defined to measure. This was followed by an analysis of each indices' robustness to inter-user variability. Next the definitions of the metrics were examined for clear problems in the definition or application of each metric, with

sensitivity and user-variability taken into account. This was followed by a factor analysis of the metrics that were determined to be sufficiently robust in order to determine which metrics were highly inter-correlated, and which morphological characteristics described the most variance in the given populations. All statistics were performed using the R statistical package. The results of this process were then used to adjudicate as to which variables most uniquely and robustly described the largest amount of morphological variance and should therefore be used in future longitudinal cohort studies.

Study on robustness of morphological indices to inter-user variability

Motivation

Any computerized algorithm that utilizes user feedback as part of its processes is subject to inter-user variability. Depending on the robustness of the algorithm it could be highly sensitive to small changes in user input for an otherwise similar dataset. A study of user variability was performed in order to determine the robustness of the study protocol and morphological indices.

Study data

A subset of 8 aneurysms from this dataset was selected, by random selection, such that one aneurysm was within a size category of every 2mm from 0mm up to the largest collected aneurysm size of greater than 14mm, as measured using the definition of Dperp by the Ramachandran et al. group.

Procedure

Two users performed the entirety of the Aim 1 morphological index extraction protocol on the data subset of 8 aneurysms using both the automatic and manual clipping plane isolation techniques. The automatic clipping plane was inspected for errors, and as specified by the protocol, the manual clipping plane isolation technique was only utilized if an error was present. The results from the analysis of User 1, the expert user, and User 2, the novice user, were plotted against one another for each index. The slope of a regression line and the Pearson correlation coefficient were also calculated for each index. All statistics were performed using the R statistical package.

Results

All of the morphological indices were calculated and the results compared between the two users. Three of the eight cases experienced errors within the calculation of the automatic clipping plane isolation, and as such the results were taken from the manual clipping plane isolation. User 1-User 2 scatter plots can be seen in Appendix B, and renderings of the planar and non-planar ostia can be seen in Appendix C.

The inter-user variability was assessed using a combination of the plots from Appendix B, the regression line slope, and the Pearson coefficient. This variability is outlined in Table 3.

Table 3. Inter-user variability statistics, regression line slope and Pearson coefficient, for each morphological index.

Index	Regression line slope	Pearson coefficient
Vnp	1.1	1.0
V	1.0	1.0
Vvdc	1.1	1.0
Hperp	1.0	1.0
Hmed	1.1	0.9
Hang	1.0	1.0
Dperp	1.0	1.0
Dmed	0.9	1.0
Dang	1.1	0.9
SRperp	0.9	1.0
SRmed	0.9	0.9
SRang	0.9	1.0
ARperp	0.8	1.0
Armed	0.9	0.9
ARang	1.0	1.0
BF	0.6	0.8
BFarea	0.7	1.0
BLperp	1.0	1.0
BLmed	0.4	0.4
BLang	0.5	0.8

Table 3 – continued

Cov12	0.8	1.0
Cov23	1.1	0.9
CovRatioMagnitude	0.9	1.0
CRhnorm	0.9	1.0
MaxD1	1.0	1.0
MaxD2	1.0	1.0
MaxD3	1.1	0.9
MaxDRatio12	0.8	1.0
MaxDRatio23	0.4	0.5
MaxDRatioMagnitude	0.4	0.4
NSI18	1.0	1.0
NSI36	1.0	1.0
NSIImis	0.9	1.0
NSIvdc	1.0	1.0
EI18	1.0	1.0
EI36	1.0	1.0
EIImis	0.9	1.0
EIvdc	1.1	1.0
UI	0.9	1.0
IRRvdc	1.1	1.0
TSR	1.0	1.0
VOR	0.8	1.0
VORvdc	0.7	1.0

Table 3 – continued

ESDI	0.9	0.9
------	-----	-----

Discussion

As evidenced by the results in Table 3, while most user variability metrics trended towards 1.0 for both regression line slope and Pearson correlation coefficient there were some indices that were less robust to inter-user variability. For instance, BLang, BLmed, MaxDRatio23 and MaxDRatioMagnitude showed both poor Pearson inter-correlation coefficients and a poor regression line slope. The MaxDRatioMagnitude metric likely only displayed poor inter-user variability robustness because of its direct calculation from MaxDRatio23. MaxDRatio23 itself is likely sensitive to inter-user variability because of its dependence upon the perpendicular orientation of MaxD2 and MaxD3 to the MaxD1 orientation axis. Depending on a small variation in orientation of MaxD1, MaxD2 and MaxD3 may experience highly different measurements depending on the geometry of the aneurysm, as demonstrated in Figure 32.

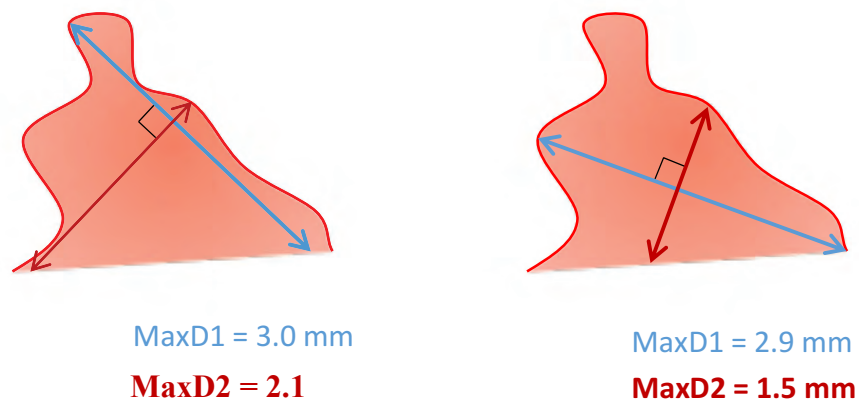


Figure 32. Demonstration of sensitivity of MaxD2 (and MaxD3) to different orientations of the MaxD1 measurement axis caused by a slight change in the ostium.

Bulge location in general is very sensitive to user variation because of its nature of locating the largest cross-section. A small variation in orientation of the angled height point and medial axis orientation could significantly affect the measurement of the bulge location because of the possibility that multiple locations have similar diameters.

Study on sensitivity of morphological indices

Motivation

The morphological indices introduced in Aim 1 were each designed to measure a particular morphological characteristic. However, in order to verify that each metric does in fact measure the morphological characteristic that is designed to measure a sensitivity analysis was performed. In this experiment hypothetical, idealized aneurysm models were developed in which one particular shape characteristic was perturbed. These models were then used to verify that a given metric sufficiently measured the morphological characteristic that it was designed to measure. These models were designed such that they approximately mimicked realistic ranges of the shape characteristics observed in patient-specific aneurysm geometries.

Procedure

Hypothetical idealized models were used for the sensitivity analysis. They were designed in order to test the sensitivity of morphological indices by perturbing the specific morphological characteristics as listed in Table 4. Each one of the three hypothetical idealized models for each morphological characteristic represents either a high, medium or low presence of the particular morphological characteristic. In max measured dimensions and non-sphericity models there were more than three possible

configurations of the morphological characteristic, and those models were represented appropriately. All models were created using either PTC Creo 3 or Rhinoceros 5 CAD packages, and re-meshed to a surface element target area of 0.1 mm^2 . Examples of the idealized aneurysm models used in these analyses are shown in Figure 33.

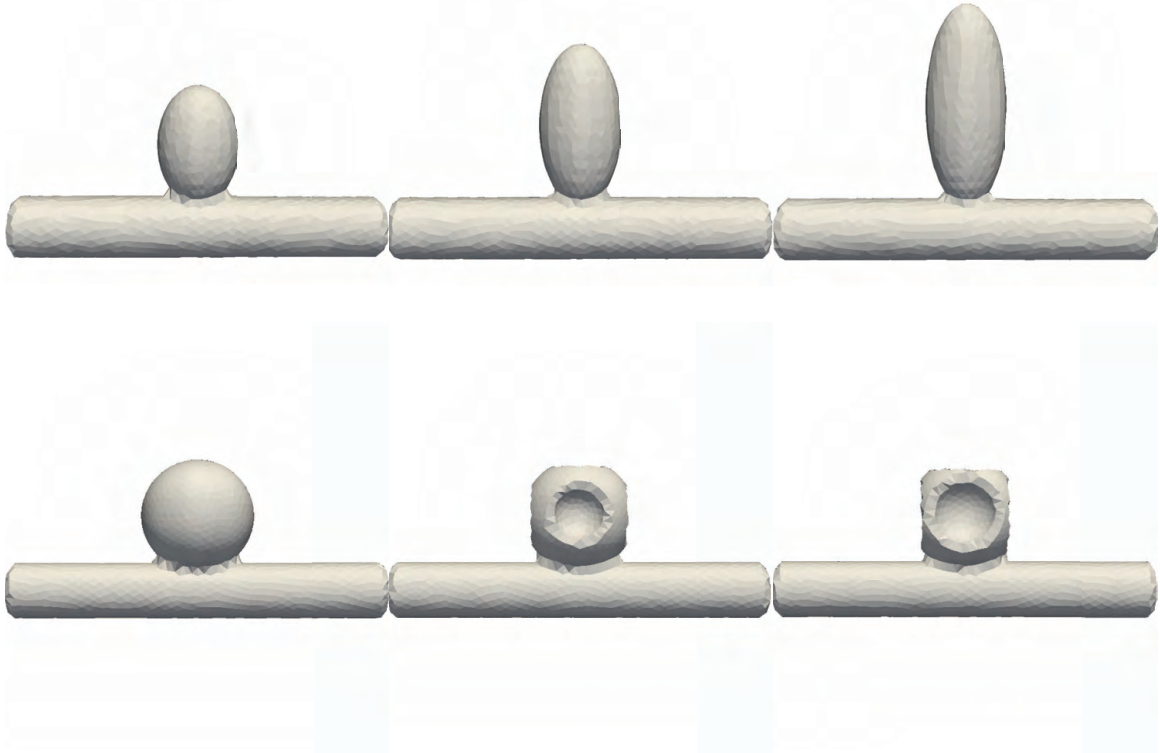


Figure 33. Examples of prescribed morphological changes in hypothetical idealized models. From left to right, the top row contains the models for low, medium and high prescribed height, and the bottom row contains the low, medium and high prescribed concave surface undulation.

Table 4. Description of the idealized aneurysm models used for the sensitivity analysis.

Morphological characteristic	Aneurysm models	Vessel models	Indices measured
Height	10x4x4mm, 8x4x4mm and 6x4x4mm ellipsoids placed 0.5mm below vessel surface	3mm diameter, lateral orientation	Hang, Hmed, Hperp
Diameter	10mm, 6mm and 4mm spheres placed 0.5mm below vessel surface	3mm diameter, lateral orientation	Dang, Dmed, Dperp
Max measured dimensions	10x10x10mm, 10x10x6mm, 10x6x6mm, 10x6x2mm and 10x2x2mm, 6x6x6mm and 2x2x2mm ellipsoids placed 0.5mm below vessel surface	3mm diameter, lateral orientation	MaxD1, MaxD2, MaxD3
Volume	10mm, 6mm and 2mm spheres placed 0.5mm below vessel surface	3mm diameter, lateral orientation	V, Vvdc, Vnp
Size ratio	10mm and 6mm spheres placed 0.5mm below vessel surface	3mm and 4mm diameter, lateral orientation	SRang, SRmed, SRperp
Bulge location	Rotational surface created by splines created with points (0,1,0), (3,2,0) and (0,7,0); and (0,1,0),(3,4,0) and (0,7,0) placed 0.5mm below vessel surface	3mm diameter, lateral orientation	BLang, BLmed, BLperp

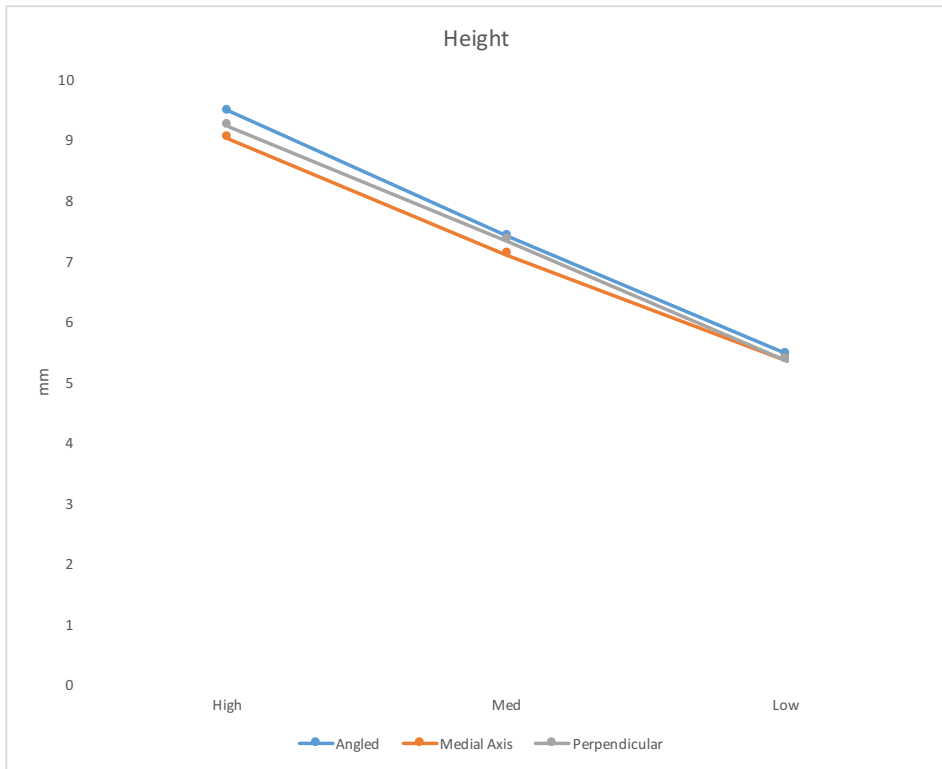
Table 4 – continued

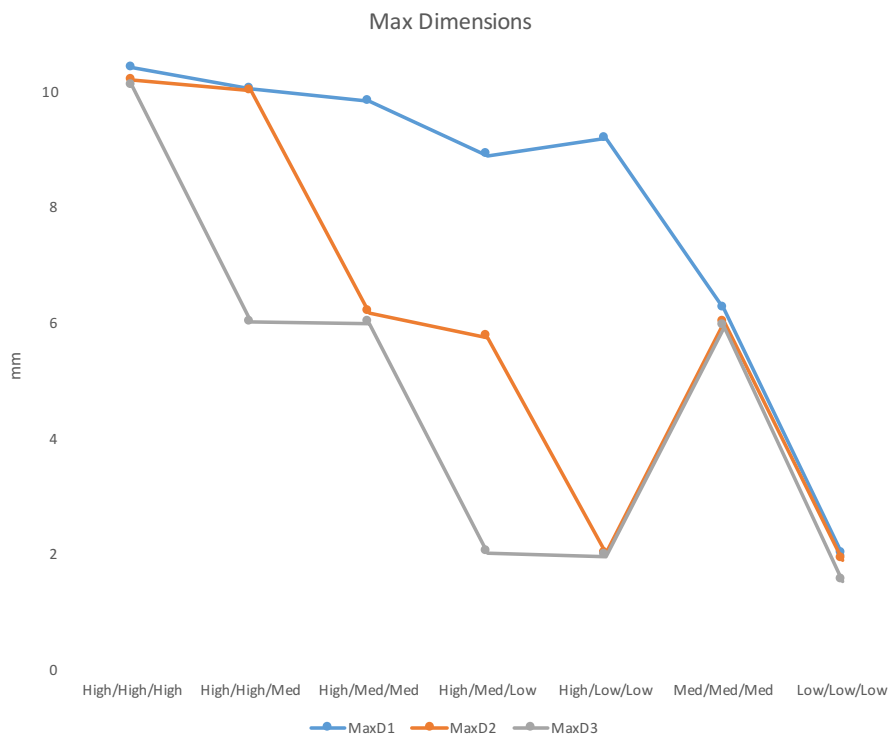
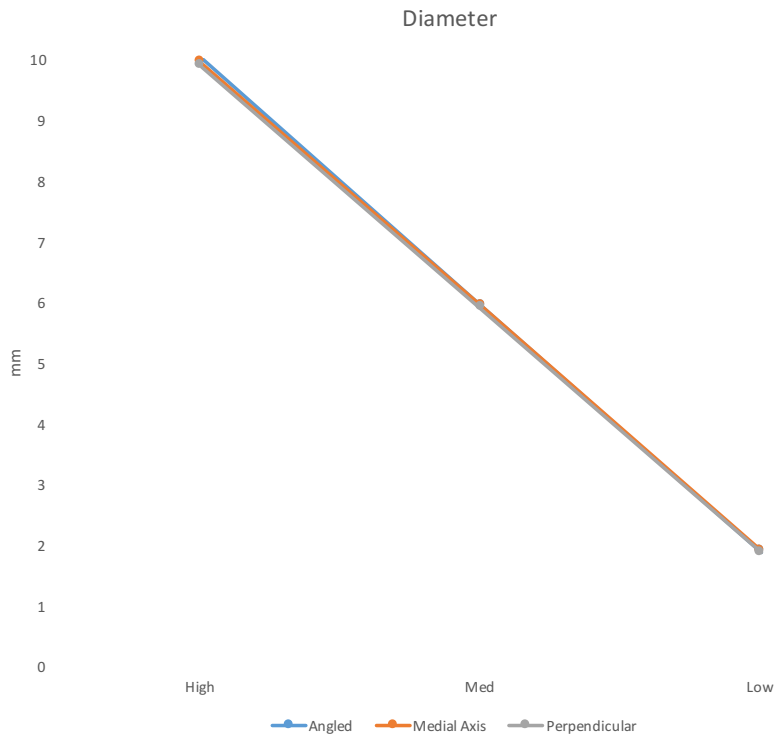
Bottleneck	10mm, 6mm and 2mm spheres placed 0.5mm below vessel surface	3mm diameter, lateral orientation	BF, BFarea
Neck-sac size relation	10mm, 6mm and 2mm spheres placed 0.5mm below vessel surface	3mm diameter, lateral orientation	TSR, VOR, VORvdc, ARang, ARmed, ARperp
Prolateness	10x10x10mm, 10x6x6mm, 10x2x2mm ellipsoids placed 0.5mm below vessel surface	3mm diameter, lateral orientation	MaxDRatio12, Cov12
Oblateness	10x10x10mm, 10x10x6mm, 10x10x2mm	3mm diameter, lateral orientation	MaxDRatio23, Cov23
Ellipticity	10x6x6mm, 8x6x6mm and 6x6x6mm	3mm diameter, lateral orientation	EI18, EI36, EIImis, EIvdc, CovRatioMagnitude, MaxDRatioMagnitude
Irregularity	6mm spherical with divots which decrease the volume of the aneurysm by 10%, 25% and 50%	3mm diameter, lateral orientation	UI, IRRvdc
Non-sphericity	Utilize the same models from both ellipticity and irregularity		NSI18, NSI36, NSIImis, NSIvdc, CRhnorm
Fusiformity	6mm spherical placed 0.5mm, 1.5mm and 2.5mm below the vessel surface	3mm diameter, lateral orientation	ESDI

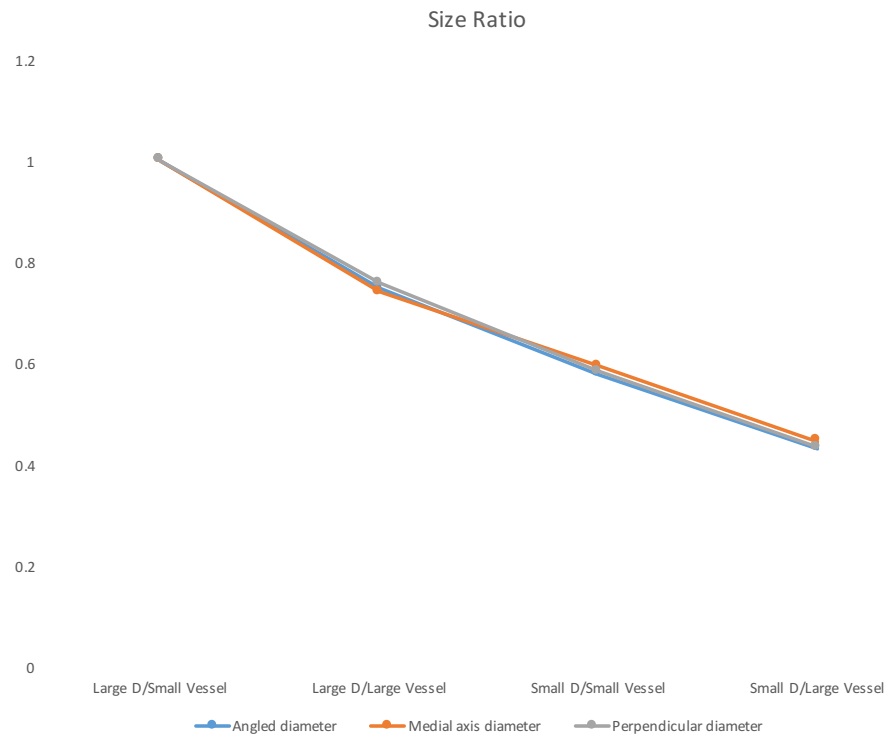
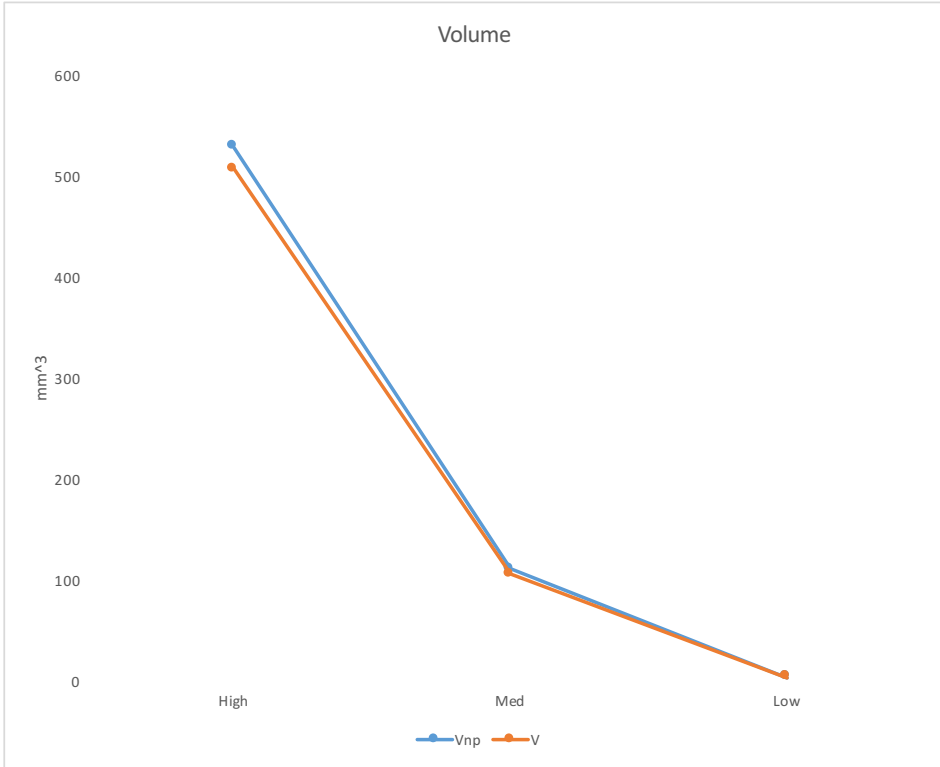
Following the creation of the hypothetical idealized models, each model was processed using the Aim 1 protocol in order to calculate all morphological indices.

Results

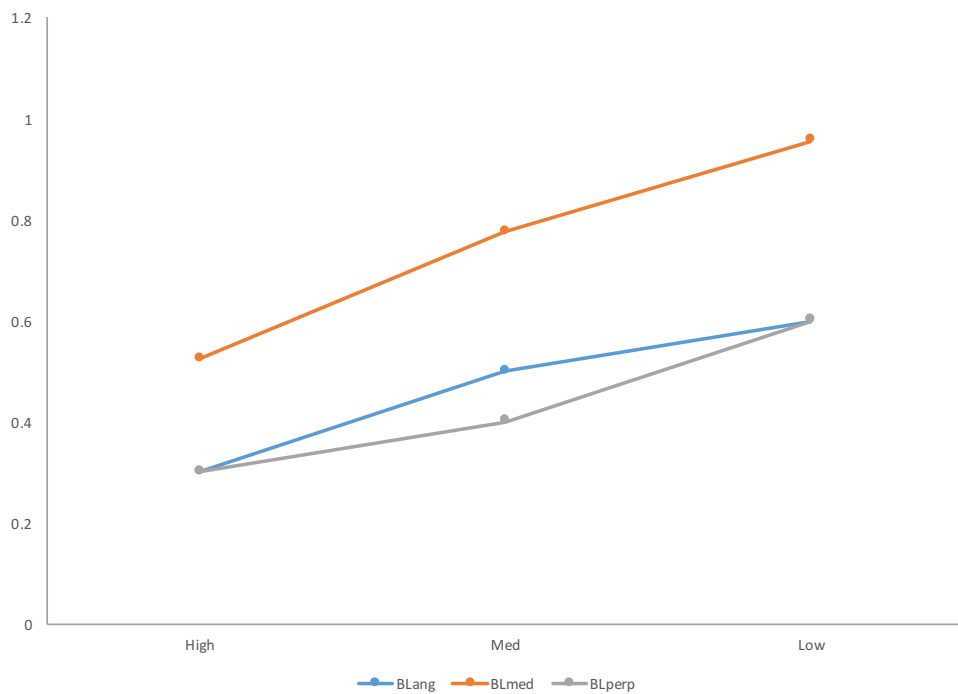
The plots show in Figure 34 are representative of the morphological metric values measured from each hypothetical idealized model with, in most cases, a high, medium or low presence of a morphological characteristic.



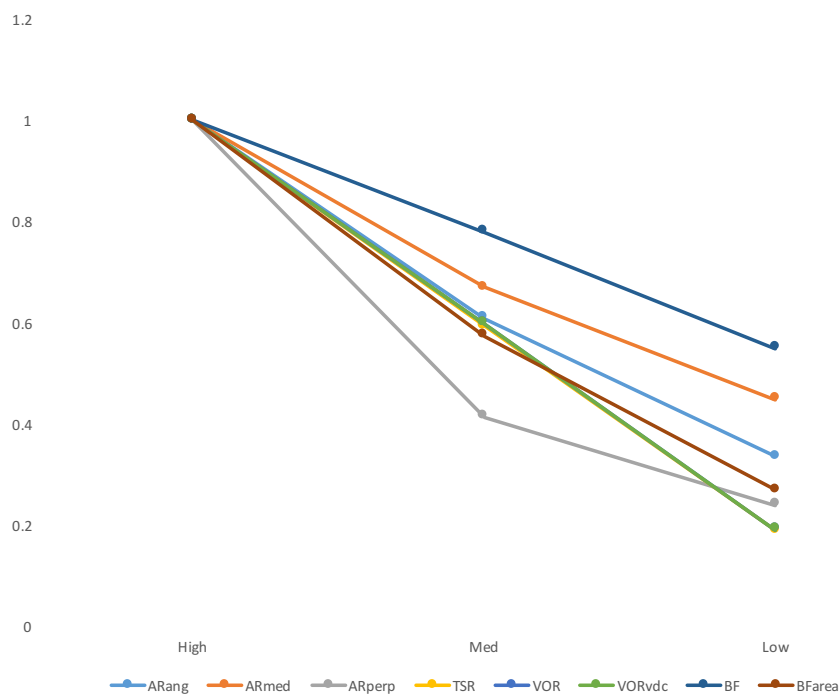




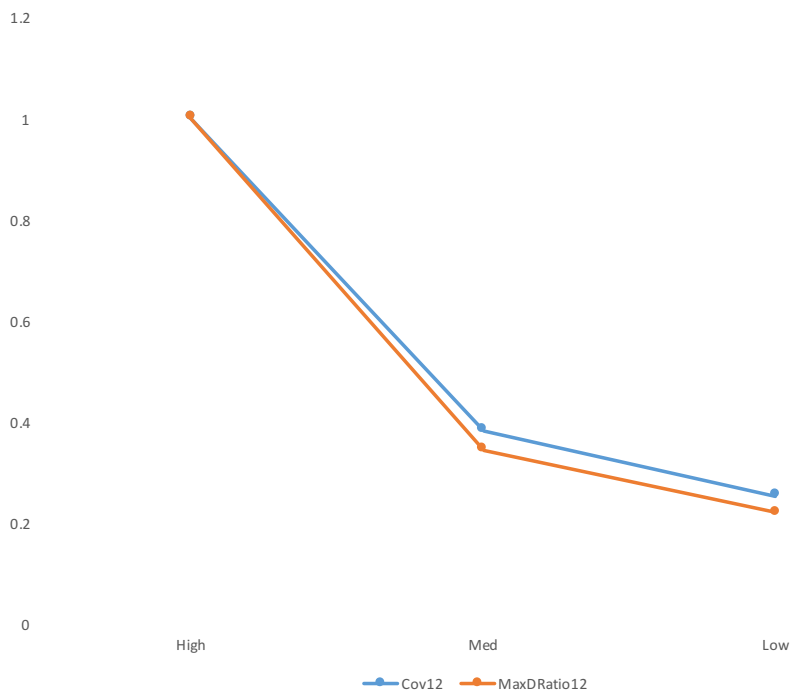
Bulge location



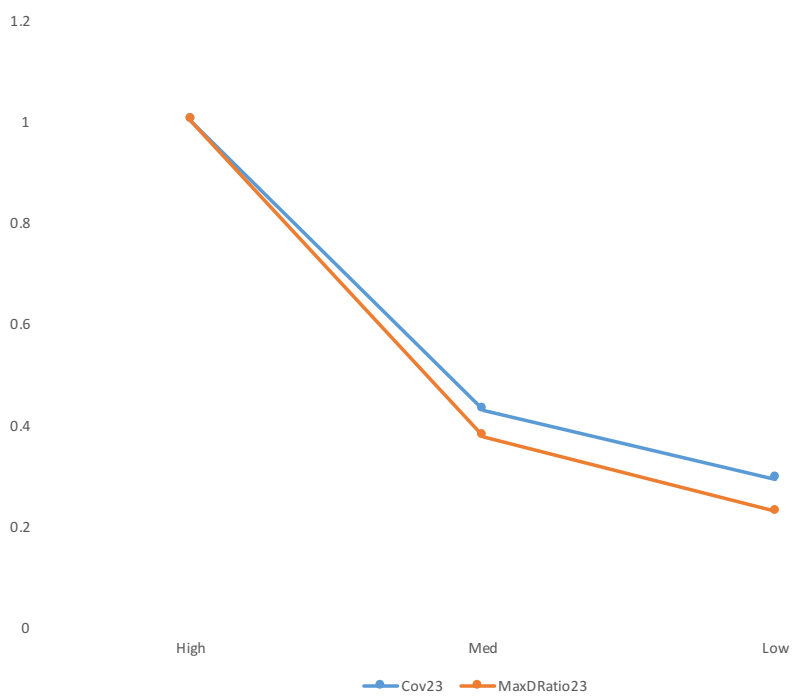
Neck Sac Size Relation

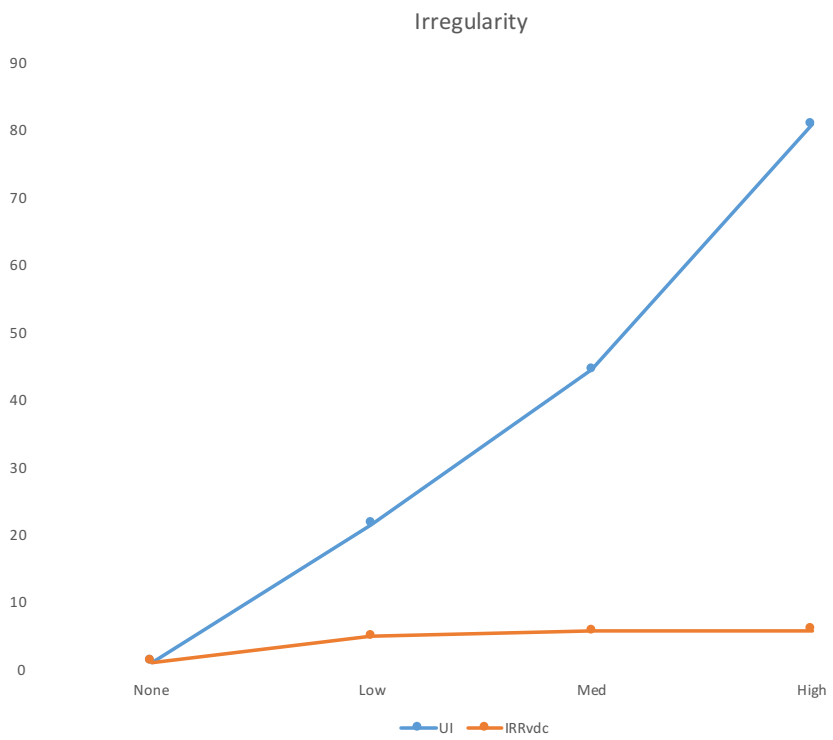
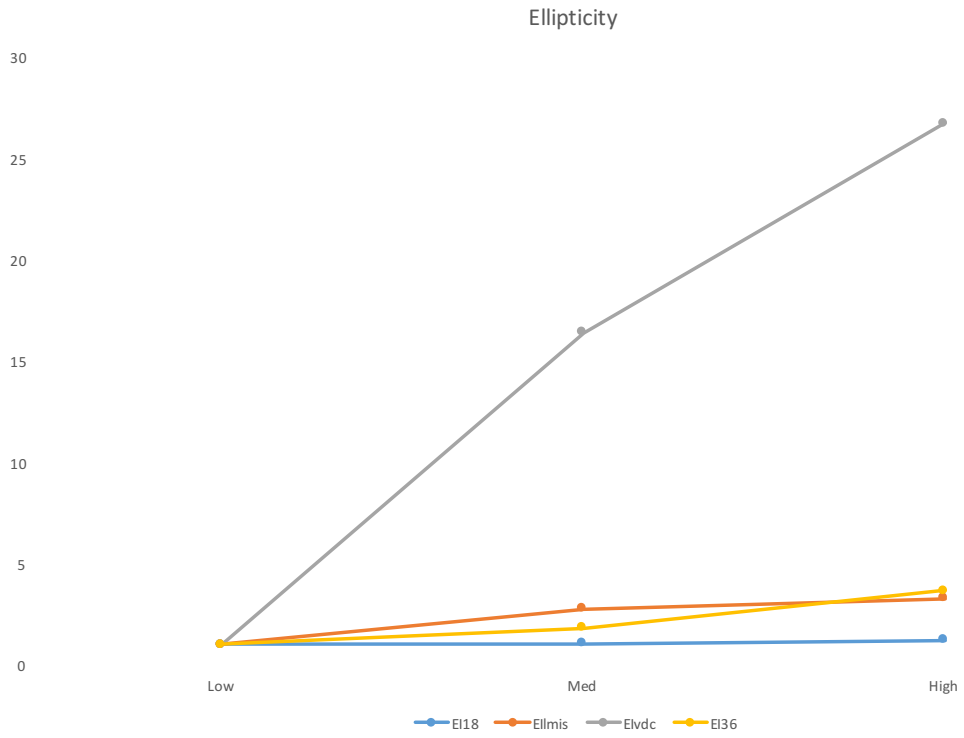


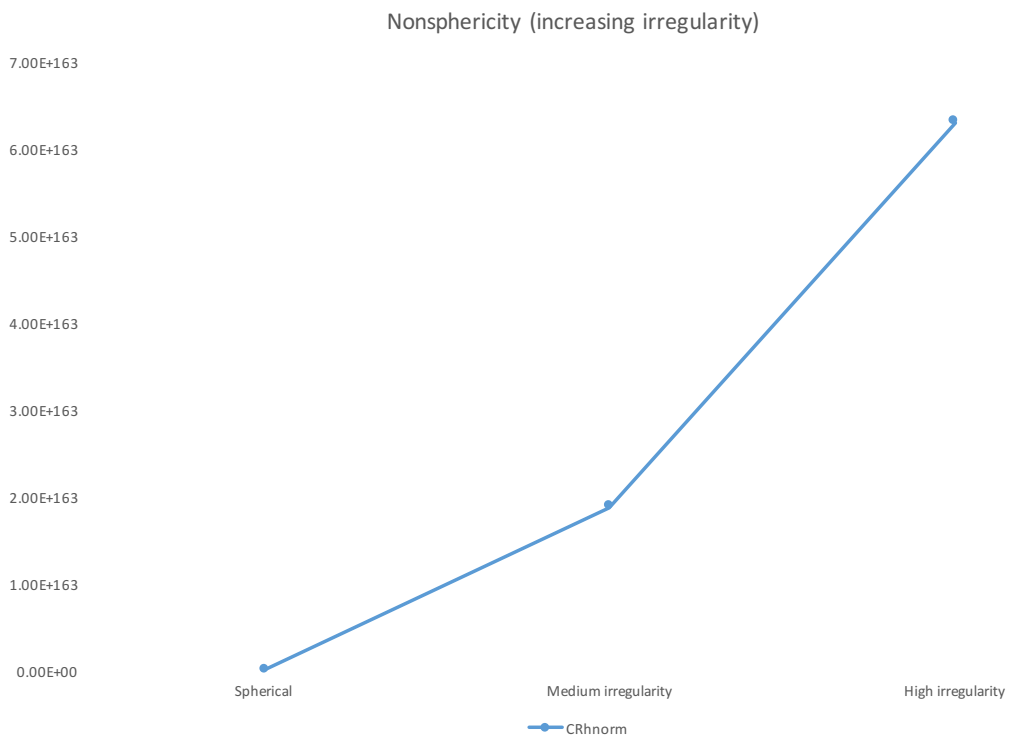
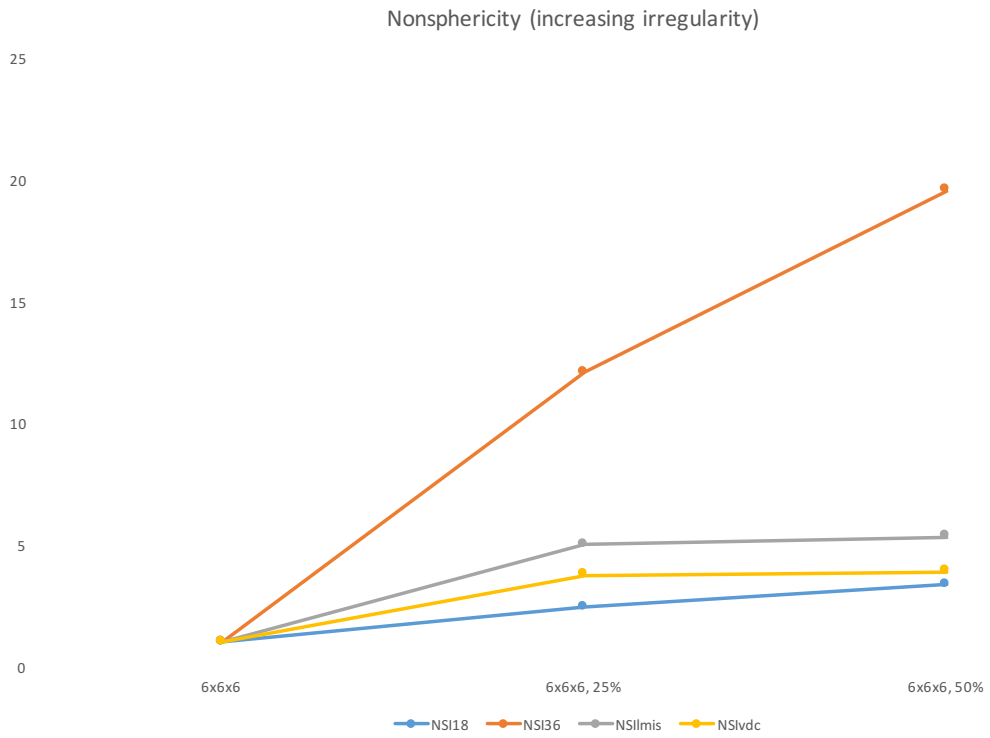
Prolateness

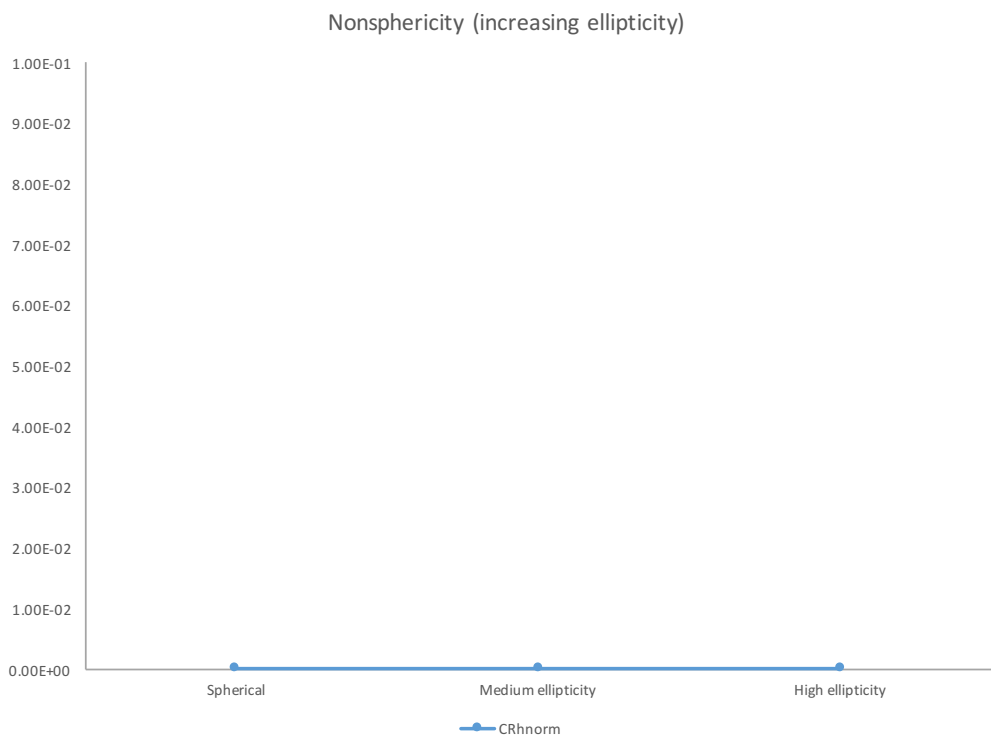
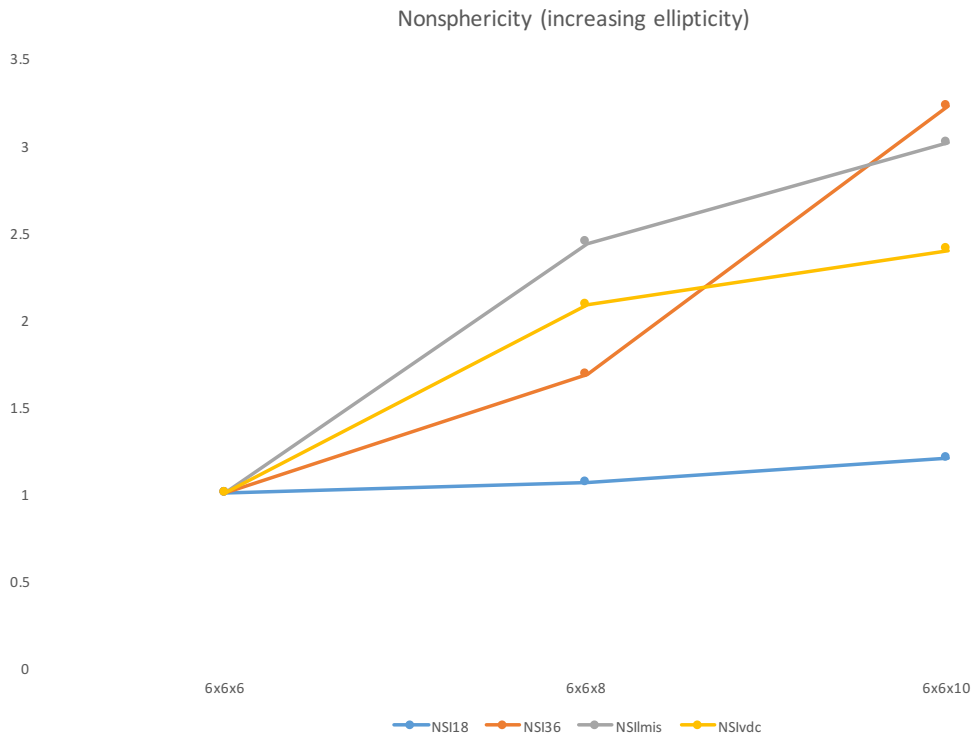


Oblateness









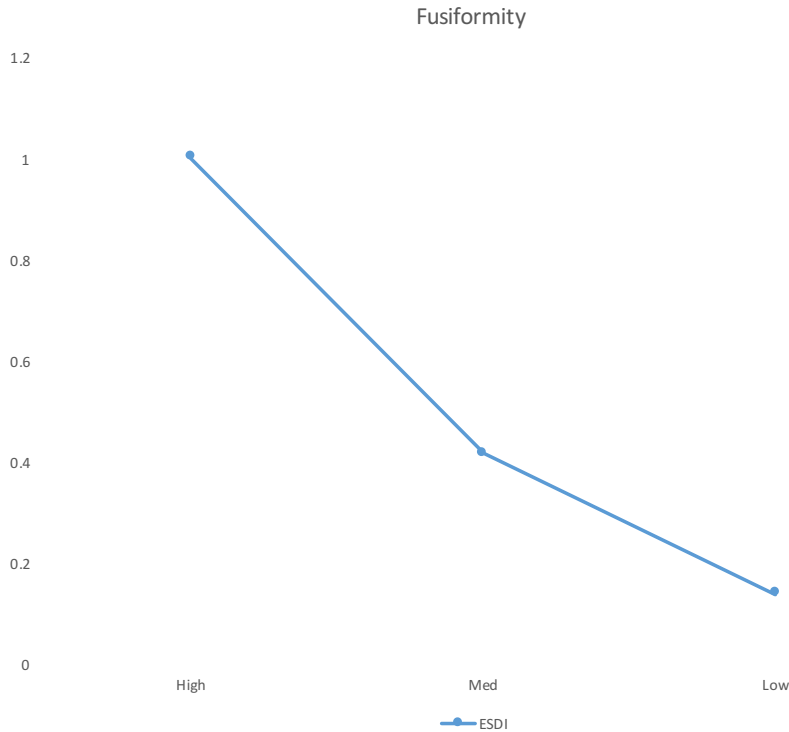


Figure 34. Plots of the morphological index measurements from hypothetical idealized aneurysm models that modulate the morphological characteristic the index is designed to measure. Plots for Size Ratio, Neck-Sac Size Relation, Irregularity, Non-sphericity, Ellipticity, Prolateness, Oblateness and Fusiformity are normalized to the initial value of each index.

Discussion

In analyzing the individual sensitivity of the morphological indices, it should be noted that some morphological indices are dimensional measurements and some are non-dimensional. Of the dimensional measurements, the measurements of height, diameter, maximum dimension and volume all accurately represented the prescribed values of the models. Because of the similar measurements of height between the height metrics, all of the size ratio metrics displayed similar results. For bulge location BLmed provided

different results than the other two metrics, but the sensitivity appeared to be similar within the shape characteristics of the prescribed models. For bottleneck, however, BFarea appeared to be much more sensitive to varying shape characteristics than BF. This is likely due to its use of two-dimensional rather than one-dimensional measurements. In examining the relationship between neck and sac size, VOR and VORvdc exhibited higher sensitivity than TSR or the aspect ratio metrics. However, TSR and the aspect ratio metrics also did appear to be sufficiently sensitive to the prescribed morphological changes. For prolateness and oblateness, the covariance-fit ellipse metrics and the MaxDRatio metrics appeared to be sufficiently sensitive to the prescribed morphological changes, with MaxDRatio metrics slightly more so. Sensitivity to Ellipticity was sufficient in MaxDRatioMagnitude, CovRatioMagnitude and Eivdc. However, it appeared as though EI18 and EI36 hardly changed at all with increasing prescribed ellipticity, and EIImis was only sensitive to the lower range of prescribed ellipticity, which is likely the range in which most aneurysms will occur. Irregularity was sufficiently represented by both metrics, however IRRvdc appeared to be more sensitive in the lower ranges of prescribed irregularity, while UI was more sensitive in the higher ranges of prescribed irregularity. When examining the measurement of prescribed non-sphericity two components needed to be examined – the sensitivity of the non-sphericity to increasing irregularity and to increasing ellipticity. Non-sphericity metrics were intended to capture both morphological characteristics equally, so it is important that a metric be sensitive to both. When increasing prescribed irregularity, it appeared that NSIvdc and NSIImis were very sensitive in the lower ranges, CRhnorm was more sensitive in the upper ranges, while NSI18 and NSI36 presented more of a linear trend.

However, similarly to EI18 and EI36, NSI18 and NSI36, along with CRhnorm, almost entirely failed to reflect prescribed changes in ellipticity. NSI1mis was more sensitive, while NSIvdc was the most sensitive. Finally, ESDI appeared to be sufficiently sensitive to fusiformity. These sensitivity results are summarized in Table 5.

Table 5. Summary of the sensitivity analysis.

Morphological characteristic	Index	Sensitivity
Height	Hang	Good
	Hmed	Good
	Hperp	Good
Diameter	Dang	Good
	Dmed	Good
	Dperp	Good
Max measured dimensions	MaxD1	Good
	MaxD2	Good
	MaxD3	Good
Volume	V	Good
	Vvdc	Good
	Vnp	Good
Size ratio	SRang	Good
	SRmed	Good
	SRperp	Good
Bulge location	BLang	Good
	BLmed	Good
	BLperp	Good
Bottleneck	BF	Good
	BFarea	Good
Neck-sac size relation	TSR	Good
	VOR	Good
	VORvdc	Good
	ARang	Good
	ARmed	Good
	ARperp	Good
Prolateness	MaxDRatio12	Good

Table 5 – continued

	Cov12	Good
Oblateness	MaxDRatio23	Good
	Cov23	Good
Ellipticity	EI18	Poor
	EI36	Poor
	EIImis	Good
	EIVdc	Good
	CovRatioMagnitude	Good
	MaxDRatioMagnitude	Good
Irregularity	UI	Good
	IRRvdc	Good
Non-sphericity	NSI18	Poor
	NSI36	Poor
	NSIImis	Good
	NSIVdc	Good
	CRhnorm	Poor
Fusiformity	ESDI	Good

Discussion of robustness in definition and application

In examining the morphological indices that were calculated as part of the protocol it is clear that, as discussed in Specific Aim 1, metrics that relate surface area to volume are often unreliable. For this reason, several metrics were chosen to be eliminated as recommendations for future use. Those metrics were NSI18, NSI36, EI18, EI36, VOR and VORvdc.

The bulge location metrics, BLang, BLperp and BLmed, were not recommended for use. These metrics are generally non-robust because of their tendency to change drastically with small differences in orientation or position of the height measurement axis. Because these metrics search the cross-sections along the height measurement axis for a single maximum of the cross-sectional area, there are many instances in which one

maximum may be very similar in value to another area in cross-sectional area. With a slight change in orientation the cross-sectional area could change very slightly but cause a drastic change in the location of the maximum value along the height measurement axis.

The indices for prolateness and oblateness each accomplish this measurement by measuring the ratios of the first and second, and second and third axes of either a best-fit ellipse or a covariance fit ellipsoid. Practically these do not provide much information on their own, but rather would be meaningful in conjunction. This is accomplished by the inclusion of MaxDRatioMagnitude, so MaxDRatio12 and MaxDRatio23 were eliminated from the analysis. This is also the case for Cov12 and Cov23.

While reviewing the results for the calculation of ESDI, many of the datasets presented a negative value. Ideally there should not ever be a negative value for ESDI, which would mean that the planar isolation contained more volume than the non-planar isolation. In fact, this was seen frequently throughout the data. It appeared that the planar ostium was frequently more deeply inset into the vessel than the non-planar ostium. This index was built under the assumption that this would not occur. Because of this faulty logic, ESDI was eliminated from the analysis.

Factor analysis

Motivation

A factor analysis was performed in order to understand which morphological variables measured similar morphological characteristics, and how much variance each variable described. Factor analysis is a statistical method for uncovering underlying

structures of associations between variables. Each variable is assumed to be a linear function of the factors, in which each variable is loaded to a different extent onto each factor (Gie Yong & Pearce 2013). In fields like psychology it may be used for understanding how answers to certain survey questions might give insight into general personality traits. This study aimed to use factor analysis to uncover how morphological indices vary together to describe physical characteristics of aneurysms.

Procedure

Prior to performing the factor analysis, the data was ensured to be appropriate for a factor analysis. According to Zygmunt and Smith, the sample size should be greater than 5 times as large as the number of variables (Zygmunt & Smith 2014). A sample size of 276 data sets and 30 variables per data set yields an acceptable sample-to-variable ratio of 9.2. Another consideration is the normality of the variable distributions. In order for a reliable factor analysis, each variable must be normally distributed. The normality of the distribution affects how the variables group together into factors, and depending on the amount of skew could produce incorrect results from a factor analysis. The distributions of each variable can be viewed in Appendix A. A Shapiro-Wilk (S-W) test of normality was performed for each variable, and depending on the amount and direction of skew a transformation was applied (McDonald 2014), as indicated in Table 6, in order to bring the distribution into a normal or nearly-normal distribution.

Table 6. Normality and transformations of variables.

Variable	Initial S-W p-value	Direction of skew (if present)	Transformation applied	Final S-W p-value
ARang	3.65E-14	+	Log	0.0003
ARmed	4.99E-18	+	Log	1.59E-05
ARperp	9.15E-14	+	Log	0.0379
BF	1.01E-21	+	Sqrt, Log	3.40E-18
BFarea	8.52E-26	+	Log, Sqrt	1.66E-07
CovRatioMag	2.22E-09	+	Log, 8rt	0.0005
Dang	1.76E-10	+	Log	0.0516
Dmed	8.60E-11	+	Log	0.2702
Dperp	6.70E-12	+	Log	0.0100
EIlmis	6.65E-07	+	Sqrt	0.0048
EIVdc	0.1197	None	None	0.1197
Hang	1.37E-10	+	Log	0.0180
Hmed	4.33E-13	+	Log	0.0231
Hperp	3.06E-11	+	Log	0.0648
MaxD1	1.18E-10	+	Log	0.0258
MaxD2	7.41E-12	+	Log	0.2871
MaxD3	4.45E-10	+	Log	0.0047
MaxDRatioMag	7.78E-11	+	Log, 8rt	0.0005
NSIlmis	2.72E-05	+	Sqrt	0.1053
NSIVdc	0.0066	None	None	0.0066
SRang	6.46E-09	+	Log	0.0004
SRmed	8.64E-11	+	Log	0.0128
SRperp	2.93E-10	+	Log	0.0021
TSR	7.44E-25	+	Sqrt, Log	0.1971
UI	5.13E-19	+	Sqrt, Sqrt	0.0227
IRRvdc	0.0058	None	None	0.0058
V	1.84E-24	+	Log	0.0047
Vvdc	7.87E-25	+	Log	0.0161
Vnp	5.39E-25	+	Log	0.0433

All of the variables except for NSIvdc, EIVdc and IRRvdc were highly non-normal and required transformation using a log, square-root or combination thereof. Most were successfully transformed to a nearly normal distribution, as shown in Table 6. However, ARmed, BF, and BFarea could not successfully be transformed to a normal distribution and were excluded from the factor analysis to prevent incorrect factor loadings.

Next, a preliminary factor analysis was performed with a parallel analysis of random normally distributed data generated by the statistical package.

Scree plots with parallel analysis

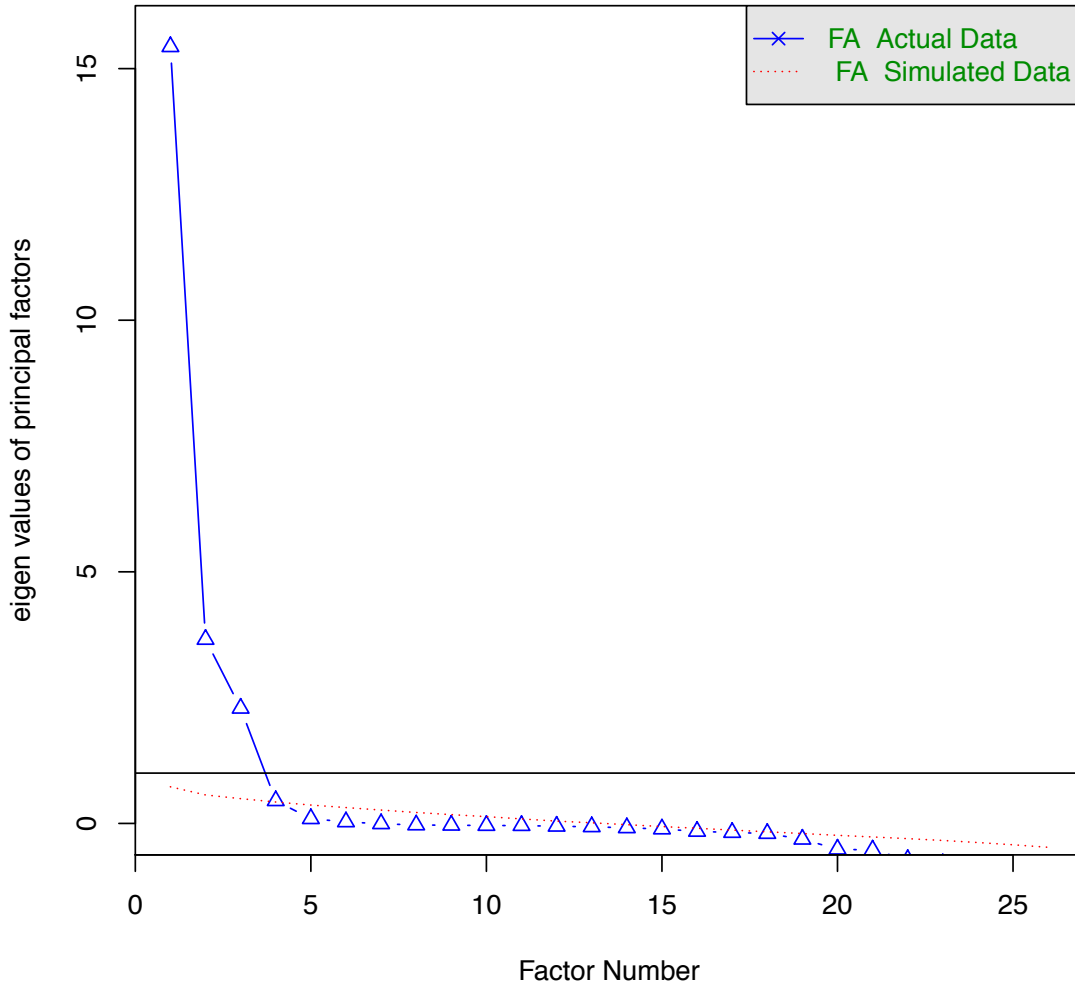


Figure 35. Scree plots with parallel analysis of simulated data. Four factors were extracted as a result.

There are many methods for determining how many factors to extract using a scree plot. In the Kaiser method all eigenvalues greater than one are extracted, because an eigenvalue of 1 is equivalent to the amount of variance explained by a single variable on

its own; however, this method has been shown to often over- or underestimate the appropriate number of factors (Zygmunt & Smith 2014; Gie Yong & Pearce 2013). Alternatively, the scree test involves denoting which factors are above a sharp elbow in the scree plot (Gie Yong & Pearce 2013). A third test involves a parallel analysis of a number of matrices of simulated data, in this case 100 (Kabacoff 2011). This scree plot shown in Figure 35 indicated that four factors were both above the elbow of the scree plot and above the simulated data, so four factors were chosen for the factor analysis. Because it was not known whether the underlying factors varied orthogonally, with no inter-correlation, a promax non-orthogonal rotation scheme was used to rotate the factors to align with the variance of the variables.

Results

The factor analysis produced a pattern matrix, Table 7, that indicates the factor score of the variables. This factor score indicates the correlation of the variables with each factor (Factor 1, Factor 2, Factor 3 and Factor 4). The communalities indicate the amount of variance within each variable that could be explained using the four factors. The proportion of variance explained by each factor is presented in Table 8. The correlation of each factor with each other factor is presented in the factor correlation matrix, Table 6. A visual representation of the alignment of each variable with each factor is presented in Figure 37. The factor diagram, Figure 36, presents a visual summary of several of the factor analysis tables. This factor diagram indicates the top correlation between each variable and factor with an arrow between the two and that correlation's factor loading displayed on the arrow. The inter-correlation between factors

is indicated by the arrows between factors, and the correlation values associated with each arrow. Values less than $|0.3|$ were considered low and not displayed on the chart.

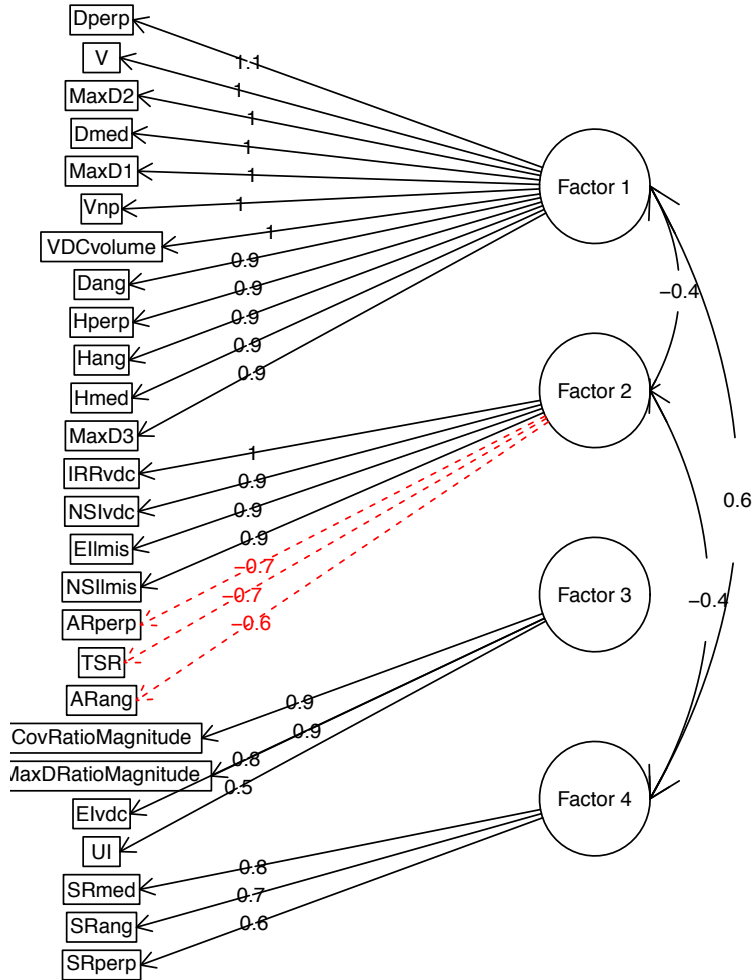
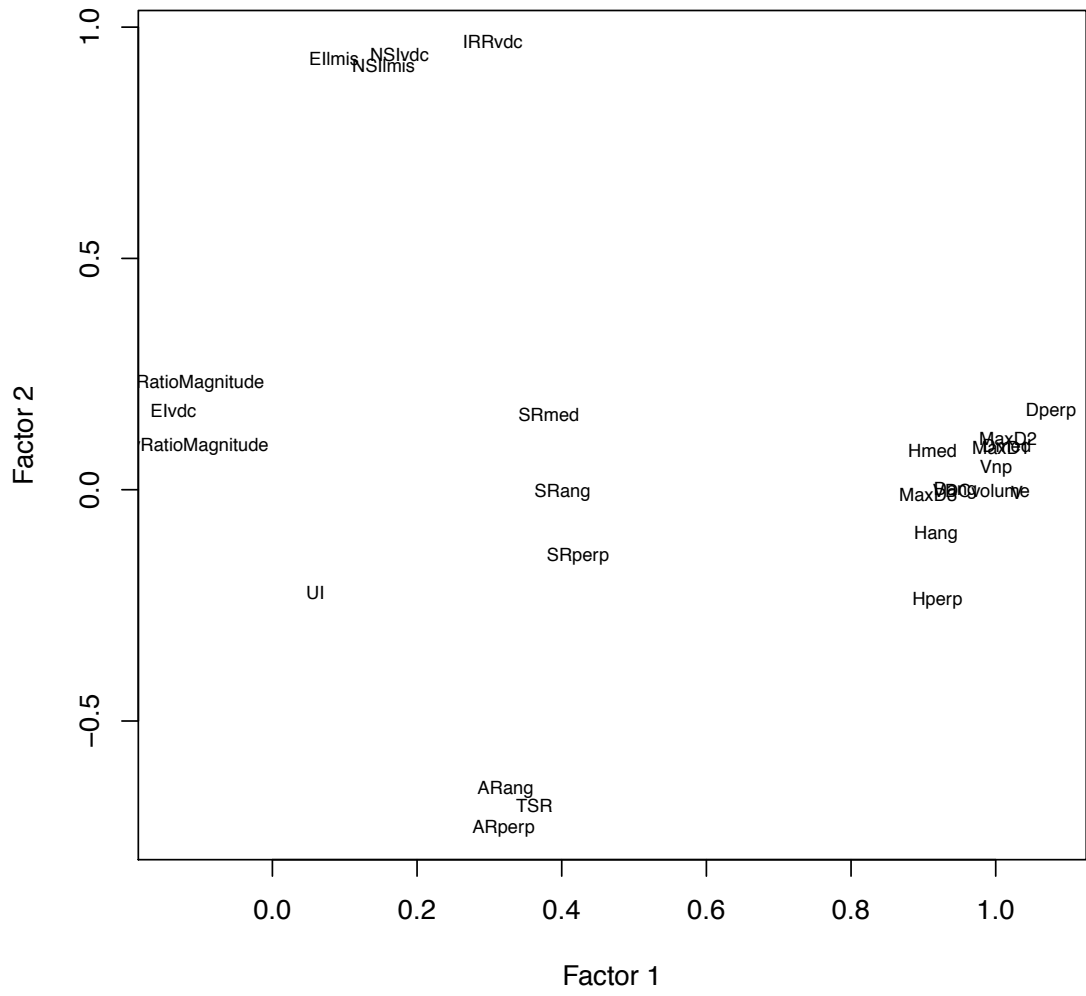
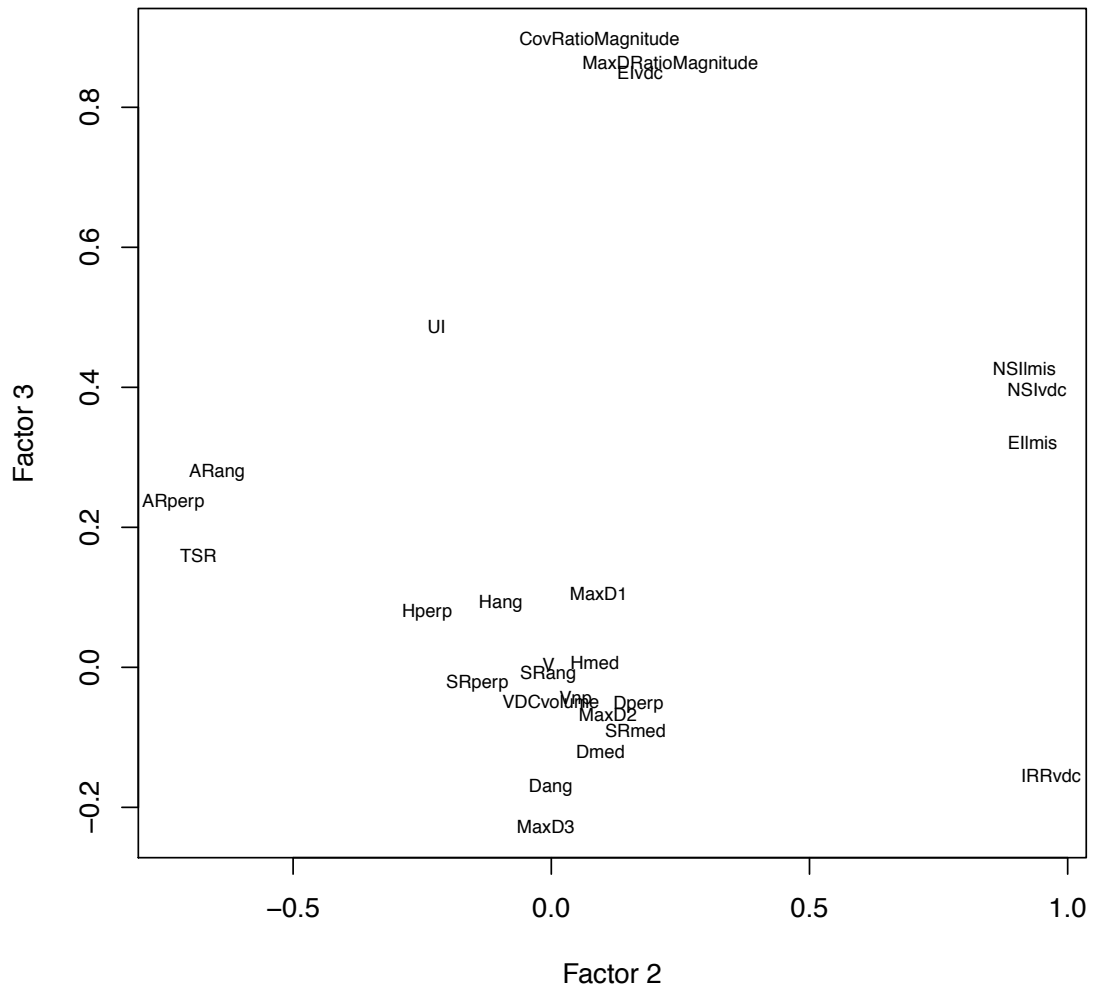


Figure 36. Factor diagram. The arrows indicating association between a variable and its underlying factor associate the variable with its factor of highest loading.





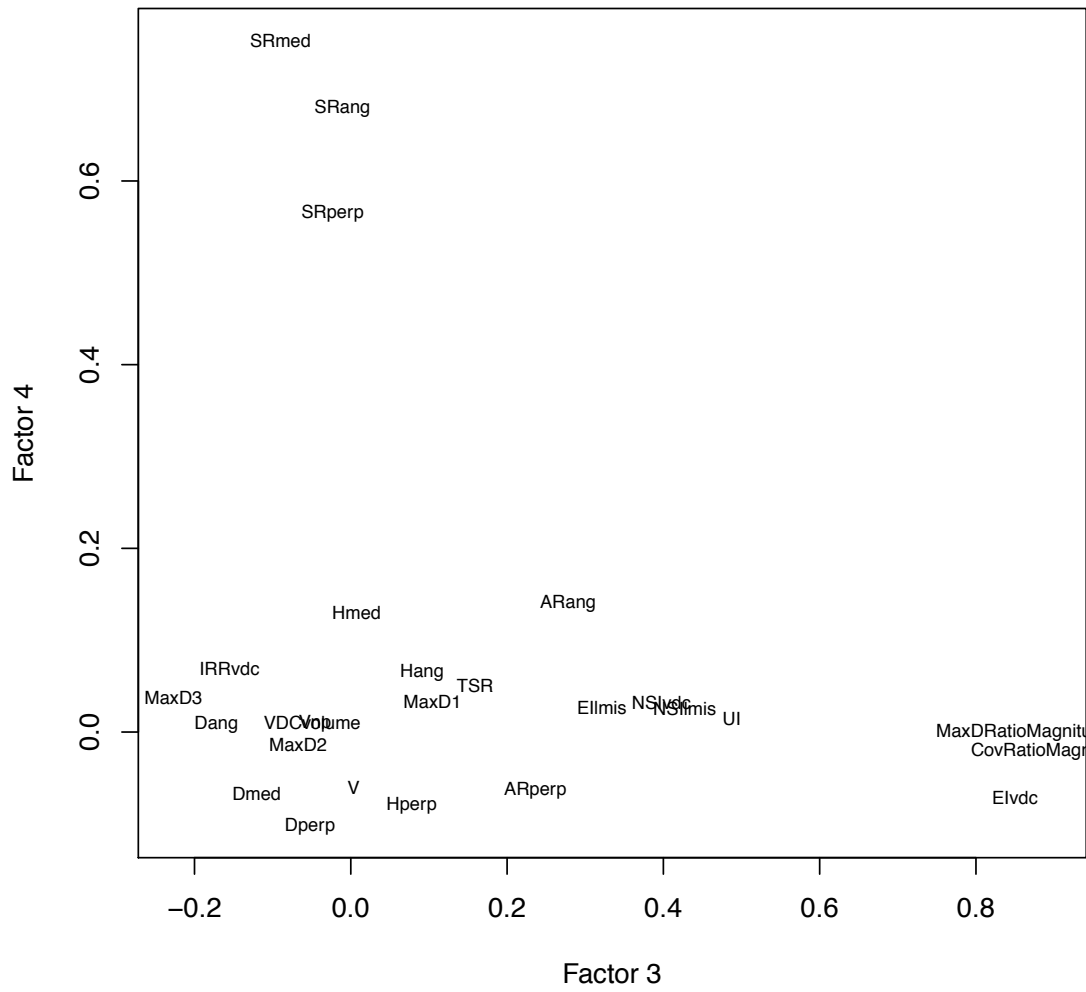


Figure 37. Biplots showing the alignment of the variables with each factor.

Table 7. Pattern matrix for the factor analysis.

Variable	Factor 1	Factor 2	Factor 3	Factor 4	Communalities
Dperp	1.08	0.17	-0.05	-0.10	0.96
V	1.03	-0.01	0.00	-0.06	0.99
MaxD2	1.02	0.11	-0.07	-0.01	0.97
Dmed	1.02	0.10	-0.12	-0.07	0.94
MaxD1	1.01	0.09	0.10	0.03	0.98
Vnp	1.00	0.05	-0.05	0.01	0.99
VDCvolume	0.98	0.00	-0.05	0.01	0.99
Dang	0.94	0.00	-0.17	0.01	0.98
Hperp	0.92	-0.24	0.08	-0.08	0.94
Hang	0.92	-0.10	0.09	0.06	0.99
Hmed	0.91	0.08	0.01	0.13	0.94
MaxD3	0.91	-0.01	-0.23	0.04	0.98
IRRvdc	0.30	0.97	-0.16	0.07	0.81
NSlvdc	0.18	0.94	0.40	0.03	0.95
EIlmis	0.09	0.93	0.32	0.03	0.92
NSIlmis	0.15	0.92	0.43	0.03	0.95
ARperp	0.32	-0.73	0.24	-0.06	0.76
TSR	0.36	-0.68	0.16	0.05	0.83
ARang	0.32	-0.65	0.28	0.14	0.87
CovRatioMag	-0.12	0.09	0.90	-0.02	0.87
MaxDRatioMag	-0.13	0.23	0.86	0.00	0.89
Elvdc	-0.14	0.17	0.85	-0.07	0.86
UI	0.06	-0.22	0.49	0.01	0.29
SRmed	0.38	0.16	-0.09	0.75	0.98
SRang	0.40	-0.01	-0.01	0.68	0.98
SRperp	0.42	-0.14	-0.02	0.56	0.94

Table 8. Proportion of variance explained by each factor.

	Factor 1	Factor 2	Factor 3	Factor 3	Total
Proportion of variance explained	50%	20%	13%	7%	91%

Table 9. Factor correlation matrix.

	Factor 1	Factor 2	Factor 3	Factor 4
Factor 1	1.00	-0.36	-0.14	0.65
Factor 2	-0.36	1.00	0.04	-0.43
Factor 3	-0.14	0.04	1.00	0.00
Factor 4	0.65	-0.43	0.00	1.00

Discussion

In examining the factor loadings in the factor diagram, Figure 36, there was a clear pattern behind the groupings of the variables. The first factor, Factor 1, explained the highest portion of the variance. It contained all of the morphological indices that measured size alone, and only morphological indices that measure size alone. In examining the variables' factor loadings, it appeared that all of these metrics mainly had a strong association exclusively with the first factor. Hperp had a slight factor loading on Factor 2. Therefore, this factor can be interpreted as describing sac size.

The second factor, Factor 2, was associated most highly with variables that, at first, appeared to measure a myriad of morphological traits. IRRvdc, NSIvdc, EIlmis and NSIImis all aligned closely and positively, and measured some form of non-sphericity. ARperp, TSR and ARang all measured the size relationship between the neck and the sac, and aligned less closely and negatively. However, in reviewing the definition for the metrics that described non-sphericity this relationship was clear. All of these metrics – IRRvdc, NSIvdc, EIlmis, NSIImis – measured the irregularity of the sac, including the

ostium region. Therefore, as the ostium region increased in size with respect to the aneurysm dome, the aneurysm shape naturally became more irregular, as demonstrated in Figure 38.

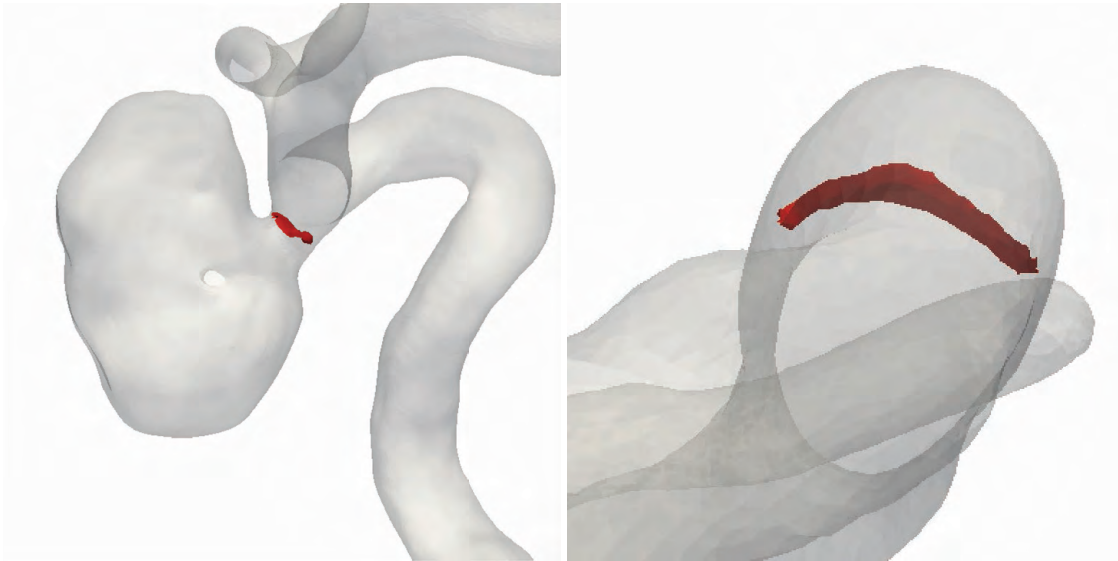


Figure 38. Aneurysm with ARang of 4.72 and IRRvdc of 0.36, left; and ARang of 0.6 and IRRvdc of 0.64, right. The increased IRRvdc in the aneurysm with a lower aspect ratio was likely caused by the indentation and sharp-edged regions of the aneurysm geometry near the ostium.

EII_{mis}, which has strong attachment to Factor 2 and moderate attachment to Factor 3, should not logically align with a factor that describes irregularity. However, it is possible that while EII_{mis} does effectively measure ellipticity, as was examined in the

Specific Aim 1 sensitivity study, it is also possible that it closely mirrors NSIImis as well, which would be worth examining in a study on its specificity.

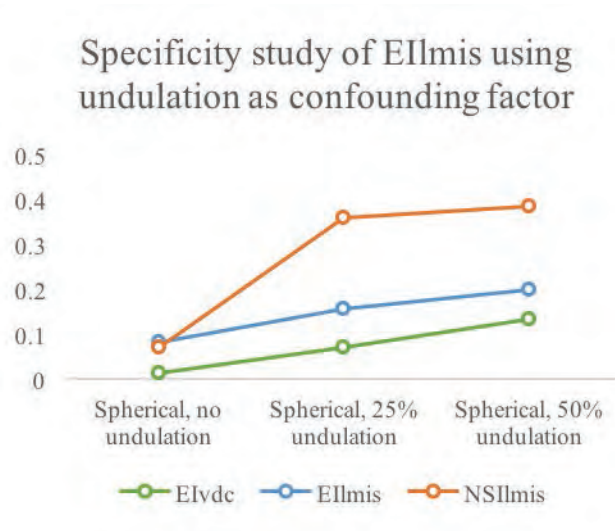


Figure 39. Specificity study of EIlmis using a spherical hypothetical idealized aneurysm with increasing irregularity (or undulation). Ellipticity should not theoretically increase, while non-sphericity should increase.

Figure 39 represents a quick examination of the specificity of EIlmis to ellipticity. The same 6mm spherical model used in the sensitivity study of non-sphericity was used, with increasing concave irregularities of 25% and 50% of the aneurysm's volume. Because the shape was symmetrical and only increased its surface undulation, the non-sphericity metrics should have increased, while the ellipticity metrics should not have increased. In this case the ellipticity metrics only increased slightly, presumably due to an unavoidable slight increase in ellipticity due to the asymmetry near the ostium region. It appears that EIlmis did not align more closely to NSIImis than other ellipticity metrics. The explanation above may not explain the alignment of EIlmis to Factor 2, and the alignment may have been due to another reason. However, as irregularity increased a slight increase in both metrics of ellipticity was present. UI, the only other variable

besides EIlmis that utilized the convex hull, had a very low communality of 29%, which indicates that the portion of the variable's variance that the rotated factors are able to successfully describe was low. It is possible that the convex hull was simply an ineffective measurement tool in specific situations, which lead to both of these phenomena. EIlmis and UI should therefore be removed from the list of recommended metrics.

The rest of the metrics that aligned most strongly with Factor 2 – ARperp, TSR and ARang – had a negative association. They also aligned moderately with both the size (Factor 1) and ellipticity (Factor 3) factors. They were all designed to simply describe the size relationship between the neck and the height, although as mentioned earlier Raghavan et al. also recognized that they would also indicate prolate/oblate nature for hemispherical aneurysms (Raghavan et al. 2005). While it is somewhat unclear why these variables were most associated with a factor that otherwise describes non-sphericity, it is likely that increased ostium size in relation to height (or lower ostium ratio) also leads to higher irregularity values. If this is the case it is most likely due to the interface of the ostium and the dome, which the non-sphericity values would view as an irregularity, encompassing a larger portion of the aneurysm geometry. Understanding that IRRvdc, NSIvdc and NSIImis all directly measure irregularity in this manner, and that the ostium-sac size relation inversely affects the likelihood that the aneurysm shape is irregular, it is clear that Factor 2 describes sac irregularity. Although the ostium-sac size relation metrics most heavily align with Factor 2, it would be most prudent to include both a metric for irregularity and a metric for ostium-sac size relation in the final set of metrics in order to most fully describe the variance.

The third factor, Factor 3, was most highly associated with variables that described ellipticity. However, the variable UI, which measures irregularity, also attached to this factor. The most plausible explanation is that the communality from Table 7 was only 29%. This is in contrast with most other variables that had communalities in the high ninety percent-range, and could lead to incorrect factor attachment. It could also be due, as discussed above, to the convex hull as a poor measurement tool.

The fourth factor, Factor 4, was most highly associated with only variables that described the relation between the aneurysm size and the vessel size.

In examining the relationships between the factors themselves in the factor correlation matrix in Table 9, there is a decent amount of correlation between Factor 1 and Factor 1. This is likely the case because as discussed above, many of the variables associated with Factor 1 are directly used in the calculation of those in Factor 4.

As a result of the factor analysis it appears that are four clear factors underlying the morphological indices: size (Factor 1), non-sphericity (Factor 2), ellipticity (Factor 3) and vessel-sac size relation (Factor 4).

As an experiment of whether including further factors in the factor analysis would alter the interpretation, the number of factors included was increased from 4 factors to 5 factors. The same procedure was run as earlier, and the resulting factor diagram is shown in Figure 40.

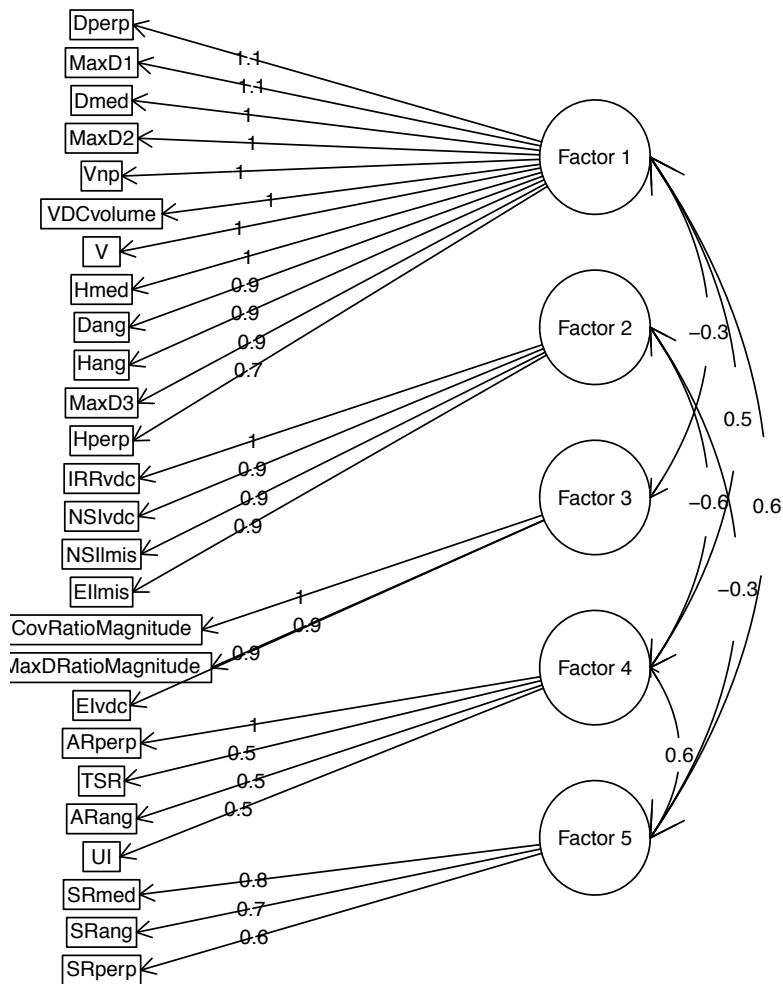


Figure 40. Factor diagram using 5 factors.

In this analysis the variables that describe the sac-ostium size relation move to a new factor, suggesting that they do, in fact, likely describe another aspect for morphology that should be analyzed independently. However, all other variables remain grouped as in the previous analysis, further reinforcing the conclusions of the factor analysis.

Conclusions toward an optimal set of morphological indices

Table 10. Overall assessment results.

Morphological characteristic	Index	Sensitivity	User Var.	Logic & Application	Predominant Factor Loading
Height	Hang	Good	Good	Good	Factor 1
	Hmed	Good	Good	Good	Factor 1
	Hperp	Good	Good	Good	Factor 1
Diameter	Dang	Good	Good	Good	Factor 1
	Dmed	Good	Good	Good	Factor 1
	Dperp	Good	Good	Good	Factor 1
Max measured dimensions	MaxD1	Good	Good	Good	Factor 1
	MaxD2	Good	Good	Good	Factor 1
	MaxD3	Good	Good	Good	Factor 1
Volume	V	Good	Good	Good	Factor 1
	Vvdc	Good	Good	Good	Factor 1
	Vnp	Good	Good	Good	Factor 1
Size ratio	SRang	Good	Good	Good	Factor 4
	SRmed	Good	Good	Good	Factor 4
	SRperp	Good	Good	Good	Factor 4
Bulge location	BLang	Good	Poor	Poor	-
	BLmed	Good	Poor	Poor	-
	BLperp	Good	Good	Poor	-
Bottleneck	BF	Good	Poor	Good	-
	BFarea	Good	Good	Good	-
Neck-sac size relation	TSR	Good	Good	Good	Factor 2
	VOR	Good	Good	Poor	-
	VORvdc	Good	Good	Poor	-
	ARang	Good	Good	Good	Factor 2
	ARmed	Good	Good	Good	-
	ARperp	Good	Good	Good	Factor 2
Prolateness	MaxDRatio12	Good	Good	Poor	-
	Cov12	Good	Good	Poor	-
Oblateness	MaxDRatio23	Good	Poor	Poor	-
	Cov23	Good	Good	Poor	-
Ellipticity	EI18	Poor	Good	Poor	-

Table 10 – continued

	EI36	Poor	Good	Poor	-
	EIImis	Good	Good	Good	Factor 2
	EIVdc	Good	Good	Good	Factor 3
	CovRatioMag	Good	Good	Good	Factor 3
	MaxDRatioMag	Good	Poor	Good	Factor 3
Irregularity	UI	Good	Good	Good	Factor 3
	IRRvdc	Good	Good	Good	Factor 2
Non-sphericity	NSI18	Poor	Good	Poor	-
	NSI36	Poor	Good	Poor	-
	NSIImis	Good	Good	Good	Factor 2
	NSIVdc	Good	Good	Good	Factor 2
	CRhnorm	Poor	Good	Good	-
Fusiformity	ESDI	Good	Good	Poor	-

As a result of the sensitivity analysis, user-variability analysis, and assessment of application and definition of the original metrics, the factor analysis assessed the most robust morphological indices, as summarized in Table 10. The factor analysis then uncovered the underlying constructs of morphology that these indices measured. Using this information, an educated decision can be made as to what morphological indices should be used in a longitudinal cohort study. In this case, because the factor loadings are generally high and some of the variables loaded on a factor by definition measure a very similar quantity, the call could be made to reduce the number of metrics in such a study; and therefore the number of hypotheses, power and costs; to one or more metrics per factor. These choices are summarized in Table 11. Some studies may lack the resources or expertise to perform an advanced morphological analysis using the algorithm developed as part of Specific Aim 1. Therefore, a surrogate measurement that could be performed manually by a clinician using only one-dimensional measurements should also

be provided. These indices should either be a directly measured index, such as Dang, or a derived index, such as SRang.

In order to describe the most prominent latent morphological structure, size, it would likely be inadvisable to simply measure MaxD2 or MaxD3 alone in order to ascertain aneurysm size. These metrics are constrained in that their measurement such that MaxD1 is always representative of the largest dimension, MaxD2 and MaxD3 must be equal to or less than MaxD1, and therefore by definition not representative of an aneurysm's full size. However, MaxD1 is unconstrained by any other metric and meaningfully represents the size of the aneurysm, and would therefore be acceptable as a single representative of size. It is interesting to note, though, that as MaxD1 varies, MaxD2 and MaxD3 also vary similarly. In describing aneurysm size, MaxD1, Dang, Dperp, Dmed, MaxD1, Hmed, Hperp, Hang, V, Vnp and Vvdc have been shown to be robust morphological indices that have strong co-variance. Therefore, it is recommended that only one of these indices should be chosen to represent aneurysm size, depending on whether a direct 1D measurement will be made by a clinician, or 3D analysis will be performed by researchers using the segmentation. MaxD1 gives the closest approximation of a physician's direct measurement of size on an angiogram. Vnp more accurately represents the volume in aneurysms that are not fully saccular when compared with V. Vvdc, while providing a volume that is less sensitive to blebs or other relatively irrelevant morphological features, may not provide a full representation of the volume due to the somewhat arbitrary 75% VDC cutoff. Therefore, although it would be valid to use any of the recommended size metrics to characterize the sac size morphological

characteristic, it is most recommended to use Vnp for automated measurements and MaxD1 for manual measurements.

In assessing sac irregularity, it appears that there are two methods by which this shape characteristic should be measured to describe the most variance. IRRvdc, NSIvdc, EIlmis and NSIImis all align very closely to Factor 2. EIlmis, as mentioned in the discussion section of the factor analysis, was not recommended for measurement because of its use of the convex hull. ARperp, TSR and ARang all align to a lesser extent, and in an inverse orientation. So in order to best describe the variation of the underlying factor for sac irregularity one of the factors that aligned most closely should be chosen. However, none of these factors are easily measured by hand, so for manual measurement a subjective classification of either “irregular” or “not irregular” should be assessed. For automatic calculation, although IRRvdc, NSIvdc, and NSIImis were all valid for measurement of the sac irregularity morphological characteristic, IRRvdc is most suggested because it logically most directly measures irregularity.

Because of the logical disconnect between the morphological indices that describe the sac-ostium size relation and those that describe sac irregularity, and the results of the analysis with the inclusion of a 5th factor, it is recommended to assess these metrics in addition to the irregularity metrics. ARang is less sensitive to orientation of the ostium, the most likely source of user variability, than ARperp and therefore most recommended, although both metrics have been shown to be sufficiently robust.

Sac ellipticity can be characterized by MaxDRatioMagnitude for manual measurements. CovRatioMagnitude and EIVdc can be extracted using automated

measurements to describe sac ellipticity. UI has poor alignment with this factor, and poor overall communality, so it is not recommended for use. EIVdc is a more thorough measurement for ellipticity because it captures ellipticity that may not be aligned with the principal axes of a best fit ellipse and compliments nicely to IRRvdc, so it is most highly recommended for automated measurements. MaxDRatioMagnitude, while shown to have relatively poor inter-user variability, is easily calculated using manual measurements.

Sac-vessel size relation can be described using any of SRmed, SRang or SRperp. All three are very similar in definition and had good alignment with the factor, and would all work for either manual or automated measurement. SRang was chosen as the most highly recommended metric for sac-vessel size relation because it is less sensitive to orientation of the ostium, the most likely source of user variability.

Table 11. Recommended choices for morphological indices using either automated or manual measurements. The most highly recommended morphological index for each morphological factor is highlighted in bold.

Underlying Morphological Factor	Recommended choices for morphological indices using automated measurement	Recommended choices for morphological index using manual measurement
Sac size	Vnp	MaxD1
	V	Dmed
	Vvdc	Dperp
		Dang
		Hmed
		Hperp
		Hang
Sac Irregularity	IRRvdc	Subjective visual assessment [irregular / not irregular]
	NSIvdc	
	EIIImis	
	NSIImis	
Sac-ostium size relation	TSR	ARang
		ARperp
Sac ellipticity	EIVdc	MaxDRatioMagnitude
	CovRatioMagnitude	
Sac-vessel size relation	SRang	SRang
	SRperp	SRperp
	SRmed	SRmed

Limitations

As with any study that utilizes imaging data in assessing cerebral aneurysm morphology, the extent to which the morphology of an aneurysm can be characterized is dependent upon the quality and resolution of the medical images. MR and CT, for instance, produce images with resolutions that may be lower than certain morphological

features such as small surface irregularities. Additionally, all of these images can only capture the portion of the lumen into which blood circulates, so in areas of low flow within the aneurysm sac, certain morphologies may be obscured by low contrast.

In terms of limitations specifically of this study, several morphological characteristics remained undescribed because of unforeseen problems. The angle metrics, such as $\theta_{\text{neck-vessel}}$, could not be included because of oversight in the protocol to include blood-flow orientation when choosing vessel reconstruction direction. Fusiformity was not included because it was discovered that ESDI did a poor job of characterizing the morphological characteristic in certain circumstances. Due to the inability to transform highly skewed distributions, BF, BFarea and ARmed could not be included in the factor analysis.

SPECIFIC AIM 3:
DEMONSTRATION OF USE OF OPTIMAL METRICS TO TEST
HYPOTHESIS

Background

When a patient is diagnosed with a cerebral aneurysm the physician makes his or her recommendation to treat or not to treat based on certain characteristics of the patient and the aneurysm. Etminan et al. in 2014 suggested that physicians do already look at certain aspects of morphology as an indicator of rupture risk, and that selection bias likely varies by clinical site. Ramachandran et al. in 2016 hypothesized that in their small longitudinal cohort study a selection bias may be present. A measurement of this selection bias would be helpful in constructing future studies to determine if study populations of unruptured, untreated aneurysms are representative of the total population prior to physician treatment selection.

Study groups

The study population consisted of 54 unruptured cerebral aneurysms of patients presenting at two clinical centers – University of Iowa Hospitals and Clinics (UI) and the Pennsylvania State University Hershey Medical Center (PSU). Study subjects were placed in one of two groups – observation group and treatment group. Observation group consists of unruptured aneurysms that were placed on untreated observation while the treatment group consists of unruptured aneurysms that were chosen for treatment. In addition, to perform a controlled investigation, the aneurysms in these groups were size and location matched. To recruit subjects, a retrospective search was conducted at UI and

PSU clinical database. For each aneurysm in the BioMOST database (these are observation-only unruptured aneurysms reported in Ramachandran et al. 2006) from each of these two centers, size and location matched counterpart unruptured aneurysm that was chosen for treatment was identified retrospectively. Size matching allowed for ± 1 mm in clinically measured sac size.

The retrospective search yielded 13 matched pairs from the University of Iowa Hospitals and Clinics (UI) and 14 matched pairs from the Pennsylvania State University Hershey Medical Center (PSU).

Procedure

The treatment group data-sets were segmented using the VMTK level-set segmentation technique. A surface mesh was then extracted and optimized using an element target area of 0.1mm. Each data-set was then processed using the isolation and morphological analysis protocol as detailed in Specific Aim 1. The indices chosen as an outcome of Specific Aim 2 (except sac size and sac-vessel size relation, which were prescribed as part of the enrollment criteria in this study) were analyzed using a paired Wilcoxon signed rank test to test each metric for the hypothesis that each would be different in the treated group versus the untreated group. This analysis was performed using the marquee indices for manual measurement and for automated measurement. All statistical analysis was performed using the R statistical package.

Results

The values for each morphological index are plotted with the box plots in Figure 41 and Figure 42. The statistical results of the Wilcoxon signed rank test are listed in Table 12 and Table 13.

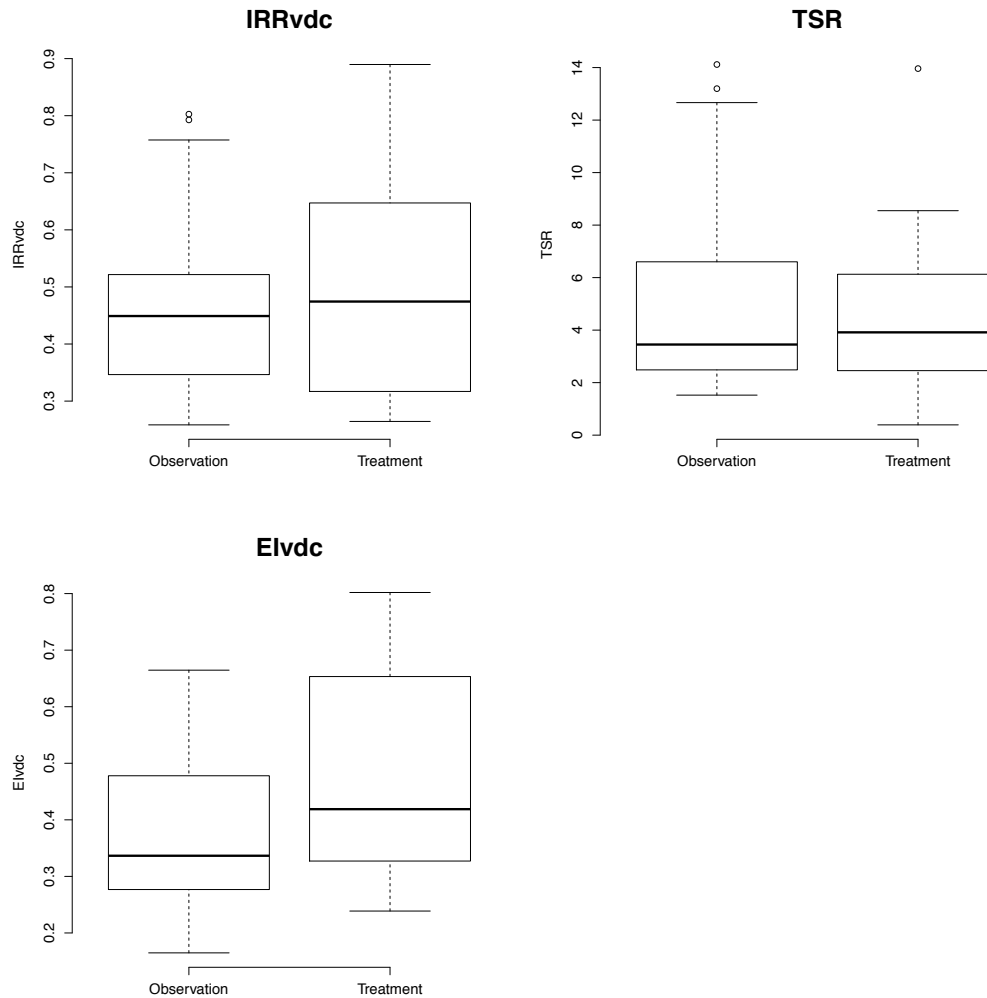


Figure 41. Comparison of observational and treatment groups using marquee morphological indices for automated measurement. EIVdc showed a significant difference between the observational and treatment groups.

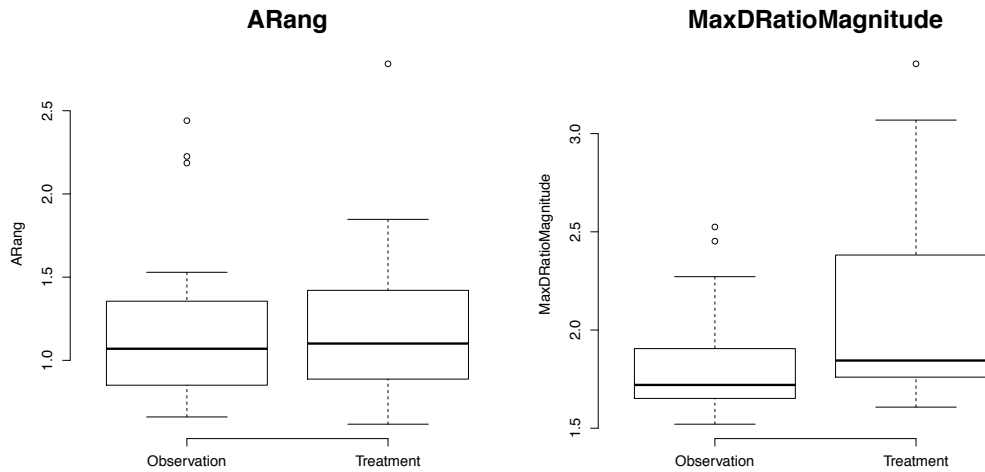


Figure 42. Comparison of observational and treatment groups using marquee morphological indices for manual measurement. MaxDRatioMagnitude was significantly different between the observational and treatment groups.

Table 12. Results from Wilcoxon test between observational and treatment groups using the marquee morphological indices derived using automated measurement. Elvdc was significantly different between the treated aneurysms and the follow-up aneurysms.

Morphological Index	Treatment			Observational			P-Value
	Min	Med	Max	Min	Med	Max	
IRRvdc	0.26	0.47	0.89	0.26	0.45	0.80	0.485
TSR	0.39	3.92	13.96	1.52	3.45	14.12	0.953
Elvdc	0.24	0.42	0.80	0.16	0.34	0.66	0.012

Table 13. Results from Wilcoxon test between observational and treatment groups using the marquee morphological indices derived using automated measurement. MaxDRatioMagnitude was significantly different between the treated aneurysms and the follow-up aneurysms.

Morphological Index	Treatment			Observational			P-Value
	Min	Med	Max	Min	Med	Max	
ARang	0.62	1.10	2.78	0.66	1.07	2.44	0.546
MaxDRatioMag	1.61	1.84	3.36	1.52	1.72	2.52	0.009

Discussion

This study serves to examine the morphological features that physicians might already be selecting as criteria for aneurysm treatment. The morphological index that measured irregularity, IRRvdc, was not significantly different between the two groups. Neither were morphological indices that measured sac-ostium size relation, ARang and SRang. However, the two indices that measured ellipticity, EIVdc and MaxDRatioMagnitude, were significantly different between the observational and treatment groups. This indicates that physicians might already be accounting for shape characteristics such as ellipticity in assessing rupture risk. In fact, in a survey of aneurysm clinicians sac ellipticity was listed as one of the factors that was used in selecting between treatment and observation, although it was determined to be considered of low importance (Etminan et al. 2014). Another interesting finding is the fact that the ellipticity metrics were found to be significantly different between the two study groups for both manual and automatic measurement, while the other morphological metrics were not significantly different between the study groups. This serves to highlight the fact that

the morphological indices that are grouped to measure a particular morphological characteristic do, in fact, produce similar results, and are independent from indices that measure other morphological characteristics.

CONCLUSIONS

Many studies have introduced novel morphological indices. While a large number of indices has been developed, there has been no consolidation of such metrics. Some indices are poorly defined for their application in measuring their intended morphological characteristic, and many redundantly measure similar morphological characteristics. Many studies have demonstrated particular morphological differences between ruptured and un-ruptured aneurysms, but the field has not yet seen a large longitudinal cohort study to sufficiently assess the use of aneurysm morphology in the assessment of aneurysm rupture risk. One small longitudinal study has been performed, but was limited in that no ruptures occurred, and that the group of morphological indices it analyzed may not have been sufficient to fully assess all relevant aspects of cerebral aneurysm morphology.

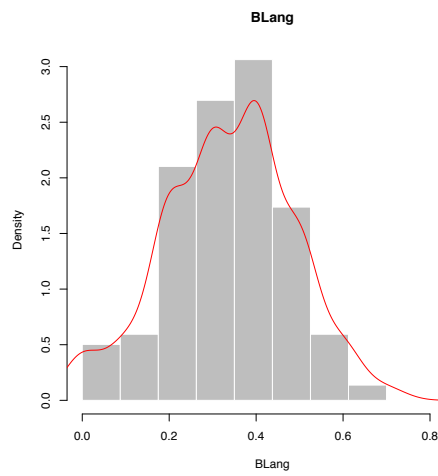
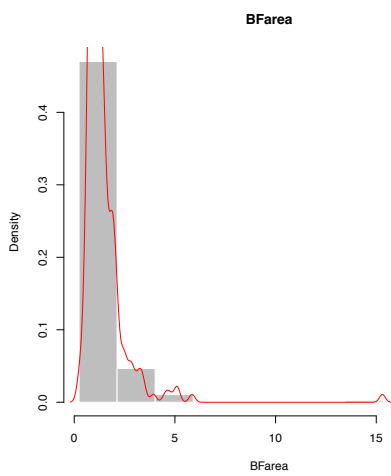
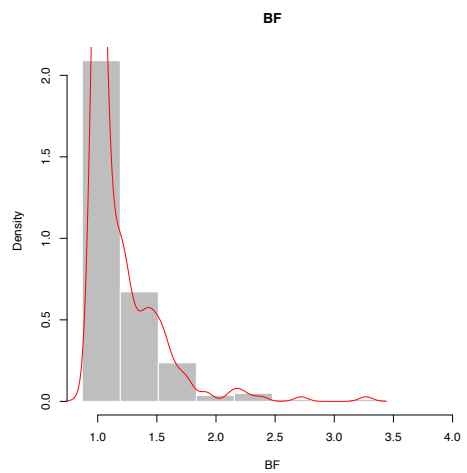
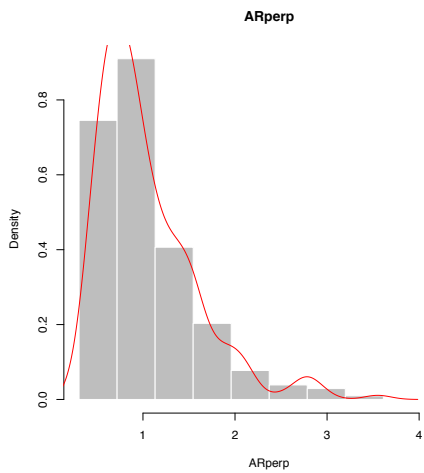
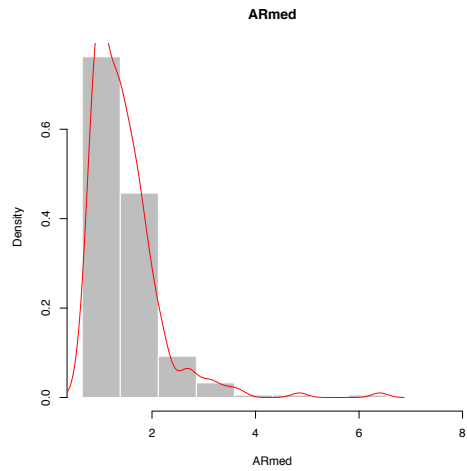
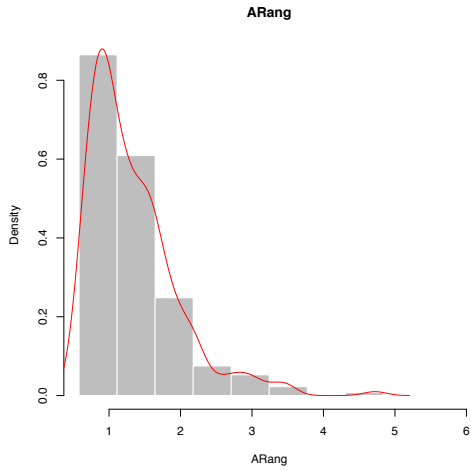
This dissertation assessed all relevant morphological traits for cerebral aneurysms. It then consolidated indices from the literature, and developed novel morphological indices to quantify the morphological traits that were not yet been described in the literature. Fully automated software was developed using popular open-source platforms, and a protocol was developed for efficiently and accurately processing segmented medical image data sets and obtaining morphological index measurements. A population of 276 unruptured patient specific aneurysms was assessed using these morphological index calculations. Each morphological index's susceptibility to inter-user variability was assessed using an 8-aneurysm patient-specific subset. Each morphological index's sensitivity to variations in the morphological trait it was designed to measure was assessed using hypothetical idealized aneurysm models. Each morphological index was

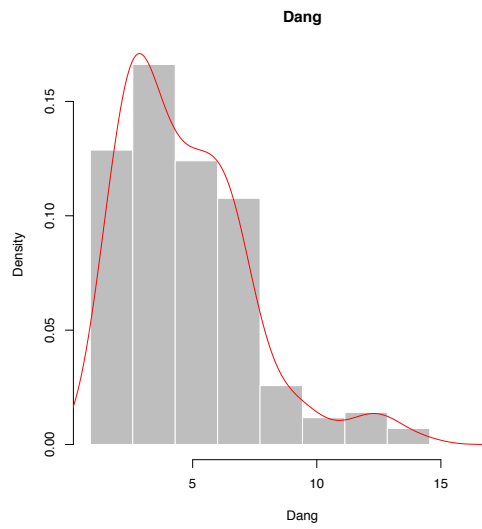
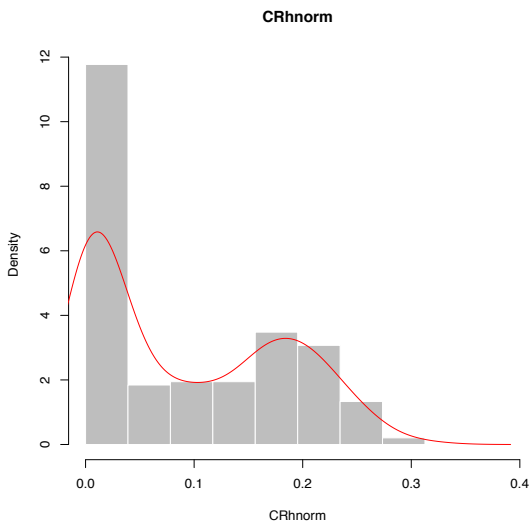
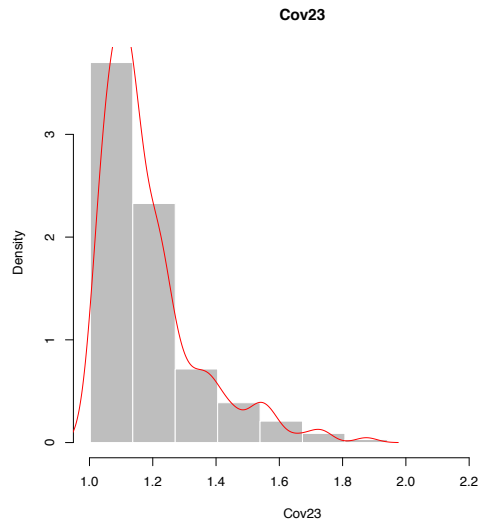
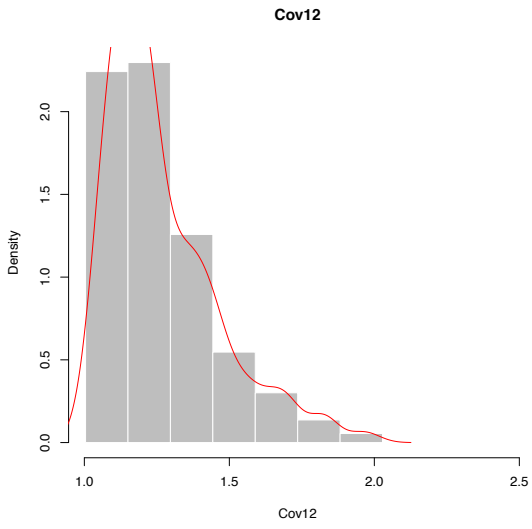
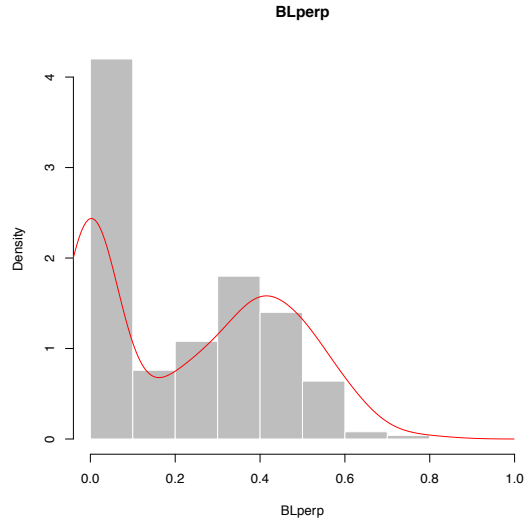
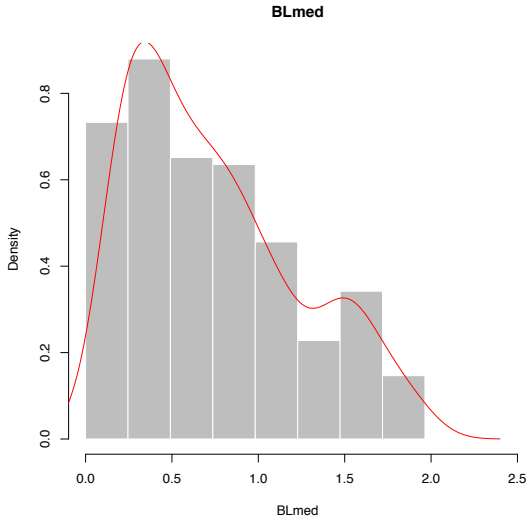
analyzed logically to ensure that it was defined in a manner that appropriately assessed cerebral aneurysm morphology. A factor analysis was then performed using a data set of 276 unruptured aneurysms. This factor analysis revealed the underlying morphological traits that the morphological indices measured, and provided an estimate of the amount of variance in the population that those morphological traits described. The morphological traits that described the most variance in the data set were interpreted to be size, sac irregularity, neck-sac size relation, sac ellipticity, and vessel-sac size relation. From this information an optimal set of morphological indices was defined for studies that would use manual measurements of aneurysm morphology and for studies that would use automated measurements of aneurysm morphology. A study was then performed as a demonstration of the use of this optimal set of morphological indices. It assessed the hypothesis that these morphological indices were different in aneurysms that had been selected for treatment than those that aneurysms that had been selected for untreated observation. The morphological indices that described sac ellipticity were found to be different between the treatment and untreated observation groups. It also demonstrated that different morphological indices that measured the same morphological factors produced similar results when assessing aneurysm morphology in patient populations.

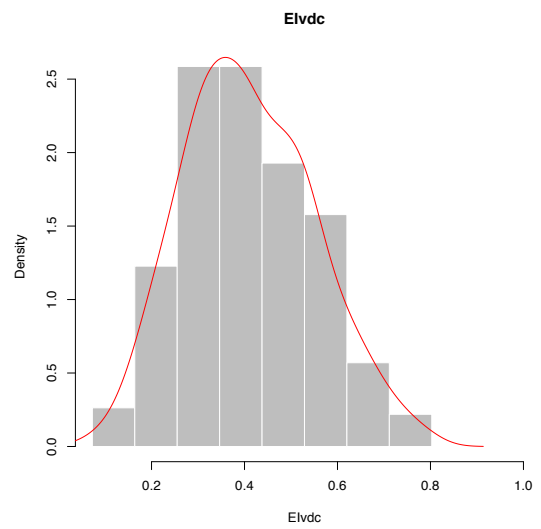
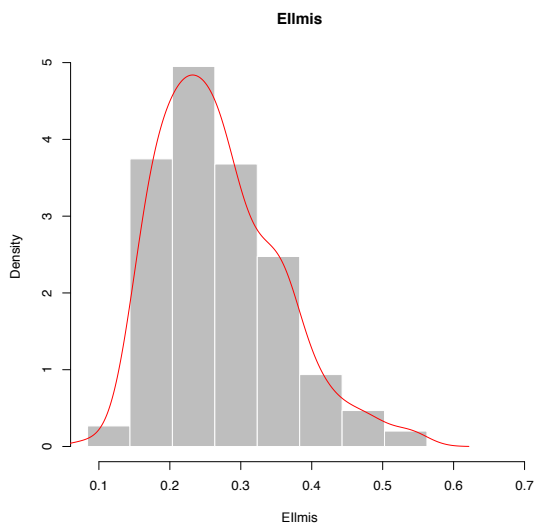
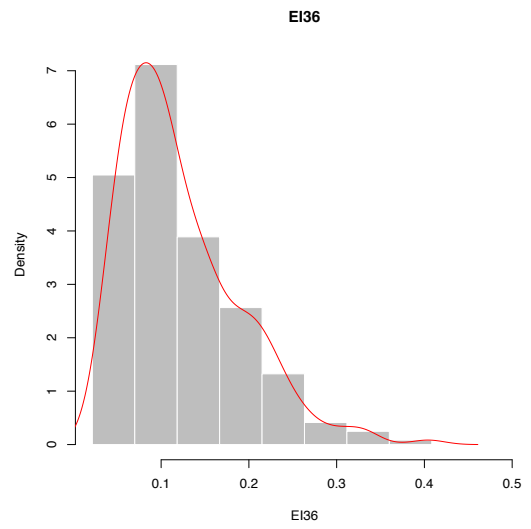
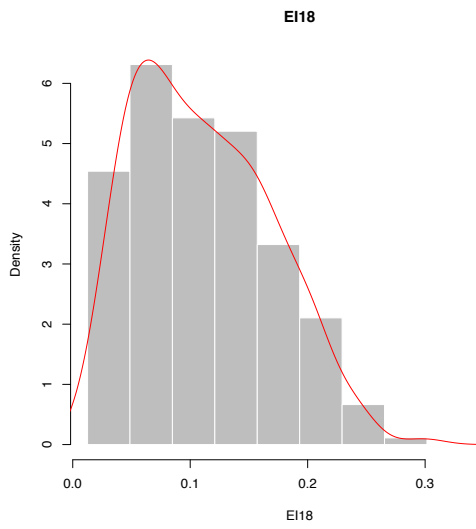
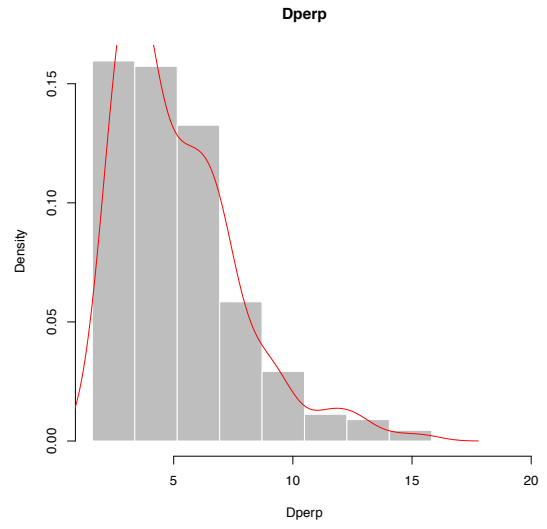
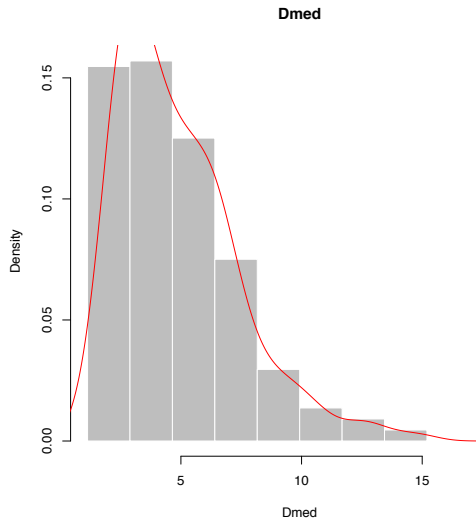
Ultimately, this dissertation progressed the field by defining methods to fully assess the relevant morphological features of aneurysms using an optimal set of morphological indices – a necessary step prior to performing the sweeping longitudinal cohort study that the field requires. It also suggested to the field that physicians may already be recommending aneurysms for treatment or observation based upon certain aspects of morphology, which merits further research.

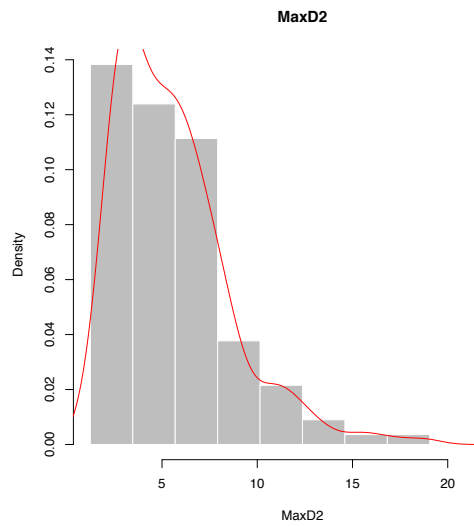
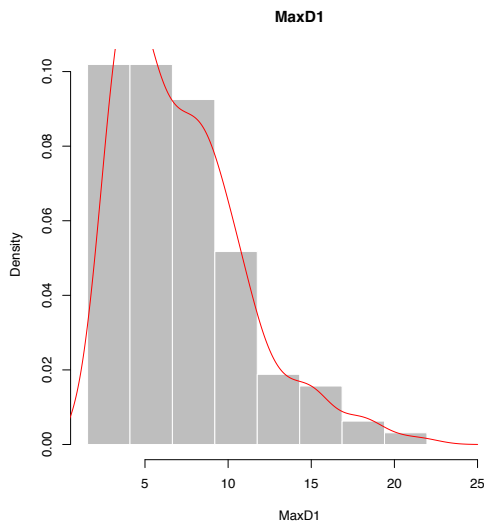
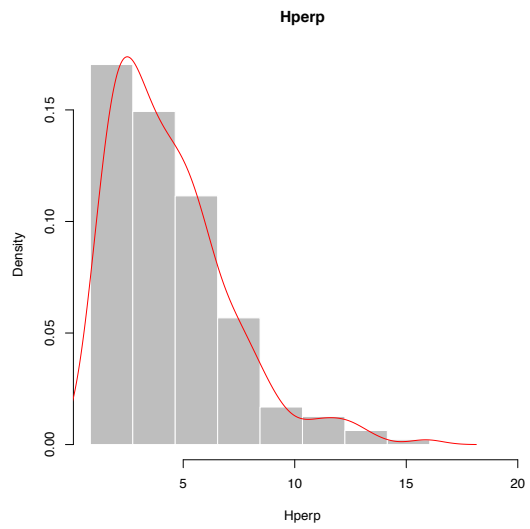
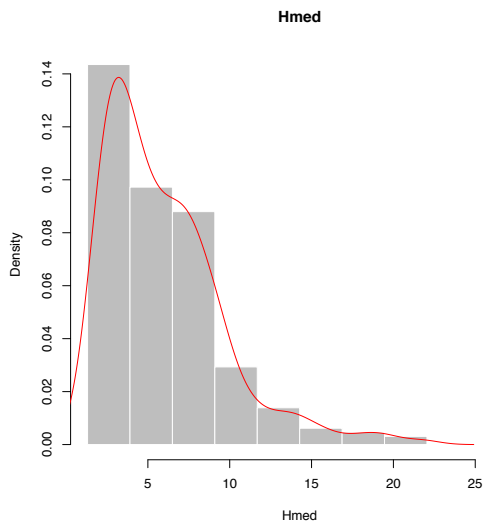
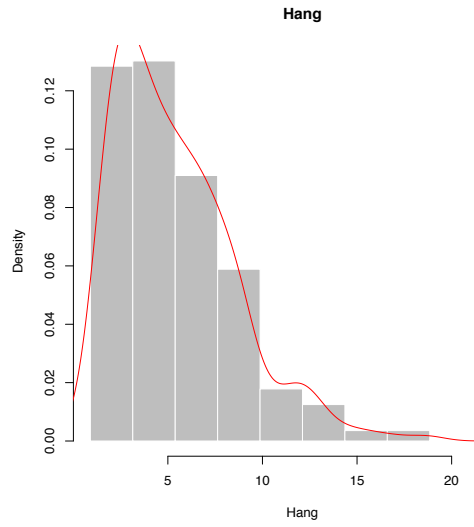
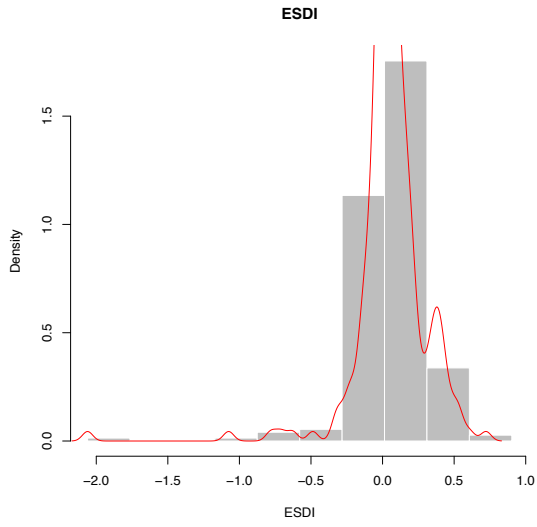
APPENDIX A

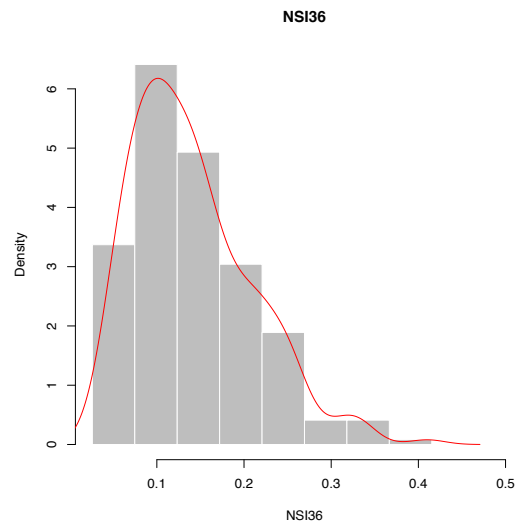
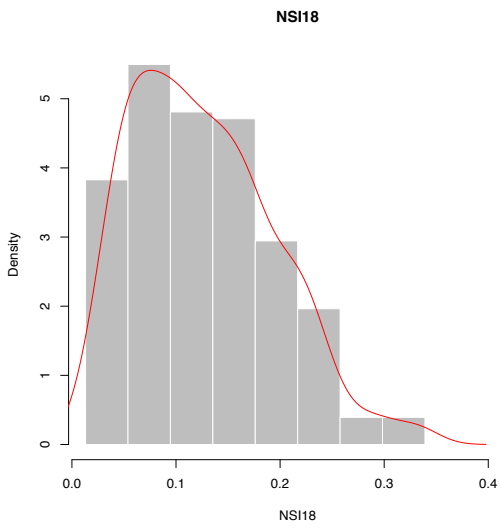
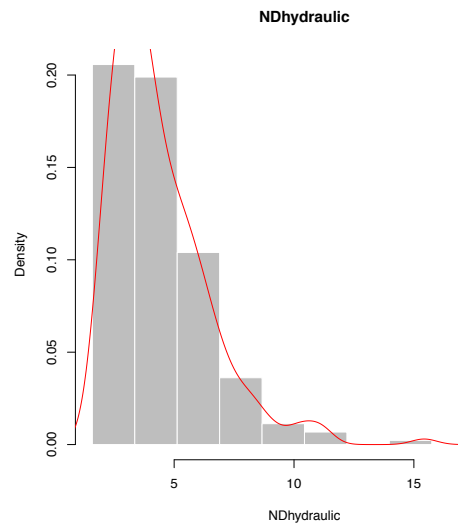
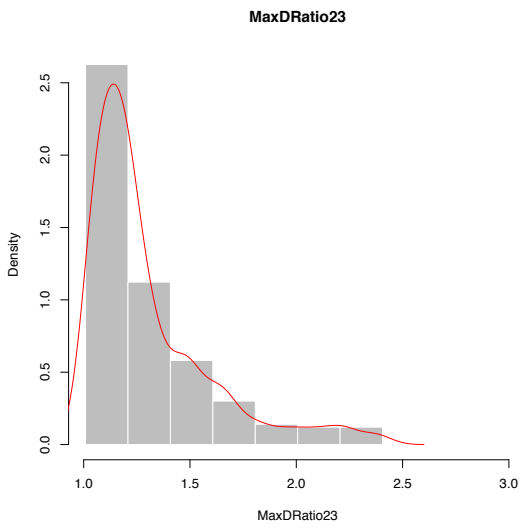
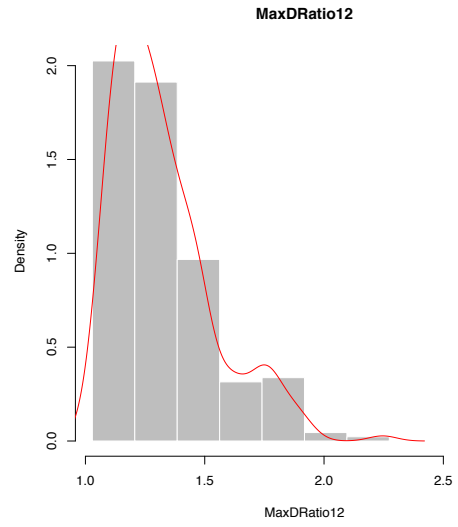
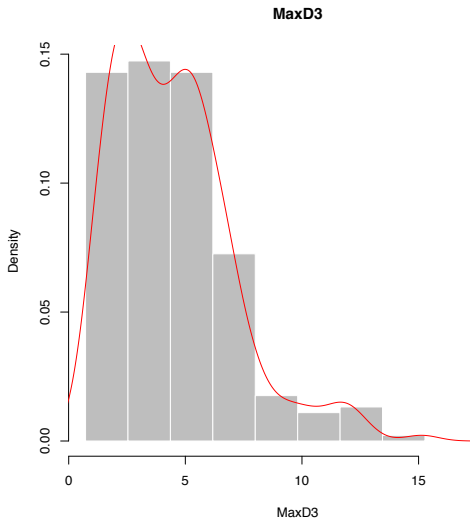
DISTRIBUTIONS OF THE MORPHOLOGICAL INDICES

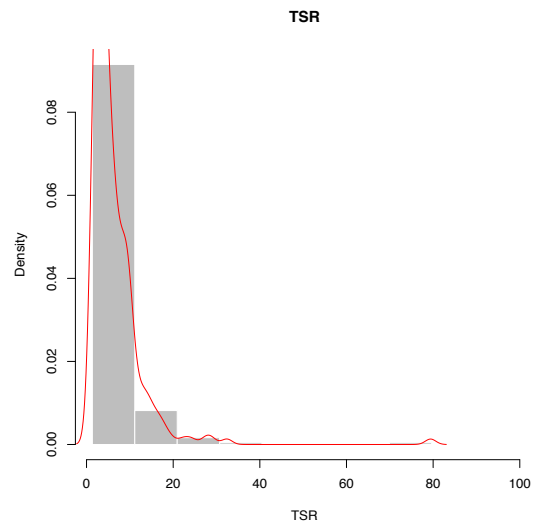
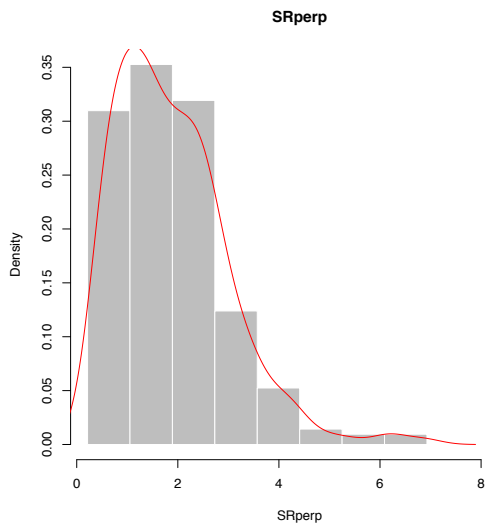
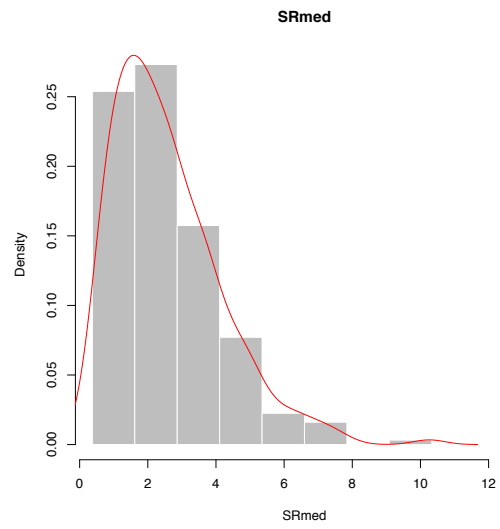
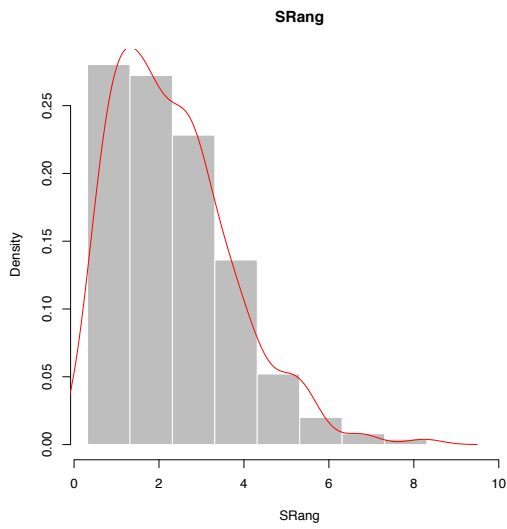
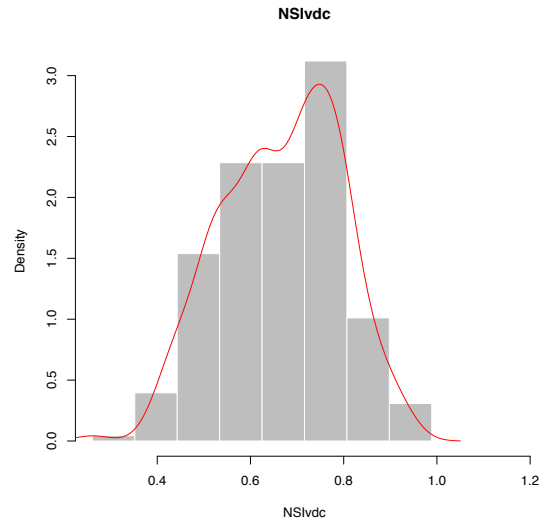
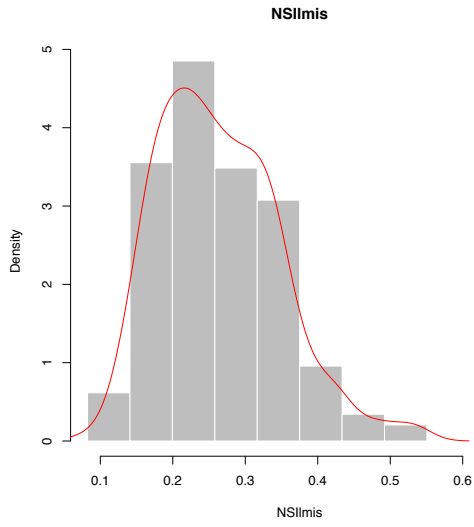


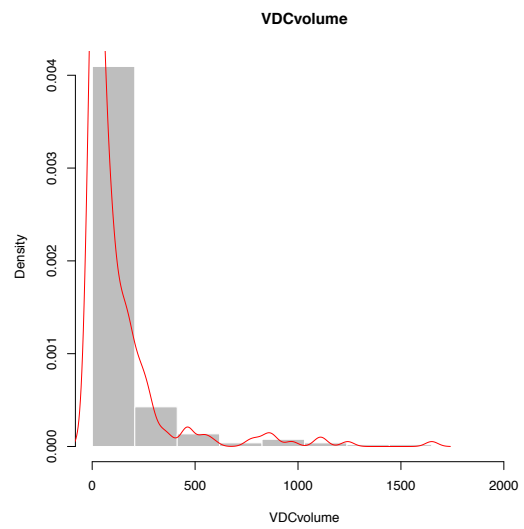
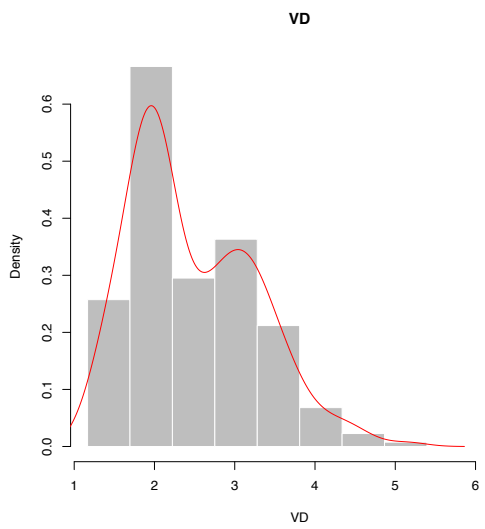
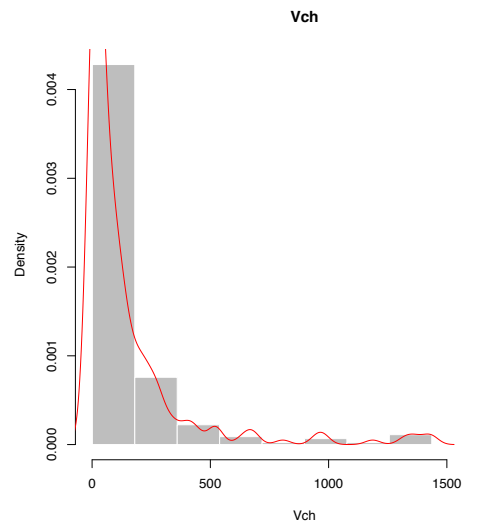
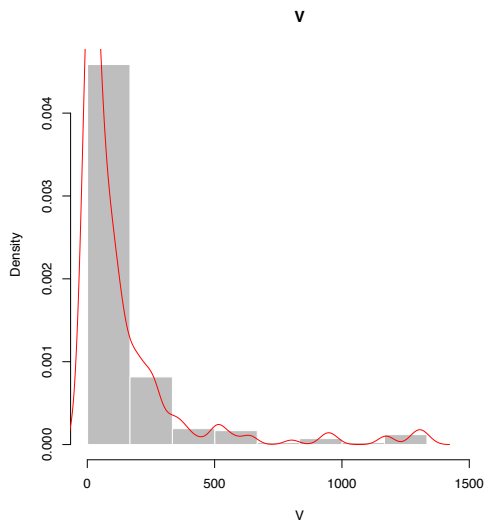
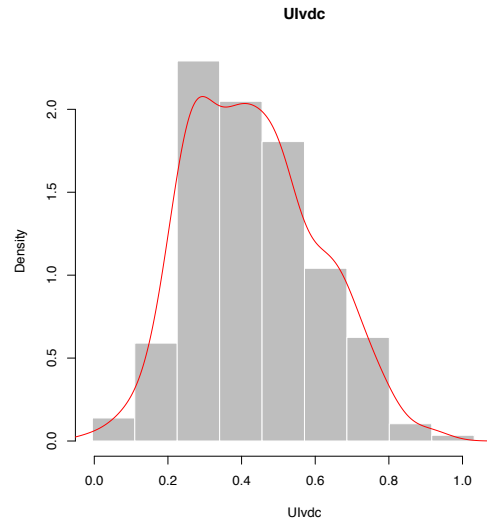
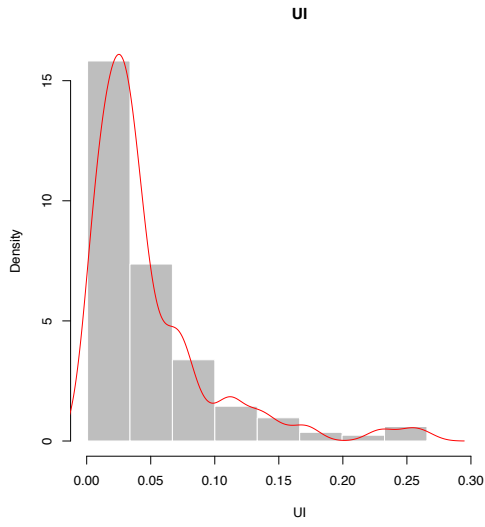












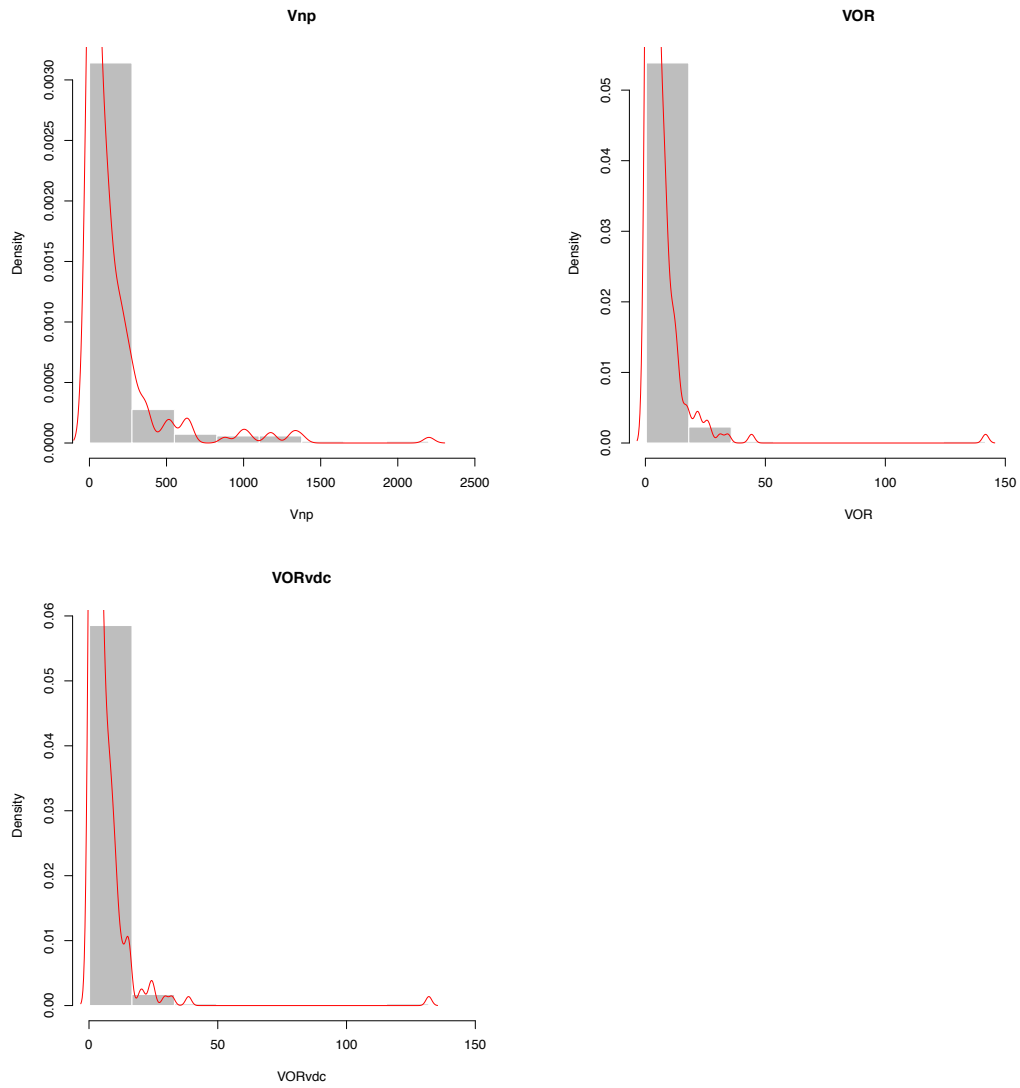
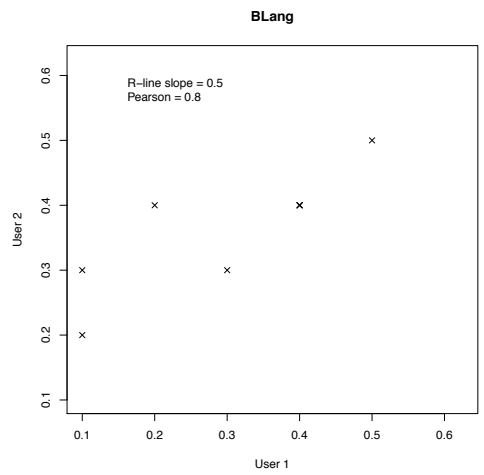
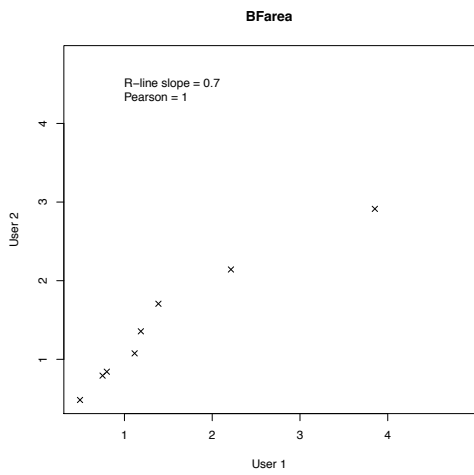
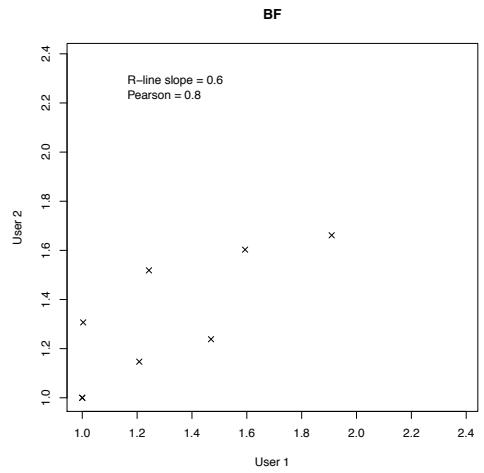
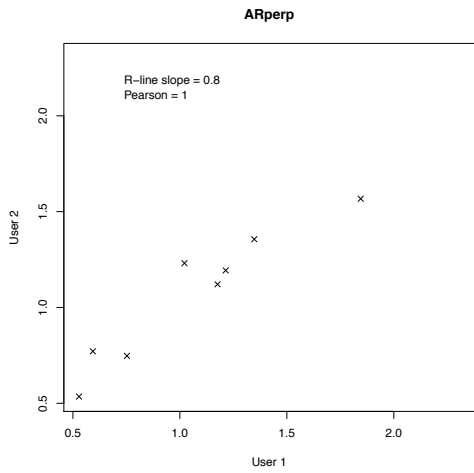
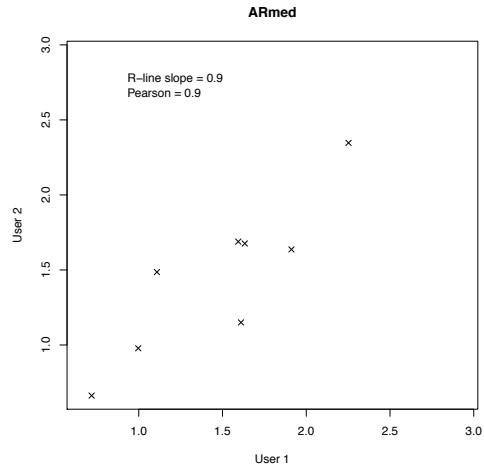
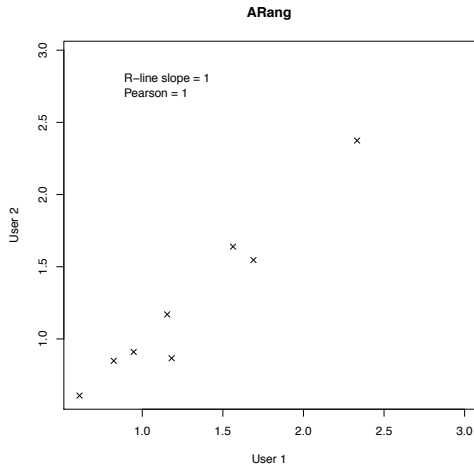
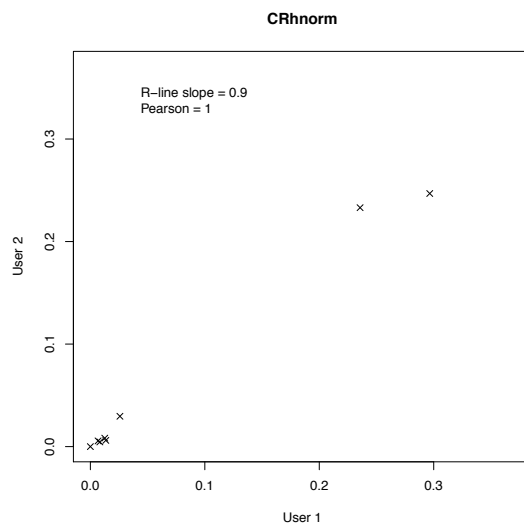
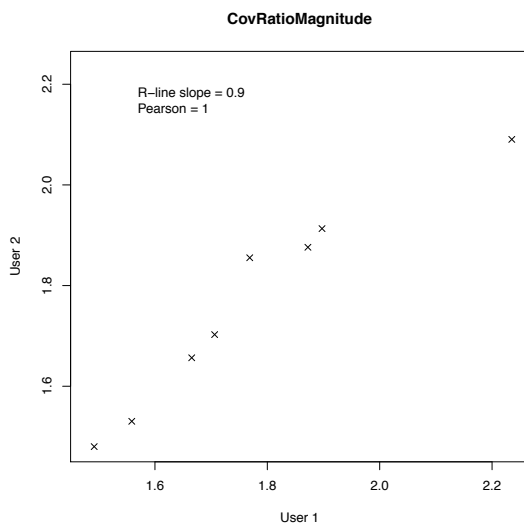
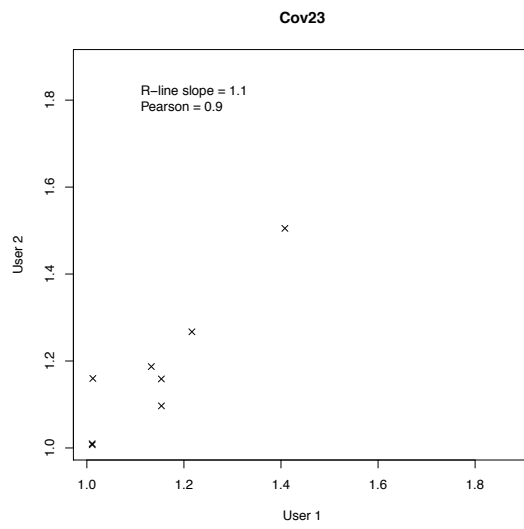
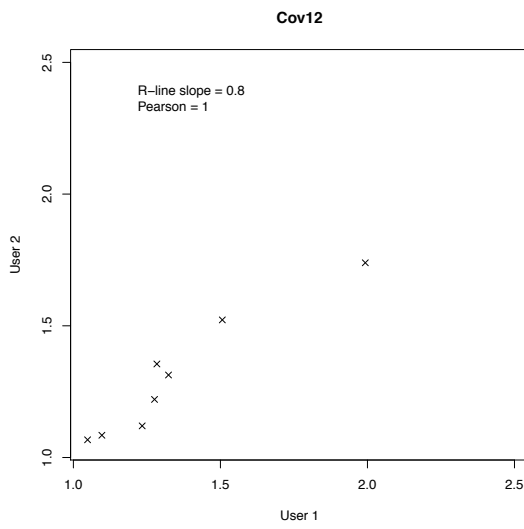
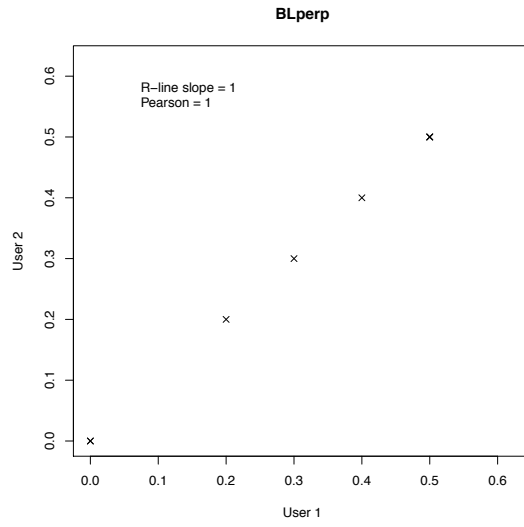
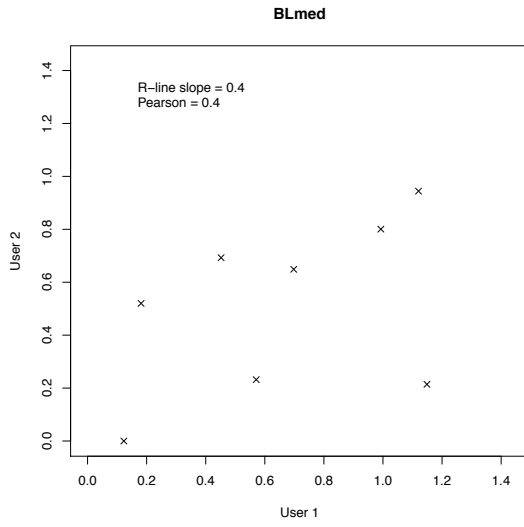


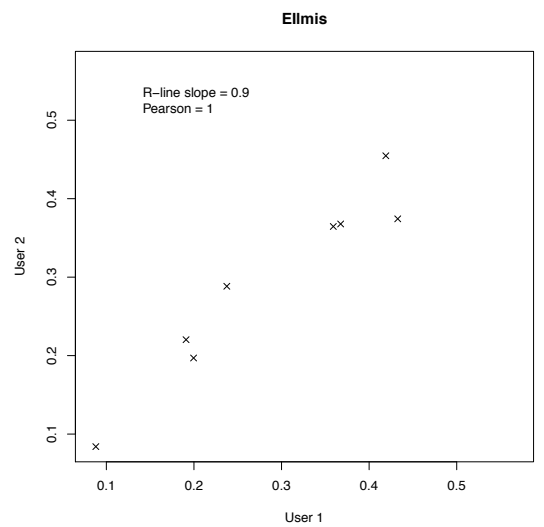
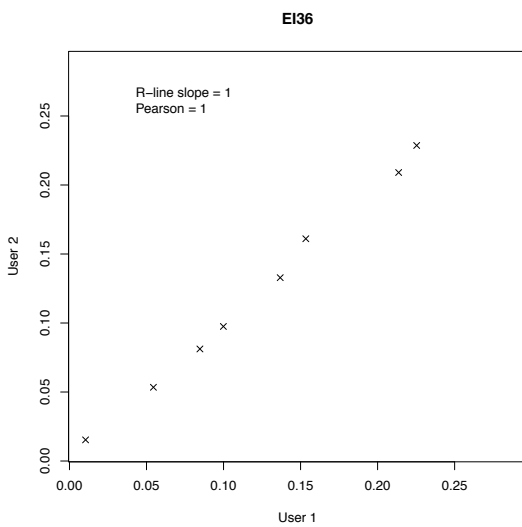
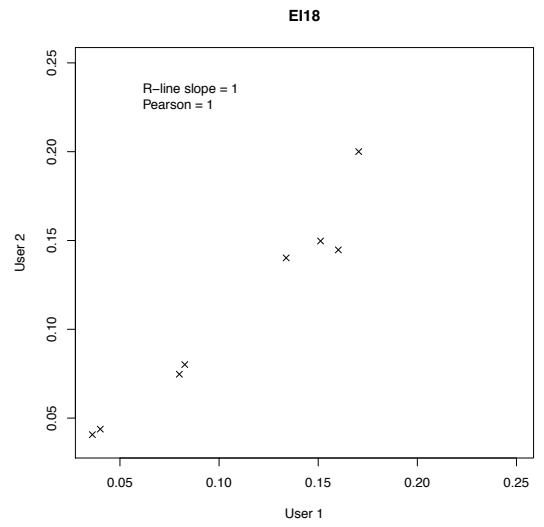
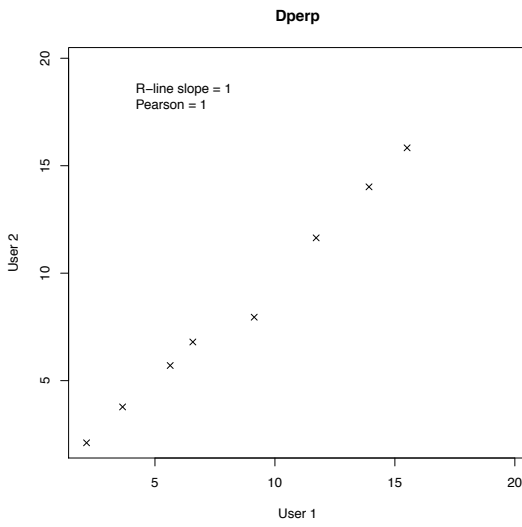
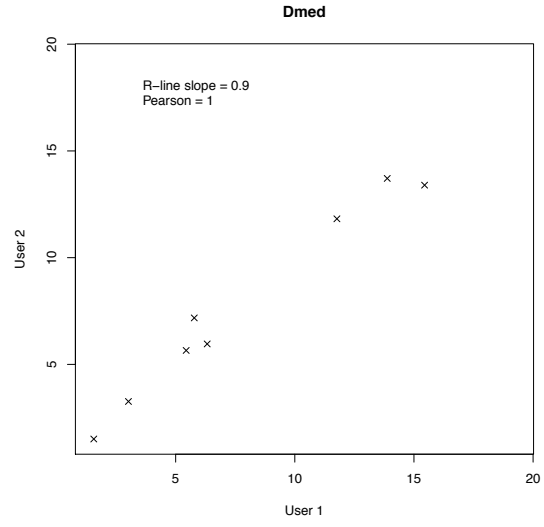
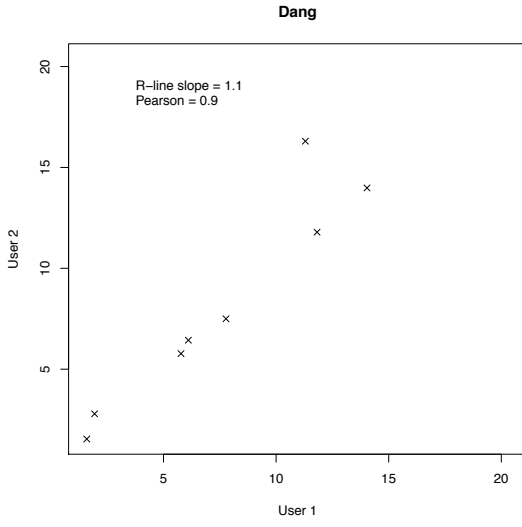
Figure A.1. Distribution plots of the morphological indices prior to transformation.

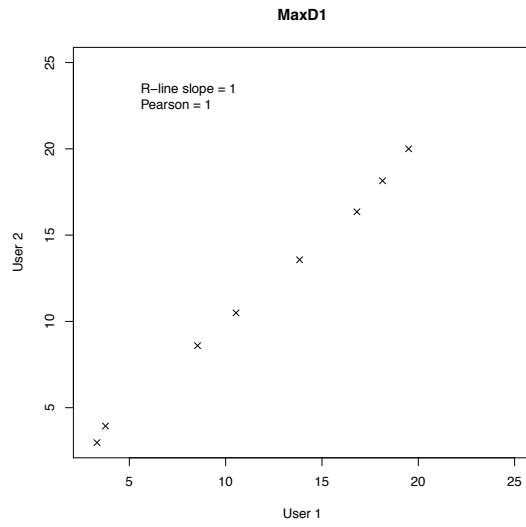
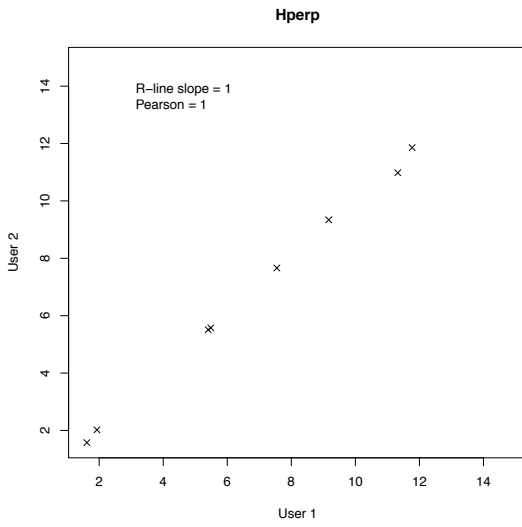
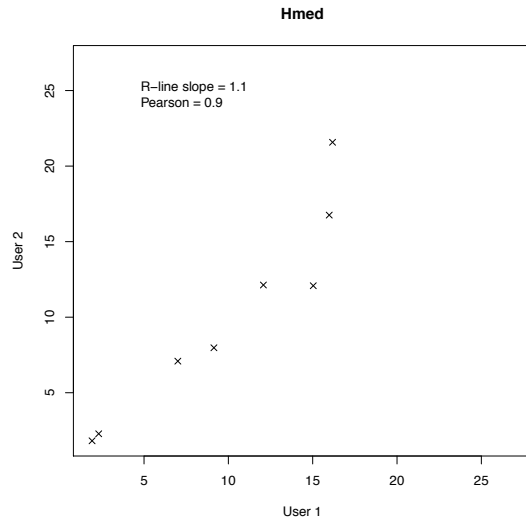
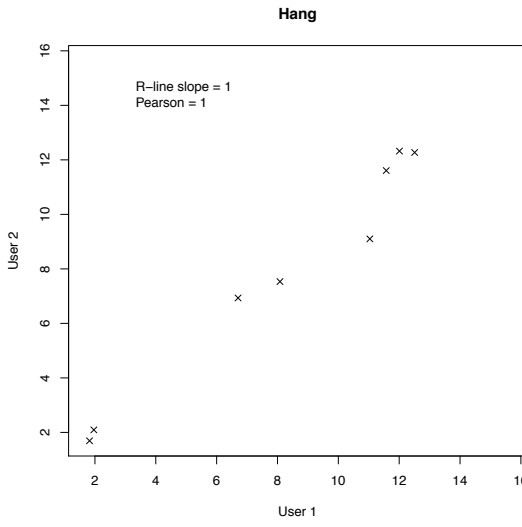
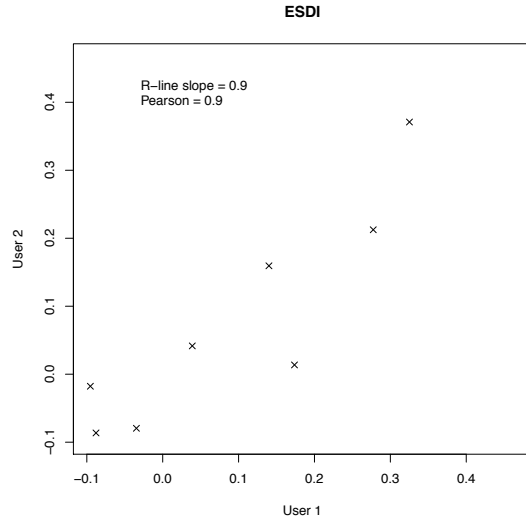
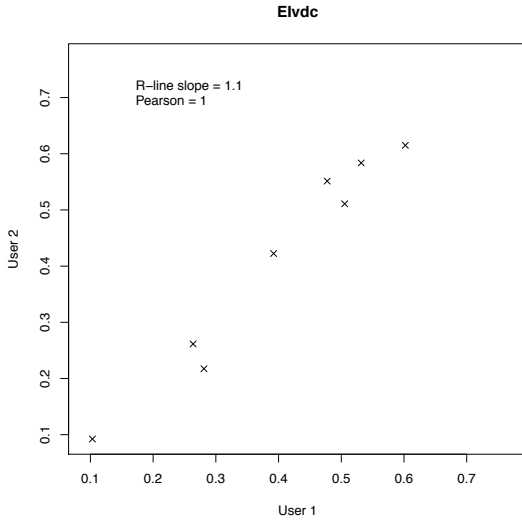
APPENDIX B

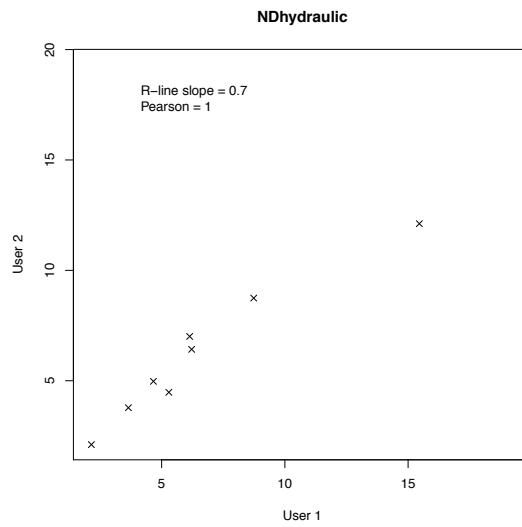
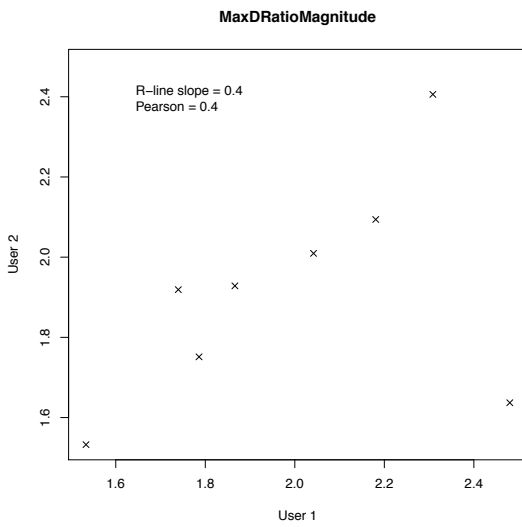
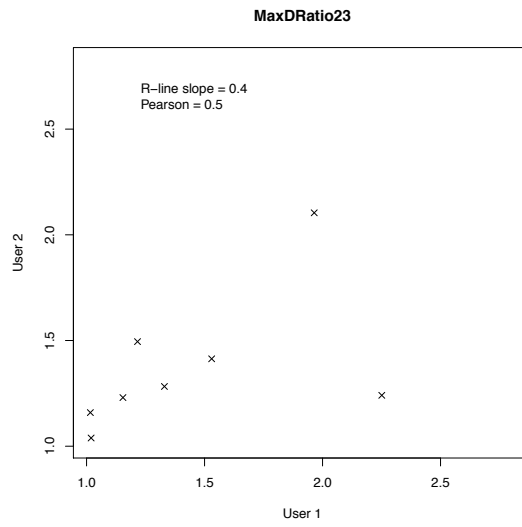
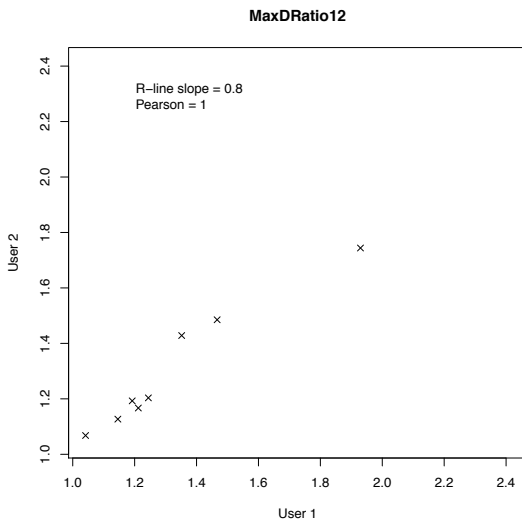
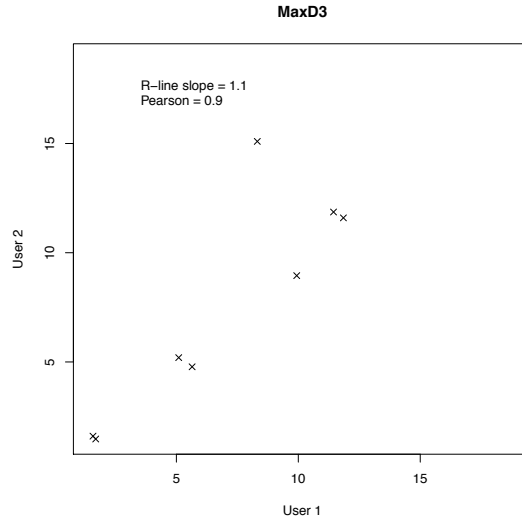
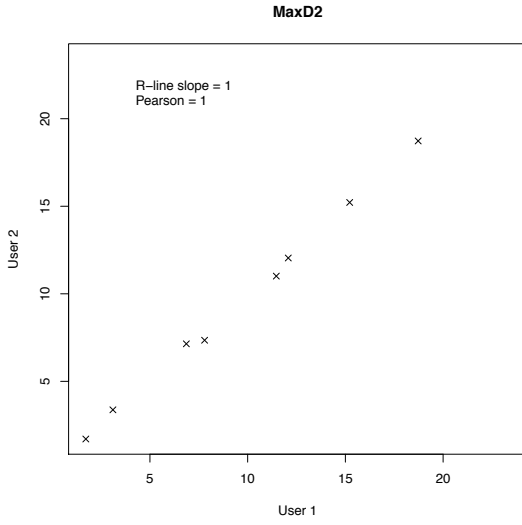
USER VARIABILITY PLOTS

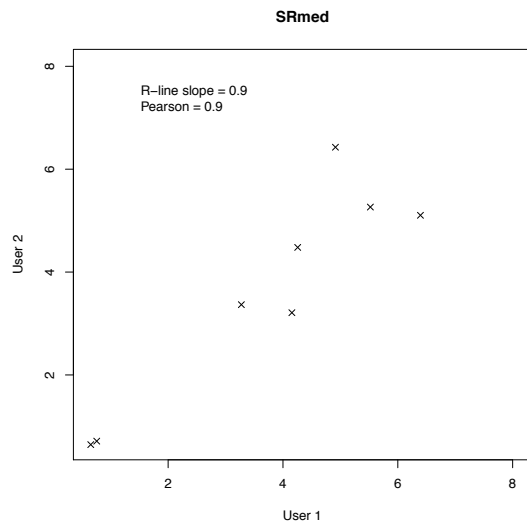
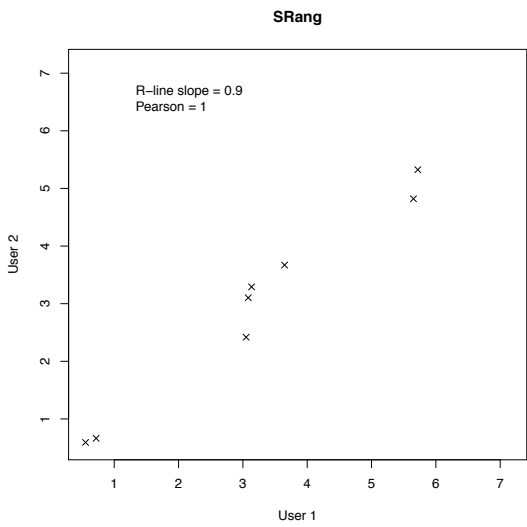
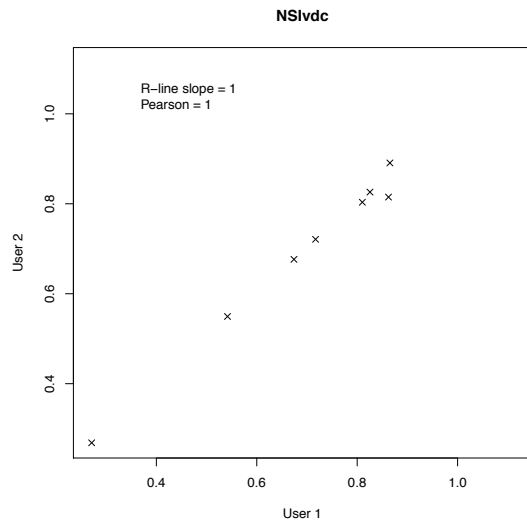
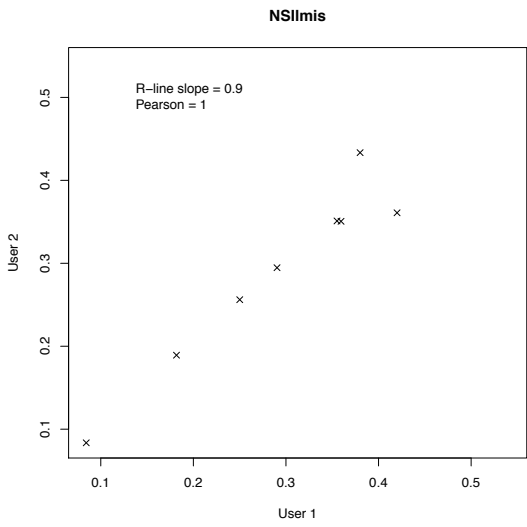
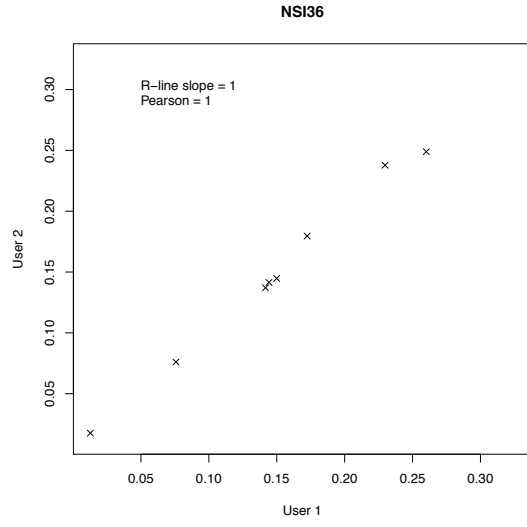
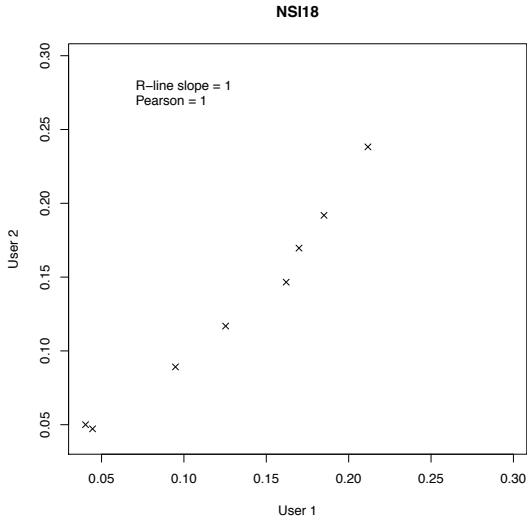


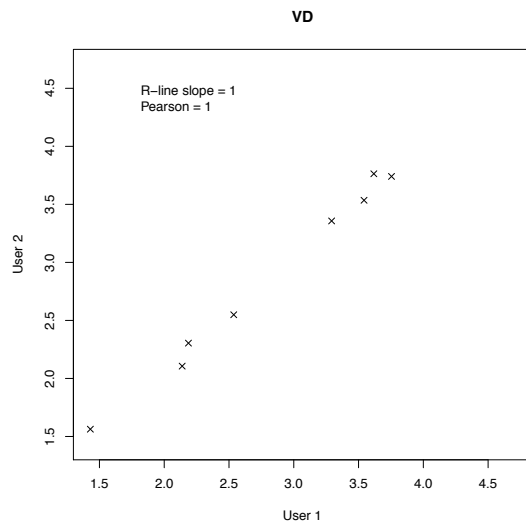
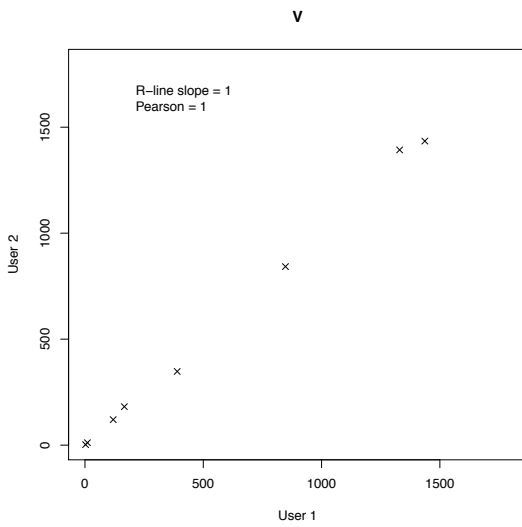
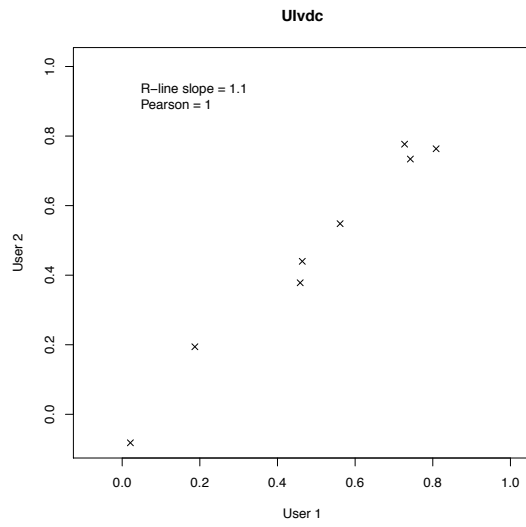
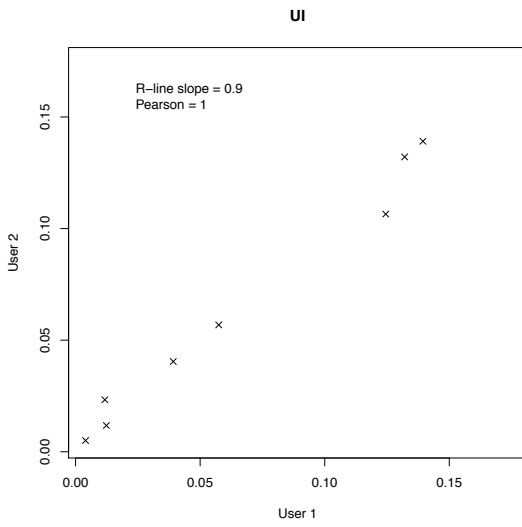
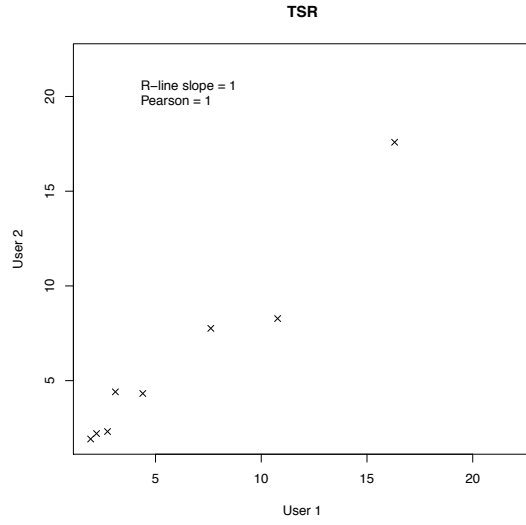
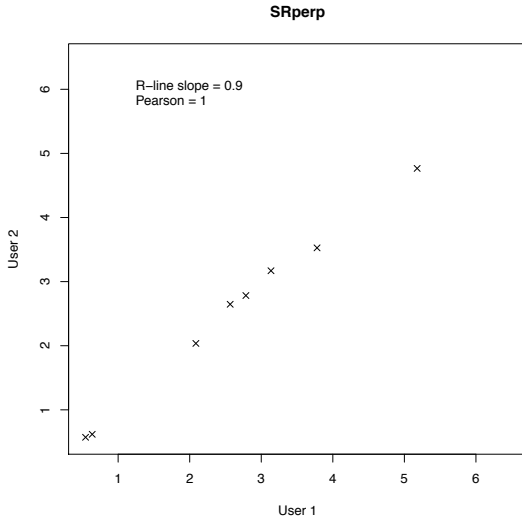












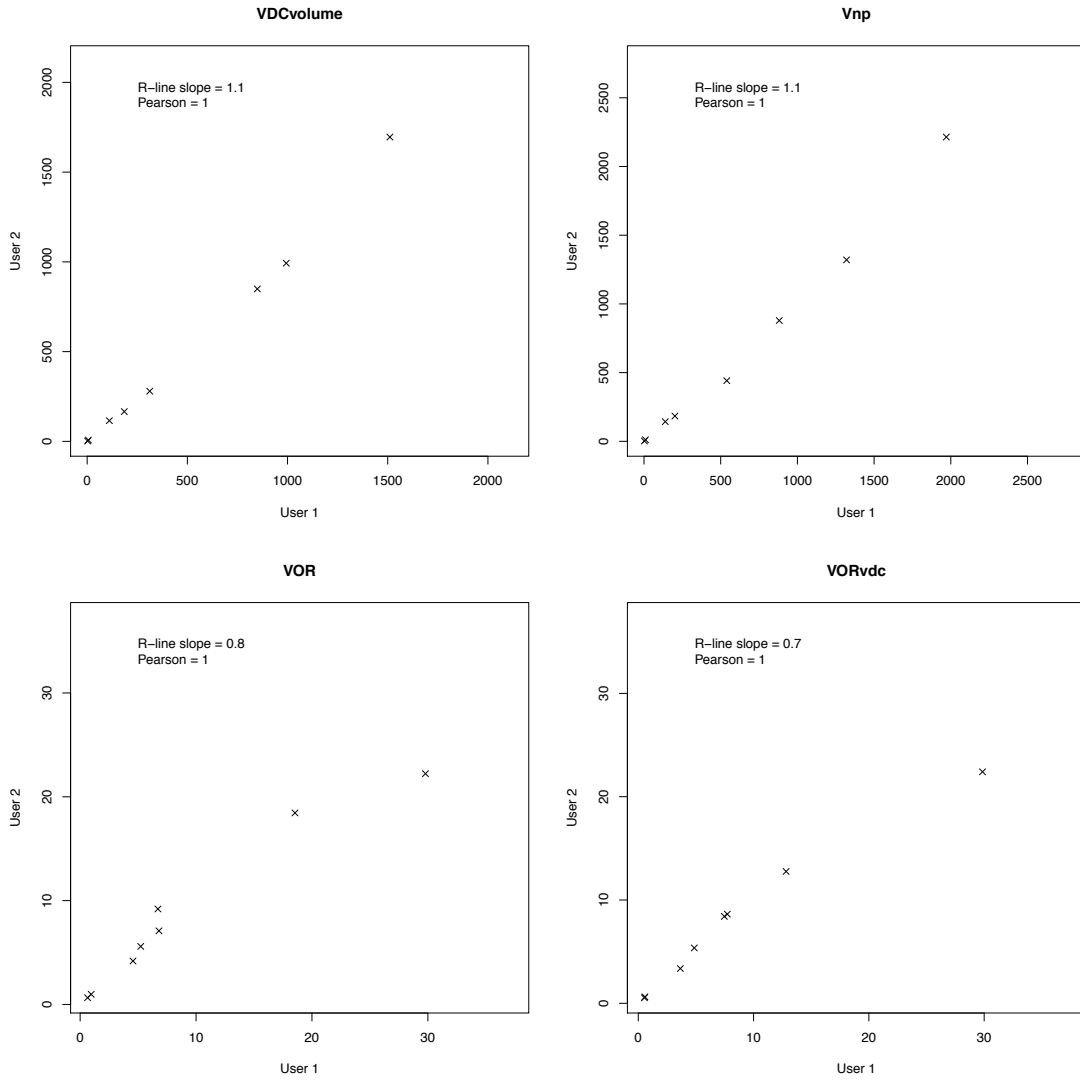
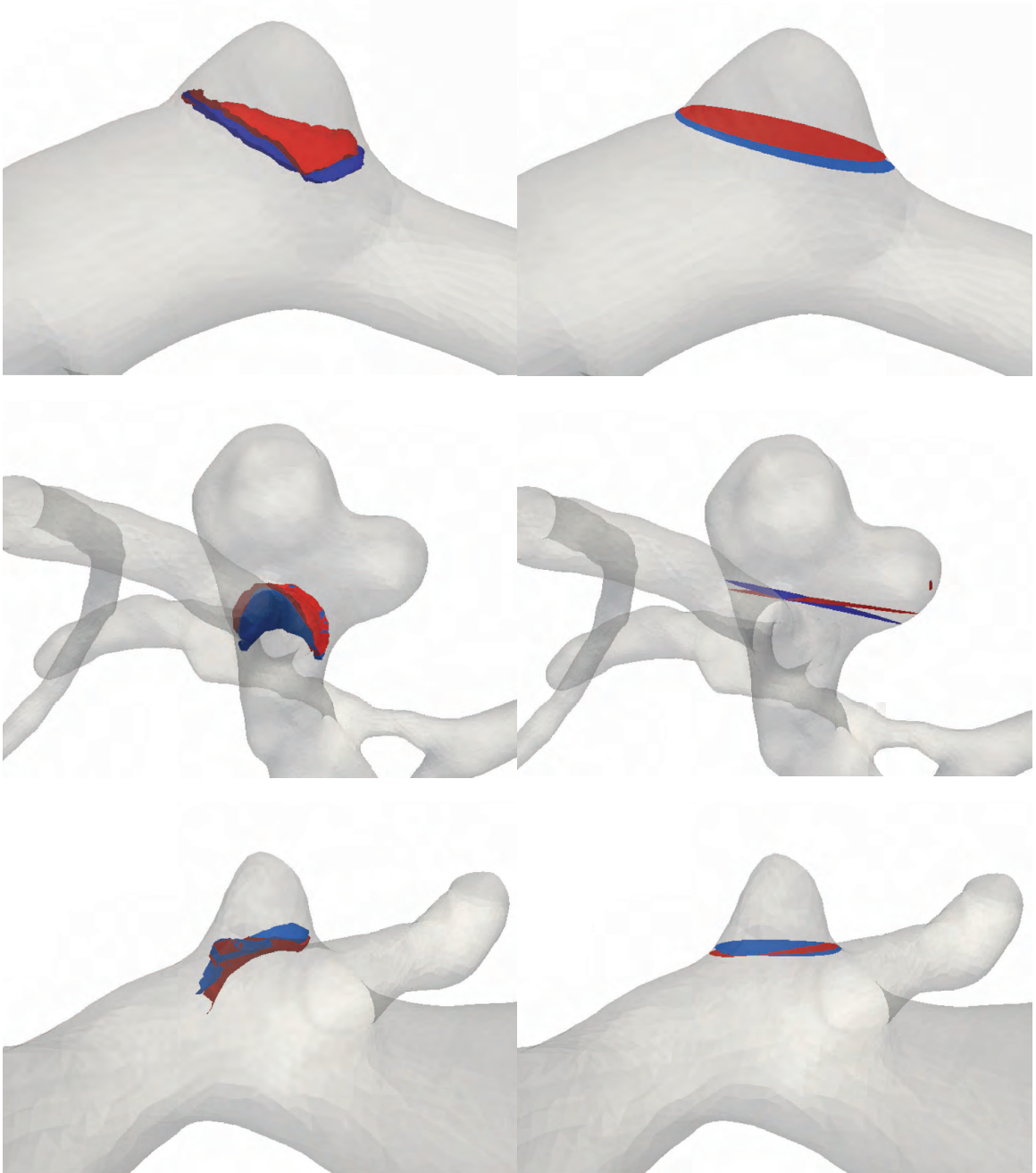
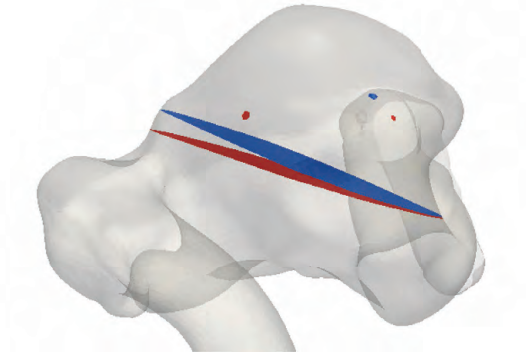
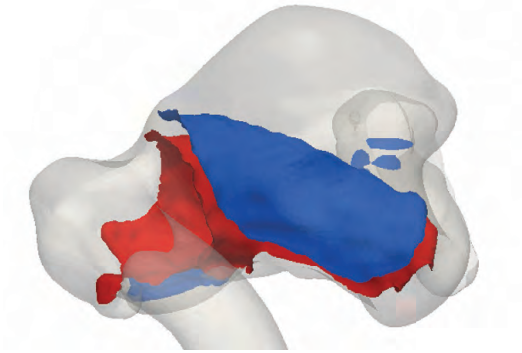
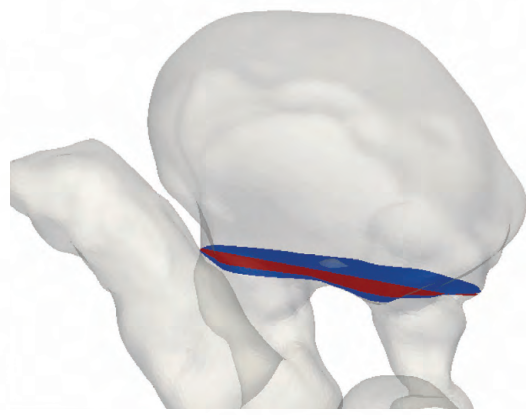
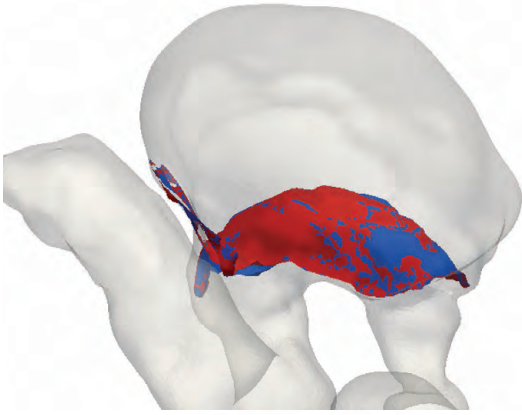


Figure B.1. Comparison of the results of the analysis by User 1 and User 2.

APPENDIX C

USER VARIABILITY ISOLATIONS





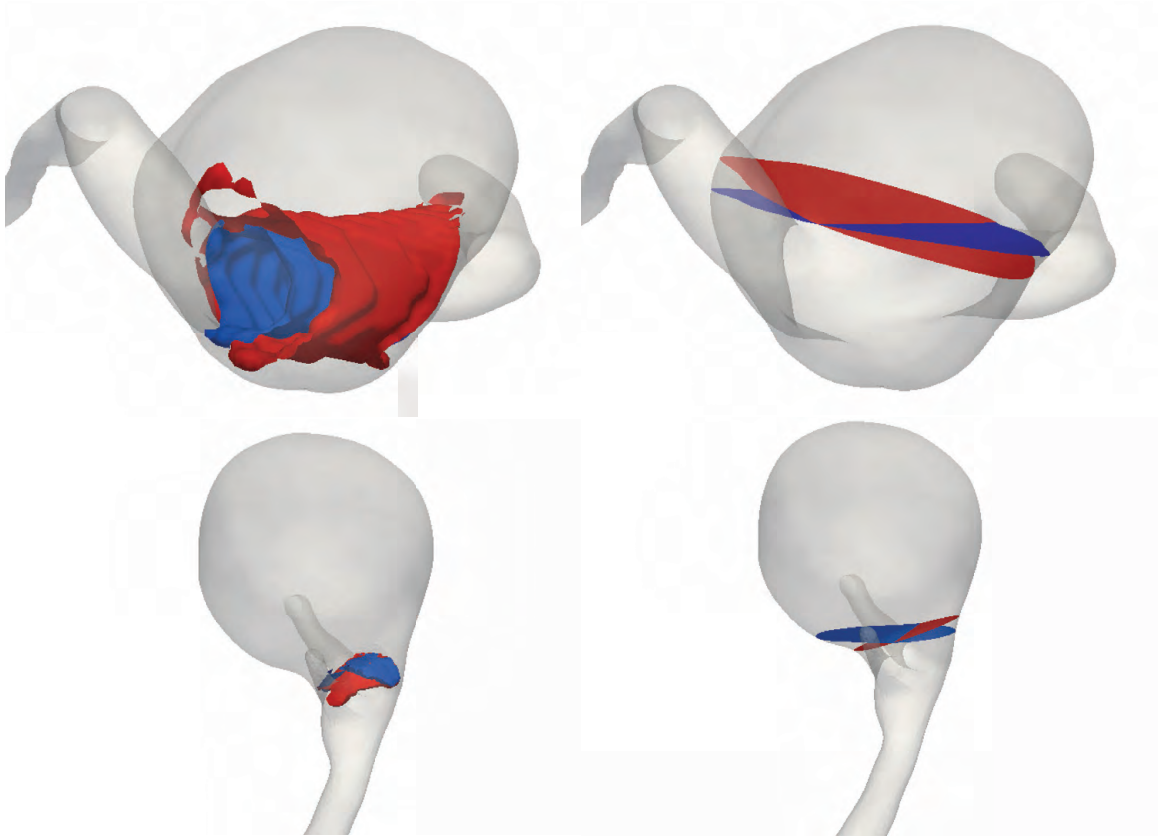


Figure C.1. Renderings of the non-planar ostium (left) and planar ostium (right) from user 1 (red) and user 2 (blue).

REFERENCES

- Antiga, L. et al., 2008. An image-based modeling framework for patient-specific computational hemodynamics. *Medical & biological engineering & computing*, 46(11), pp.1097–112.
- Antiga, L., 2002. Patient-Specific Modeling of Geometry and Blood Flow in Large Arteries.
- van den Berg, R., Rinkel, G.J. & Vandertop, W.P., 2003. Treatment of ruptured intracranial aneurysms: implications of the ISAT on clipping versus coiling. *European Journal of Radiology*, 46(3), pp.172–177.
- Berkowitz, B., 2012. *Development and demonstration of an automated method for deriving novel morphometric indices of cerebral aneurysms*. University of Iowa.
- Cebral, J.R. et al., 2011. Association of hemodynamic characteristics and cerebral aneurysm rupture. *AJNR. American journal of neuroradiology*, 32(2), pp.264–70.
- Cebral, J.R., Hendrickson, S. & Putman, C.M., 2009. Hemodynamics in a lethal basilar artery aneurysm just before its rupture. *AJNR. American journal of neuroradiology*, 30(1), pp.95–8.
- Dhar, S. et al., 2008. Morphology parameters for intracranial aneurysm rupture risk assessment. *Neurosurgery*, 63(2), pp.185-96–7.
- Emory University Department of Math and Computer Science, 2012. AneuriskWeb project website. Available at: <http://ecm2.mathcs.emory.edu/aneuriskweb>.
- Etmnan, N. et al., 2014. Multidisciplinary consensus on assessment of unruptured intracranial aneurysms: proposal of an international research group. *Stroke; a journal of cerebral circulation*, 45(5), pp.1523–30.
- Ford, M.D. et al., 2009. An objective approach to digital removal of saccular aneurysms: technique and applications. *Br. J. Radiol.*, 82, pp.S55–S61.
- Gie Yong, A. & Pearce, S., 2013. A Beginner's Guide to Factor Analysis: Focusing on Exploratory Factor Analysis. *Tutorials in Quantitative Methods for Psychology*, 9(2), pp.79–94.
- Grunwald, I.Q. et al., 2007. Recanalization after endovascular treatment of intracerebral aneurysms. *Neuroradiology*, 49(1), p.41.
- Guglielmi, G. et al., 1991. Electrothrombosis of saccular aneurysms via endovascular approach. Part 1: Electrochemical basis, technique, and experimental results. *Journal of neurosurgery*, 75(1), p.1.
- Hop, J.W. et al., 1997. Case-fatality rates and functional outcome after subarachnoid hemorrhage: a systematic review. *Stroke*, 28(3), p.660.

- Johnston, S.C. et al., 2001. Treatment of Unruptured Cerebral Aneurysms in California Editorial Comment : Unruptured Intracranial Aneurysms: In Search of the Best Management Strategy. *Stroke*, 32(3), pp.597–605.
- Kabacoff, R.I., 2011. *R in Action Data analysis and graphics with R*,
- Kadasi, L.M., Dent, W.C. & Malek, A.M., 2012. Cerebral aneurysm wall thickness analysis using intraoperative microscopy: effect of size and gender on thin translucent regions. *Journal of NeuroInterventional Surgery*.
- Kataoka, K. et al., 2000. Difference in nature of ruptured and unruptured cerebral aneurysms. *Lancet*, 355(9199), p.203.
- Larrabide, I. et al., 2011. Three-dimensional morphological analysis of intracranial aneurysms: A fully automated method for aneurysm sac isolation and quantification. *Medical physics*, 38(5), p.2439.
- Lauric, A. et al., 2011. Rupture status discrimination in intracranial aneurysms using the centroid-radii model. *IEEE Transactions on Biomedical Engineering*, 58(10 PART 1), pp.2895–2903.
- McDonald, J.H., 2014. *Handbook of Biological Statistics* 3rd ed., Baltimore: Sparky House Publishing.
- Millán, R.D. et al., 2007. Morphological characterization of intracranial aneurysms using 3-D moment invariants. *IEEE transactions on medical imaging*, 26(9), pp.1270–82.
- NIST/SEMATECH, 2003. Mean Vector and Covariance Matrix. *e-Handbook of Statistical Methods*. Available at: <http://www.itl.nist.gov/div898/handbook/pmc/section5/pmc541.htm> [Accessed October 17, 2016].
- Piccinelli, M. et al., 2009. A framework for geometric analysis of vascular structures: application to cerebral aneurysms. *IEEE transactions on medical imaging*, 28(8), pp.1141–55.
- Piccinelli, M. et al., 2012. Automatic Neck Plane Detection and 3D Geometric Characterization of Aneurysmal Sacs. *Annals of biomedical engineering*.
- Piccinelli, M. et al., 2011. Geometry of the internal carotid artery and recurrent patterns in location, orientation, and rupture status of lateral aneurysms: an image-based computational study. *Neurosurgery*, 68(5), p.1270–85; discussion 1285.
- Raftopoulos, C. et al., 2003. Surgical Clipping May Lead to Better Results than Coil Embolization: Results from a Series of 101 Consecutive Unruptured Intracranial Aneurysms. *Neurosurgery*, 52(6), pp.1280–1290.
- Raghavan, M.L., Ma, B. & Harbaugh, R.E., 2005. Quantified aneurysm shape and rupture risk. *Journal of neurosurgery*, 102(2), pp.355–62.

- Rahman, M., 2010. Size Ratio Correlates With Intracranial Aneurysm Rupture Status A Prospective Study. *Stroke*, 41(5), pp.916–920.
- Ramachandran, M. et al., 2016. Assessment of image-derived risk factors for natural course of unruptured cerebral aneurysms. *Journal of neurosurgery*, 124(2), pp.288–95.
- Retarekar, R. et al., 2014. Stratification of a population of intracranial aneurysms using blood flow metrics. *Computer methods in biomechanics and biomedical engineering*, pp.1–11.
- Rinkel, G.J. et al., 1998. Prevalence and risk of rupture of intracranial aneurysms: a systematic review. *Stroke*, 29(1), p.251.
- Ryu, C. et al., 2011. Analysis of aneurysm rupture in relation to the geometric indices: aspect ratio, volume, and volume-to-neck ratio. *Neuroradiology*, 53(11), p.883.
- Schroeder, W., Martin, K. & Lorensen, B., 2006. *Visualization Toolkit: An Object-Oriented Approach to 3D Graphics, 4th Edition*, Kitware.
- Sforza, D.M., Putman, C.M. & Cebal, J.R., 2009. Hemodynamics of Cerebral Aneurysms. *Annual review of fluid mechanics*, 41, pp.91–107.
- Sluzewski, M. et al., 2003. Coiling of very large or giant cerebral aneurysms: long-term clinical and serial angiographic results. *American Journal of Neuroradiology*, 24(2), p.257.
- Ujiie, H. et al., 2001. Is the aspect ratio a reliable index for predicting the rupture of a saccular aneurysm? *Neurosurgery*, 48(3), pp.495-502–3.
- Vega, C., Kwoon, J. V & Lavine, S.D., 2002. Intracranial aneurysms: current evidence and clinical practice. *American Family Physician*, 66(4), p.601.
- Wakhloo, A.K. et al., 1994. Self-expanding and balloon-expandable stents in the treatment of carotid aneurysms: an experimental study in a canine model. *AJNR.American journal of neuroradiology*, 15(3), p.493.
- Wiebers, D.O. et al., 2003. Unruptured intracranial aneurysms: natural history, clinical outcome, and risks of surgical and endovascular treatment. *Lancet*, 362(9378), pp.103–10.
- Yasuda, R. et al., 2011. Aneurysm volume-to-ostium area ratio: a parameter useful for discriminating the rupture status of intracranial aneurysms. *Neurosurgery*, 68(2), pp.310-7-8.
- Zygmunt, C. & Smith, M.R., 2014. Robust factor analysis in the presence of normality violations, missing data, and outliers: Empirical questions and possible solutions. , 10(1).